USE OF EXTENDED KALMAN FILTERING FOR BATTERY MANAGEMENT SYSTEM OF A LITHIUM-ION BATTERY

by
Cansu İçöz

Submitted to Graduate School of Natural and Applied Sciences
in Partial Fulfillment of the Requirements
for the Degree of Master of Science in
Electrical and Electronics Engineering

Yeditepe University
2022

USE OF EXTENDED KALMAN FILTERING FOR BATTERY MANAGEMENT SYSTEM OF A LITHIUM-ION BATTERY

APPROVED BY:

Prof. Dr. Duygun Erol Barkana ……
(Thesis Supervisor)
(Yeditepe University)

Assoc. Prof. Dr. Engin Maşazade ……
(Marmara University)

Assist. Prof. Dr. İpek Baz ……
(Yeditepe University)

DATE OF APPROVAL: ..../..../2022

I hereby declare that this thesis is my own work and that all information in this thesis has been obtained and presented in accordance with academic rules and ethical conduct. I have fully cited and referenced all material and results as required by these rules and conduct, and this thesis study does not contain any plagiarism. If any material used in the thesis requires copyright, the necessary permissions have been obtained. No material from this thesis has been used for the award of another degree.

I accept all kinds of legal liability that may arise in case contrary to these situations.

CANSU İÇÖZ

ACKNOWLEDGEMENTS

I want to thank my esteemed teacher, Prof. Dr. Duygun EROL BARKANA, who did not spare her knowledge and support throughout my graduate education.

I would like to thank my esteemed teacher, Dr. Tolga SÖNMEZ, who did not spare his knowledge about Kalman Filtering and support and contributed to my research study.

I would like to thank ARCELİK A.Ş. for the opportunities it provided in the use of test devices.

While writing this thesis, I would like to thank my dear colleague Aybüke BİLİR, R&D Technical Leader, Osman OSMAN, İlker YILMAZ, İskender GÜRLER, Cem SASA, and İsmail ÇİMEN for their contributions to my experimental studies.

Also, I would like to thank Bekir YALIN, Test / Approval Hardware Manager of ARCELİK Electronics Plant, Mehmet ÜLKÜ, Quality Assurance Manager, and Ahmet ARAS, Design Product Quality Team Leader, who supported me during this process.

Finally, I would like to thank my family, who has always stood by me with unconditional support and love.

ABSTRACT

USE OF EXTENDED KALMAN FILTERING FOR BATTERY MANAGEMENT SYSTEM OF A LITHIUM-ION BATTERY

There are numerous energy storage applications today, but batteries that store chemical and electromechanical storage are most common. Batteries are an essential energy source preferred in various fields where electronics are used and in renewable energy systems industries. Battery technology has an utmost significance in future and present technologies such as energy storage in smart grids, electric and hybrid vehicles, consumer electronics. Lithium-ion batteries are becoming more popular among the different battery technologies with their excellently solid performance characteristics, high energy density, low weight, and high galvanic potential. One or more battery cells require a Battery Management System (BMS) circuit of which voltage, current, and temperature can be controlled safely and reliably. The primary purposes of a BMS are to protect the cells or battery from damage, prolong the battery's life, and keep the battery in a condition that can meet specified operating parameters. Therefore, the BMS may include one or more of these functions. In this thesis, a BMS system is designed to control basic functional parameters such as voltage, current, and temperature during charging and discharging. Four different operating modes have been defined as Charge, Discharge, Normal Operation, and Protection Mode. The user has been allowed to monitor the State of Charge (SoC) value on the screen by taking the OCV values measured according to the open-circuit voltage as a reference.

The BMS needs to be able to accurately predict battery states that cannot be directly measured, such as State of Charge (SoC). Within the scope of the study, the Dual Polarization Model was examined, and experimental tests and Extended Kalman Filter defined the parameters of the model. The developed Extended Kalman Filter for SoC estimation compares the measured cell voltage with the recorded current using the Coulomb Counting method with the cell voltage value predicted by the specified model. As a result, Coulomb Counting and Open Circuit Voltage (OCV) methods provide a corrected estimate for the SoC, considering the correlated and designed Extended Kalman filter measurement and model prediction accuracies.

ÖZET

LİTYUM-İYON PİLİN BATARYA YÖNETİM SİSTEMİ İÇİN GENİŞLETİLMİŞ KALMAN FİLTRE KULLANIMI

Günümüzde birçok enerji depolama uygulaması vardır fakat bunlardan en yaygın olanı kimyasal ve elektromekanik depolama yapan pillerdir. Piller, elektroniğin kullanıldığı çeşitli alanlarda ve yenilebilir enerji sistemleri endüstrilerinde tercih edilen önemli bir enerji kaynağıdır. Pil teknolojisi, akıllı şebekelerde enerji depolama, elektrikli ve hibrit araçlar, tüketici elektroniği gibi gelecek ve günümüz teknolojisinde büyük bir öneme sahiptir. Farklı pil teknolojileri arasında, Lityum iyon piller iyi performans özellikleri, yüksek enerji yoğunluğu, düşük ağırlığı, yüksek galvanik potansiyeli ile daha popüler hale gelmektedir. Bir veya birden fazla pil hücresi, güvenli ve güvenilir bir şekilde voltajının, akımının ve sıcaklığının kontrol edilebildiği bir Battery Management System (BMS) devresine ihtiyaç duyar. Bir BMS'in başlıca amaçları hücreleri veya pili hasarlardan korumak, pilin ömrünü uzatmak ve pili belirtilen çalışma parametrelerini karşılayabilecek durumda tutmaktır. Bu nedenle BMS bu işlevlerden bir tanesini veya fazlasını içerebilir. Bu tezde şarj ve deşarj esnasında voltaj, akım ve sıcaklık gibi temel işlevsel parametreleri kontrol etmeye yarayan bir BMS sistemi tasarlanmıştır. Şarj, Deşarj, Normal Çalışma ve Koruma Modu olmak üzere dört farklı çalışma modu tanımlanmış olup açık devre voltajına göre ölçülmüş açık devre voltajı (OCV) değerleri referans alınarak State of Charge (SoC) değerini de ekrandan kullanıcıya izleme imkanı verilmiştir.

BMS' in şarj durumu (SoC) gibi doğrudan ölçülmesi mümkün olmayan pil durumlarını doğru şekilde tahmin edebilmesi gerekmektedir. Yapılan çalışmada Dual Polarization Model incelenmiş, modelin parametrelerinin tanımlanması deneysel testler ve Kalman Filtresi ile sağlanmıştır. SoC tahmini için geliştirilmiş Kalman Filtresi, Coulomb Counting yöntemini kullanarak kaydedilen akım ile birlikte ölçülen hücre voltajını, belirtilen model tarafından tahmin edilen hücre voltajı değeriyle karşılaştırılmıştır. Sonuç olarak, Kalman filtresi, ölçüm ve model tahmini doğruluklarını göz önünde bulundurarak SoC için düzeltilmiş bir tahmin sağlamıştır.

TABLE OF CONTENTS

ACKNOWLEDGEMENTS iv

ABSTRACT v

ÖZET vi

TABLE OF CONTENTS vii

LIST OF SYMBOLS / ABBREVIATIONS xiv

1. INTRODUCTION 15

2. BACKGROUND 20

2.1. BATTERY MANAGEMENT SYSTEM (BMS) 20

2.2. BATTERY MODELING, OPEN CIRCUIT VOLTAGE (OCV), AND COULOMB COUNTING 21

2.3. KALMAN FILTER USED FOR BATTERY MANAGEMENT SYSTEM 23

2.4. CONTRIBUTIONS OF THE THESIS 25

3. METHODOLOGY 27

3.1. LITHIUM-ION BATTERY PACK 28

3.2. HARDWARE DESIGN 30

3.2.1. Designing the Battery Management System 30

3.2.2. Control Circuit Design 32

3.2.3. Monitor Circuit Design 35

3.3. SOFTWARE 37

3.3.1. Analog to Digital Converter (ADC) Software 40

3.3.2. Control Circuit Software 41

3.3.3. LCD (Liquid Crystal Display) Software and Test 41

3.4. SOFTWARE INTEGRATION INTO BATTERY MANAGEMENT SYSTEM 42

3.4.1. Central Processing Unit, LCD Unit, Battery Management System Protection Unit, Warning Unit Integration 42

3.4.2. Central Processing Unit, LCD Unit, ADC Unit Integration 44

3.4.3. Central Processing Unit, LCD Unit, Battery Management System (BMS) Protection Unit Integration, Warning Unit Integration, ADC Unit Integration 44

3.5. BATTERY MANAGEMENT SYSTEM AND STATE OF CHARGE 45
3.5.1. Battery Modeling 45
3.5.2. Measuring Open Circuit Voltage 46
3.5.3. Internal Resistance Calculation 49
3.5.4. Dual Polarization Model Parameter Calculation 49
3.5.5. Extended Kalman Filter and Battery Management System 50
3.5.6. State of Charge (SoC) Estimation with Extended Kalman Filter 57
4. EXPERIMENTS AND RESULTS 62
4.1. CHARGE AND DISCHARGE GRAPHS OF LI-ION BATTERY 62
4.2. TESTING ANALOG TO DIGITAL CONVERTER (ADC) SOFTWARE 63
4.3. TESTING THE CONTROL CIRCUIT SOFTWARE 64
4.4. LIQUID CRYSTAL DISPLAY (LCD) SOFTWARE AND TESTING 67
4.5. TESTING THE SOFTWARE INTEGRATION PROCESS TO THE BATTERY MANAGEMENT SYSTEM (BMS) 68
4.5.1. Central Processing Unit, LCD Unit, Battery Management System (BMS) Protection Unit, Warning Unit Integration 68
4.5.2. Central Processing Unit, LCD Unit, Analog To Digital (ADC) Unit Integration 72
4.5.3. Central Processing Unit, LCD Unit, BMS Protection Unit Integration, Warning Unit Integration, ADC Unit Integration 72
4.5.4. Measurement Results of Internal Resistance 74
4.6. CHARGE AND DISCHARGE TESTS WITH INA238 75
4.7. EXTENDED KALMAN FILTER-BASED STATE OF CHARGE ESTIMATION 79
4.7.1. Dual Polarization Model Parameter Calculation 82
4.7.2. SoC Value Graph Results with Extended Kalman Filter 83
5. CONCLUSION 88
6. FUTURE WORK 91
7. REFERENCES 92

LIST OF FIGURES

Figure 3.1. General system architecture 28

Figure 3.2. C-Code written for Cadex battery device 29

Figure 3.3 Measurements administered on the Cadex battery tester 29

Figure 3.4. Battery management system architecture 31

Figure 3.5. Hardware and software features of the battery management system 32

Figure 3.6. Battery management system control circuit diagram 33

Figure 3.7. Layout drawing 34

Figure 3.8. 3D Visualizer single-sided PCB image 34

Figure 3.9. Realized BMS protection board 34

Figure 3.10. Battery management system monitor circuit diagram 36

Figure 3.11. PCB layout drawing 36

Figure 3.12. 3D Visualizer single-sided PCB ımage 37

Figure 3.13. Realized BMS monitor board 37

Figure 3.14. Software testing and ıntegration sequence 39

Figure 3.15. Software algorithm made for ADC 40

Figure 3.16. Central processing unit, LCD unit, BMS protection unit, warning unit algorithm 43

Figure 3.17. Dual polarization model 46

Figure 3.18. EVM (left) connected to SCB controller (right) 47

Figure 3.19. INA238 high-side sensing application diagram 47

Figure 3.20. Connecting the battery to the INA238 Sensor.....48

Figure 3.21. INA238 sensor computer connection 48

Figure 3.22. Battery management system and Extended Kalman Filter relationship.....50

Figure 3.23. Extended Kalman Filter working flow chart 51

Figure 3.24. C code for pulse charge and discharge test 58

Figure 3.25. Programming steps 59

Figure 3.26. Battery model and Extended Kalman Filter flow chart.....60

Figure 3.27. SoC estimation of Lithium-ion battery with Extended Kalman Filter 61

Figure 4.1. Charge graph 62

Figure 4.2. Discharge graph.....63

Figure 4.3. Finding 0 percent and 50 percent binary value from Proteus.....64

Figure 4.4. Finding 35 percent and 70 percent binary value from Proteus.....64

Figure 4.5. CHG = 15 Volt, DSG = 15 Volt (Buzzer).....65

Figure 4.6. CHG = 15 Volts, DSG = 0 Volt (Led1).....66

Figure 4.7. CHG = 0 Volt, DSG = 15 Volts (Led2) 66

Figure 4.8. CHG = 0 Volt, DSG = 0 Volt (Led3).....67

Figure 4.9. Reading messages on the LCD screen 68

Figure 4.10. CHG = 15 Volts, DSG = 15 Volts, normal mode 69

Figure 4.11. Realization of normal operating mode on board.....69

Figure 4.12. CHG = 15 Volts, DSG = 0 Volt, Discharge Mode.....69

Figure 4.13. Realization of discharge mode on cardboard 70

Figure 4.14. CHG = 0 Volt, DSG = 15 Volt, charge mode 70

Figure 4.15. Realization of the charge mode on the cardboard 71

Figure 4.16. CHG = 0 Volt, DSG = 0 Volt, protection mode 71

Figure 4.17. Realization of protection mode on the cardboard 71

Figure 4.18. Display of central processing unit, LCD Unit, ADC unit integration on the screen 72

Figure 4.19. Reading mode and SoC on LCD screen 73

Figure 4.20. Verification of values on BMS card by measurement 73

Figure 4.21. Verifying that the SoC value is not read on the LCD Display in protection mod 74

Figure 4.22. Adjusting the INA238 EVM sampling interval and sampling number setting. 75

Figure 4.23. VBUS voltage graphic 76

Figure 4.24. Temperature and current graphics 76

Figure 4.25. Discharge graphic 77

Figure 4.26. VBUS graphic 77

Figure 4.27. VBUS temperature and current graphic 78

Figure 4.28. Charge graphic 78

Figure 4.29. Summary data of pulse charge and discharge process 79

Figure 4.30. (a) Charging with 4A and discharging with 10A (b) Graph of the first 10 data (c) Graph of the last 10 data 80

Figure 4.31. Discharge voltage pulses 81

Figure 4.32. Discharge current pulses 81

Figure 4.33. Measuring battery terminal voltage and estimation 84

Figure 4.34. Figure battery terminal voltage and OCV results 84

Figure 4.35. SoC value and current drawn 85

Figure 4.36. R_{int} value and current drawn (x 0,002) 86

Figure 4.37. U_1, U_2 and current drawn (x 0.02) 86

Figure 4.38. SoC, R_{int} and U_1 values 87

Figure 4.39. Trace of covariance matrix 88

LIST OF TABLES

Table 3.1. BMS state comparison conditions 41

Table 3.2. Calculation of OCV value and corresponding SoC percent value 44

Table 4.1. Charge-discharge summary data table 63

Table 4.2. Conditions for testing software by state comparison chart 65

Table 4.3. Table of internal values measured at different currents 75

Table 4.4. Dual polarization model parameters 83

LIST OF SYMBOLS / ABBREVIATIONS

BMS	Battery management system
ADC	Analog to digital converter
SoC	State of charge
BM	Battery management
PBM	Programmable battery management
CDM	Charging – discharging module
PPA	Programmable path array
CMU	Cell management unit
ADC	Analog-digital converter
LIB	Lithium-ion battery
OCC	Overcurrent during charge
OCD	Overcurrent during discharge
SCD	Short circuit discharge
OW	Open wire
OT	Over-temperature
UT	Under temperature
MCU	Microcontroller unit
OCV	Open circuit voltage
ECM	Equivalent circuit model
EVM	Evaluation module
SoH	State of health
EMF	Electromotive force
ANN	Artificial neural network
EKF	Extended Kalman filter
RLS	Recursive least squares
NTC	Negative temperature coefficient
PCB	Printed circuit board

1. INTRODUCTION

It is known that the importance of electrical energy storage in the transition to sustainable energy will gradually increase, and it will become widespread throughout the world. Electrical energy storage systems increase the efficient use of energy and provide energy savings. In energy conversion processes, methods such as storing waste energy, storing and reusing renewable energy sources that can only generate energy in certain periods, or converting it to other types of energy provide uninterrupted access to the required energy. There are many different types of storage technology. Battery storage technologies stand out as the most popular of these types today. The renewable energy source can be stored in battery packs; for instance, their contribution to wind and solar energy storage can be considered a crucial and significant step in reducing dependency on fossil fuels [1].

Battery storage technologies, grids, the development of green energy practices have attracted more and more attention with their use in many different industries such as electric or hybrid vehicles, renewable energy systems, autonomous and robotic systems [2-3]. For this reason, the increasing energy-saving demand for batteries and the growing use of batteries in future technology such as electric vehicles as an environmentally friendly solution has come to the fore as a critical aspect in the modern age [4]. Rechargeable batteries, which are included in battery technology, have been preferred in these systems due to their advantages, such as high energy capacity, high storage efficiency, and fast response time. Among the different battery technologies, compared with Li-ion batteries, Pb-acid, Ni-MH batteries, high capacity, high galvanic potential, low self-discharge, low weight, high specific energy, long shelf life, high rated voltage, high energy rate, low toxicity, and maintenance is the most promising technology for energy storage [5-9]. Although Li-ion batteries have higher nominal voltages than other batteries, connecting and coupling the cells in series and parallel as a shunt is necessary to obtain the required output voltage and current for medium and high power systems [5]. However, this situation causes nonequilibrium problems during recharging and discharging of battery systems, which are usually carried out with the variable current, increasing the battery system's internal resistance and decreasing capacity, significantly affecting the performance of the battery system and shortening its life [10].

Operating a battery pack in compliance with the operating parameters defined for its cells is critical for Li-ion batteries. Operation outside the specified range for temperature, cell

voltage, the charge-discharge ratio can seriously damage battery cells, shorten their life, cause fire, or even explosion. Therefore, an advanced battery management system is required for battery packs to monitor individual cells' parameters and control certain functions such as cell balancing and prevent the irreversible chemical reactions that damage cells inside the battery [11,12].

The Battery Management System (BMS) should have features that enable the user to manage the battery, prevent charge-discharge faults, monitor and optimize the battery, balance the cell voltage level to achieve maximum efficiency, collect and monitor information such as voltage, current, and temperature [6,12-15]. The battery, as mentioned above, management systems used today are widely used in various domains, from electronic devices to electric vehicle technologies. Battery packs consist of cells coupled in series or parallel. These couplings change according to the battery's current voltage. After the cells coupled in series and parallel are connected, the Battery Management System ensures that they operate in a coordinated, balanced, and safe manner, depending on where they are used in the system. These Battery Management Systems, which will be widely used in the future, are of critical importance and capacity for safety and high efficiency. The Battery Management System, which has three main tasks of calculation, data protection, and monitoring, should constantly control the battery values. This system is an integrated version of hardware and software consisting of algorithms for monitoring the battery's current, voltage, and temperature values.

A well-designed BMS should comprise voltage, current, temperature, impedance measurement, standard calculation of SoC and SoH values, ensuring that the cells work correctly within limits, algorithms where cells can be charged and discharged healthily and safely, cells that work in a balanced way, safe in out-of-control situations creation of the mode and the capacity-dependent state of charge algorithms. One of the essential algorithms is determining the battery charge rate according to the calculation algorithm. Based on the measurable data from the battery or the battery model, the BMS needs to predict battery states that cannot be directly measured, such as state of charge (SoC) [6]. The SoC describes the charge state of the Li-ion battery [16]. It is important in BMS to accurately predict the battery's SoC to guarantee the batteries' safety, the battery's peak power state, and real-time estimation of the performance characteristics [17-19,23]. The SoC is defined as the ratio of available capacity to maximum capacity when a battery is fully charged and describes the

remaining percentage of battery capacity [22]. One of the requirements for estimating the SoC is to calculate the integration of battery current and voltage per second. Due to the chemical and production stages of the battery, the batteries cannot reach the maximum voltage at the same time while the charging, causing the voltage to unbalance and low capacity between the batteries, and a cell with 100 percent SoC may not show the SoC value as it should be [24]. For this reason, to calculate the SoC correctly, while measuring the actual capacity, cell measurement should be made in charge, and discharge tests and the actual capacity should be continuously monitored.

In [26,29,63], different categories such as Open Circuit Voltage Method, Impedance Method, Impedance Spectroscopy Coulomb Counting Method, Kalman Filtering, Neural Network are mentioned for measurement approaches. Today's methods are a combination of OCV and Coulomb Counting processes by recording and controlling microprocessor-assisted data with a direct measurement method. Studies on impedance measurement, Extended Kalman Filter, and artificial intelligence-supported applications are carried out to minimize the error. The first step in SoC estimation is battery modeling to establish the estimation algorithm with these methods. An equivalent circuit model is used to simulate LIB behavior. Electrochemical, mathematical/analytical, and electrical circuit-based battery approximation models have been developed from simple models with few parameters to complex models with numerous parameters [16]. In [18], it was stated that the most accurate model for the Li-ion battery is the electrochemical model describing the electrochemical reaction inside the battery, but it is a complicated model to predict and control because partial differential equations need to be solved. Model parameters are imprecise, and noise is also present in the sensor measurements. The response of the real system will be different from the prediction made in the model [18].

The most common approach used in LIB implementations is the Extended Kalman Filter. The accuracy of the estimation is high because the actual-time estimation of the SoC can be applied effectively, and the error correction functions are good. It has a good correction capacity; even if there are errors in the system, it can go down to a specific range with self-correction, and the optimum prediction value can be obtained. An Extended Kalman filter can overcome the shortcomings of the voltage method and current integration method. This filter compares the cell voltage measured in step one with the estimated cell voltage of the battery as represented by the equivalent circuit model. The second step evaluates the

estimated accuracies in the measurement and model, corrects the situation, and ensures a more realistic estimate for the SoC [25].

In this thesis, two essential features of a BMS, namely monitoring and protection, are studied for a battery pack consisting of 4 series connected Li-ion LG 18650 HG2 3000mAh batteries. Texas Instrument BQ77915 protection IC is used for the protection circuit. With this integrated, active use of voltage, temperature, current protections, and smart passive balancing features are ensured. With the help of the microprocessor, the inbound information received from the protection circuit is defined on the screen to the user, and instantaneous monitoring is provided. A total of four messages are printed on the screen. If the battery pack falls below the voltage of 12.3, the protection system gives an audible warning, switches to the protection mode, and prints "Protection Mode". The charging mode shows the user that it is in the "Charge" mode, and in the discharge mode, it is in the "Discharge" mode. The SoC value is printed on the screen as a percentage of the measured OCV value. It is essential for a BMS to accurately predict the SoC value to manage its energy consumption. To avoid overcharging or discharging the battery, an accurate model is of utmost importance to predict the characteristics of the battery and be used as a reference during the design process.

In this thesis, a Second Order Model (Dual Polarization Model) based estimation algorithm was used for parameters that cannot be directly measured by the sensor, such as State of Charge (SoC), State of Health (SOH), and State of Life (SOL) of the battery. For the SoC of the battery, the battery circuit model parameters are estimated according to the graphs obtained by applying the charge and discharge processes to the Li-ion battery for a while. The OCV (Open Circuit Voltage) value will be read in the battery when the current is zero. It was experimentally determined that there is a nonlinear connection between OCV and SoC. According to these values, the actual measured voltage of the battery and the estimated measured voltages made with the Extended Kalman Filter were compared. When the measurement and model predictions of the Extended Kalman filter are also evaluated, it has been revealed that more corrected and higher accuracy results are obtained for the SoC.

This thesis includes monitoring the battery pack’s cell state, charging and discharging current measurement limitation, power estimation in required data conditioning situations, power cut-off in high voltage and current situations, State of Charge (SoC), and State of Health (SoH) aging effects. It can be used for control purposes in many important areas such

as electric cars, renewable energy systems, telecommunications, energy storage units, consumer electronics.

In the first chapter, an introduction has been made regarding the purpose of writing the thesis. In the second chapter, general information about what the Battery Management System is, determination of the model of the battery, Open Circuit Voltage, and Coulomb Counting Method are given in the literature. In the third chapter, the design of the monitoring and protection circuits for the design of the Battery Management System and the Extended Kalman Filter method for the correct estimation of the SoC value is mentioned. In the fourth chapter, the integration results of software and hardware tests are tested. Dual Polarization Model parameters are calculated, and Extended Kalman Filter applied graphic results are obtained. In the fifth chapter, the results of the experimental and design studies are mentioned. In the last chapter, the references used are given.

2. BACKGROUND

2.1. BATTERY MANAGEMENT SYSTEM (BMS)

Within the scope of the literature, microcontroller-based control and protection equipment have been designed and produced for batteries. With the BQ77915 integrated into the designed BMS circuit, the system is protected when the optimal values are exceeded, considering features such as passive data monitoring, charging current, and maximum discharge current. In the system designed in [20], voltage, current, and temperature data are controlled using DS2438 smart battery monitor, detection sensors, microcontroller, LCD screen, sound-light alarm unit, and RS-232 communication module. When the red light is on in the system, it is indicated by an audible warning that there is no battery power or voltage; when the yellow light is on, it means that the battery power and voltage are low when the green light is on, it indicates that the system is working normally, and when all three types of lights are on, it is understood that the system is in the adjusted state. In [15], the battery module containing the smart battery unit (it can be a battery cell or a pack) is equipped with a temperature sensor or other sensors to prevent overcharging of the battery to detect the change of the charge-discharge cycle. It consists of PBM (Programmable Battery Management) control circuit and PPA (Programmable Path Array) module. The PPA (Programmable Path Array) module includes a BM-PPA (Battery Management-Programmable Path Array) and at least one CDM-PPA (Charging Discharging Module-Programmable Path Array). Connecting BM-PPA smart battery units in series or parallel enables electrically connected battery paths, and CDM-PPA enables connect charging and discharging paths. The control circuit monitors the smart batteries and controls the switches of the PPA mode. As shown in [11], smart battery cells have extensive autonomous capabilities that manage the parameters of battery cells. Each smart cell consists of a battery cell and a Cell Management Unit (CMU) with functions such as sensing, computing, control, and communication. Smart cells communicate with each other for situations that require control beyond the cell level, such as cell balancing or SoC estimation for the battery pack. The smart cell here communicates with other cells, providing monitoring and controlling the functionality and sending and receiving messages to regulate battery level operations. The basic properties of a cell are taken as current, voltage, and temperature. Both voltage and

temperature sensing are easily measured with the analog-to-digital (ADC) converter of the cell connected to the thermistor or temperature sensor. The values obtained from the OCV voltage measurement in our system are currently printed on the screen as SoC percent value, and the user is allowed to monitor the BMS circuit operating in the four defined modes of charge, discharge, and normal operation or protection. In [21], DS2438, LCD screen, and 8051 microprocessor are used. Real-time status monitoring is obtained. The microcontroller is initiated to work according to the key operation command, and the current, temperature and voltage values are read on the screen.

2.2. BATTERY MODELING, OPEN CIRCUIT VOLTAGE (OCV), AND COULOMB COUNTING

Estimating the state of charge of the BMS is important for the safe operation of the system. Since the SoC value cannot be measured directly, it must be estimated. In this thesis, the Dual Polarization Model was examined. Model parameters were calculated according to the data measured by the sensor. In [27], the operation of BMS and the modeling analysis of batteries for SoC prediction are shown in the Matlab/Simulink and Amesim joint simulation program. BMS, including SoC and SoH estimation algorithms and active load balance system, has been developed. SoC prediction block, SoH correction block, and fast charging strategy are designed in Simulink. In [18], an equivalent circuit model for Li-ion battery was established in MATLAB/Simulink. In this model, the functions of the SoC are given approximately since the circuit parameters change according to the SoC. In this thesis, OCV and Coulomb Counting methods were calculated by associating them with each other to calculate the SoC value correctly. In [27], SoC estimation approaches are estimated based on a combination of Coulomb counting. Bi-directional DC-DC converters are used in the battery pack, and these are respectively connected to the cell array. The SoC estimation algorithm is designed based on the Extended Kalman Filter (EKF) method. In order to find the circuit model parameters, the nonlinear correlation between the INA228 sensor OCV-SoC was extracted. In the calculation made for Kalman Filter, calculations were made with the values measured per second by being charged with 4A at high current and discharged with 10A with the measurement made in the Cadex battery device. In [28], the effect of the current rate and SoC on internal resistance was tested to find the parameters used in the equivalent circuit model. The battery is charged up to the cut-off voltage, rested for 1 hour,

and the internal resistance was measured. It was discharged to 10 percent capacity with a constant current I_x, rested for an hour, and the internal resistance was measured again, and the discharge was continued with the current Ix until the battery was completely discharged. Dual and joint KFs have been used not only for SoC estimation but also for impedance parameters of the battery model [9]. In [29], the Thevenin-Extended Kalman Filter model was applied on Li-ion cells. The proposed model was set up in Matlab-Simulink to compare the calculated output voltage of the Matlab-Simpower battery model. According to [30], the Equivalent Circuit model has good dynamic performance, and the dynamic properties of the li-ion battery can be accurately simulated. If the equation of state of the system is not linear, the Kalman Filtering method cannot be used directly, and linearization with Taylor expansion is required. In [31], it is mentioned that the evaluation of the battery state of charge for electric vehicles is the key point for this new technology. Since the SoC cannot be measured directly, some methods must be used that allow it to be accurately estimated using measurable variables such as battery terminal voltage and current. It has been mentioned that the Kalman Filter is the best estimator for linear systems. In [32] it is mentioned that the SoC is a representation of the battery capacity that cannot be directly measured using any sensor. The SoC value can be determined by integrating the battery current over time into the coulomb counting method. However, this method has some disadvantages due to the need for a direct current method and the formation of error accumulations. This error rate was studied, and an ECM-based Kalman Filter was used. The Kalman filter method is a recursive process, and it has been mentioned that it is an effective method for combining noise-involved measurement data with other sensor data or a noise filter. In [7], an accurate and comprehensive SoC estimation method is proposed using the Kalman filter. The widely used Thevenin circuit model with the Simulink circuit model is compared. It explains that it predicts SoC more accurately than commonly used methods, which can help to improve battery performance and ameliorate lifespan. It is reported that open-circuit voltage and battery charge state are necessary parameters to obtain the correct value and cannot be measured directly from the battery terminal. In the proposed circuit diagram, the model parameters in the battery circuit through various tests are obtained. In the second step, the OCV was estimated with these parameters, and the OCV-SoC graph was drawn. In [30], it is stated that the estimation of the SoC state is one of the main tasks of the BMS, and it is elaborated in detail that in case this calculation is not done correctly, permanent damage to the internal structure of the battery will result. Neural Network models are very complex and

require large amounts of transaction data to train the physical model. With the Extended Kalman Filter method, a precise identification model is proposed according to the measurement data to calculate the algorithm and the value of the objects. A continuous discharge test was applied to estimate the circuit parameters. Parameter values obtained with the applied filter have been verified. In [32], three different circuit models have been proposed to calculate the SoC value of a Li-ion polymer battery: Thevenin battery model, modified battery model, and simple battery model.

2.3. KALMAN FILTER USED FOR BATTERY MANAGEMENT SYSTEM

SoC estimation is done with Coulomb Counting, open-circuit voltage (OCV), and Kalman filter. Charge and discharge tests with constant current and constant voltage were applied to the battery. While Coulomb counting and OCV could not monitor the actual value with high accuracy based on the results obtained, the Kalman Filter provided the SoC estimation correctly. In [33], the circuit parameters of the Li-ion iron phosphate battery were tried to be estimated with the Thevenin Model. Extended Kalman Filter Mathematical model calculations are made. The SoC current initial value is determined based on the previous SoC calculation value, the time interval, and the current open-circuit voltage. The values of the circuit parameters are approached to the ideal value by using the Extended Kalman Filter. In [55], the equivalent circuit model, which is a widely used model among the models in the literatüre, is proposed because it has easy and simple use. It is stated that this model does not require much calculation and that OCV is a very important parameter in terms of the equivalent circuit model. The dV/dQ method is linked to the OCV – SoC curve. It has been stated that the estimation of the real-time OCV curve is important for BMS. In this thesis, the battery is calculated according to the voltage, current, and resistance on the battery, with the current varying depending on the loaded, and unloaded voltage at different current values. It has been stated that the Recursive Least Squares (RLS) method simultaneously predicts OCV and internal resistance. For the estimation method, the OCV estimation method is proposed by using the combining method of Kalman Filter and RLS. In this thesis, in the Kalman Filter algorithm designed for Li-ion LG 18650 HG2 3000mAh battery, values for SoC estimation consist of OCV and Coulomb Counting based model equations. State equations for the designed system have been extracted. The covariance matrix has been advanced over time and the process noise has been added. By changing the experimentally

obtained process noise covariance of the Kalman filter, the experimental and estimation results are plotted. [56] presents the SoC estimation in the Extended Kalman Filter (EKF) algorithm for the LiFePO4/C cell. Important outlines characterizing the electrical behavior are demonstrated and model approaches that enable the generation of OCV properties are presented. The range of each OCV-SoC relationship is changed to reduce the SoC estimation error. A measurement noise model has been applied to compensate for simplified battery modeling errors. In this thesis, it is mentioned that the SoC estimates are estimated by coulomb counting within the range of ±5 percent of the values based on the Extended Kalman Filter. An equivalent circuit model is used to model a 2000 mAh lithium-ion battery in [57]. The parameters of the model were estimated using Simulink Design Optimization based on experimental data. In this thesis, the Extended Kalman Filter method was used. Different charge and discharge experiments were applied, and different SoC values were obtained. It can be asserted that both of the experiments carried out and the applicable methods managed to bring this value to the real-time SoC value in a timely manner, even if the SoC was not estimated correctly. [58] presented a method for estimating the SoC value for a Li-ion battery based on Kalman Filter and Artificial Neural Network (ANN). ANN is created and built for SoC prediction and then ANN is trained using Tensorflow open source library. The model used here is Thevenin Equivalent Circuit Model and Extended Kalman Filter-ANN is proposed by integrating the Extended Kalman Filter estimation according to the ANN. As a result, ANN and KF methods showed a maximum error of 2.6 percent and 2.8 percent. The Extended Kalman Filter-ANN method performed better with less than 1 percent error. In [59] offers the Extended Kalman Filter application for Li-ion batteries to obtain optimum SoC estimation. The comparison was made between Extended, and Kalman Filter with Coulomb Counting method, and SoC estimation was made using Extended Kalman Filter. It is mentioned that the Two Time Constant Model has 20 percent less absolute average error and about three times less absolute maximum error than the One Time Constant Model, and offers a higher accuracy for SoC estimation. In [60], it is mentioned that algorithms such as Recursive Algorithms and Recursive Least Squares (RLS) and Kalman Filter are widely used in estimating the electrical impedance of a battery cell. In this thesis, the impedance of the ohmic resistance was estimated in two different ways with Recursive Least Squares (RLS) approach and using Kalman Filter. The algorithm produces highly accurate predictions for the ohmic resistance and time constant of the battery cell, both in simulations and by estimating the SoC with experimental data from a Li-ion cell. It

has been mentioned that some situations should be considered, such as sensor noise, covariance windup, when these methods are used.

2.4. CONTRIBUTIONS OF THE THESIS

In this thesis, it is emphasized that electrical energy storage is a key technology that can play an important role in improving the sustainability of energy in various existing energy sectors. For this reason, it has been stated that batteries play a role in various fields such as increasing energy-saving demand, environmentally friendly solutions, increasing use of electric vehicles, consumer electronics, automotive electronics, communication technology, energy storage units, autonomous systems. In the developing technology, Li-ion battery, which has become popular day by day due to its good performance features, low cost, rechargeable, high-energy density, has been used.

The contributions of this thesis, differ from the literature, the BMS circuit and Extended Kalman filter application are not designed for electric cars. It is designed as a basic protection circuit for a 4-cell battery pack. While cell balancing, over, low current protection, extreme low voltage protection, extremely high and low-temperature protection circuits are designed separately for the protection circuit in the literature, while microprocessor-based protection circuits are designed, Texas Instruments BQ77915 used in the thesis uses current, temperature, and smart cell balancing algorithm without microprocessor control. With this, the circuit has been used more effectively and efficiently, and space has been saved in the layout design of the circuit. While BMS designs are made in simulation in the literature, in this thesis, the cards are presented in such a way that they can be used both in simulation and in protection circuits.

The second major contribution, Charge and discharge tests in the literature, is not only measured in simulation programs such as MATLAB or experimentally but also experimentally and charged and discharged in the Cadex Battery test device as a supplement. The accuracy of the tests performed by comparing the current and voltage values with the INA238 sensor has been increased.

The third major contribution, when using a multi-cell battery, a single Kalman filter is used, although separate SoC estimations are made for each cell. While OCV and Coulomb Counting methods are applied separately in the literature, in this thesis, it has been seen that the measurement values are similar in the results obtained in the OCV and Coulomb Counting Methods, and OCV and coulomb counting are methods that confirm each other. The starting values of the SoC estimation with the Extended Kalman Filter of the measurements made with Coulomb Counting and OCV were estimated as close to the real.

3. METHODOLOGY

The general structure of the system has an interpenetrated and nested structure as shown in Figure 3.1. A control and monitoring circuit is designed for the battery, which is formed by combining four series-connected Li-ion batteries. With the BQ77915 device used in the control circuit, eliminates the imbalance from over or under voltage, smart passive cell balancing from cell to cell, provides short-circuit discharge, over-current discharge, and temperature protection. The CHG and DSG pins provide packet protection via NMOS FET drivers. This device has CHG and DSG drivers for N-channel FET protection that automatically turns on the CHG or DSG FETs after the protection delay time when a fault or unexpected condition occurs. The information transmitted from the CHG and DSG pins is transferred to the AT89C51 microprocessor with the ADC. The information defined in the processor is transferred to the monitor and the defined information is provided for the user to follow. Messages printed on the screen can display “Discharge Mode” in battery discharge mode, “Charge Mode” in charging mode, “Protection Mode” in high or low voltage, current, and temperature values, and “Normal Operation” if no situation has occurred. Sensor data is NTC and current sensor. It warns the user with a buzzer in case of high or low current, voltage, and temperature. The voltage value calculated according to the open-circuit voltage and the SoC value based on this value is printed on the screen as a percentage. Accurate estimation of the SoC value is one of the most important features of BMS circuits. Model-based SoC estimation method is preferred. In order to make SoC estimation with the Extended Kalman Filter, the current and voltage values should be measured every second with the help of the sensor. Changing current and voltage values were measured with the INA228 sensor. Graphics were drawn for both OCV values and the Coulomb Counting method. The correct operation of these methods depends on working with a correct model. For model-based SoC prediction, the battery should be tested with an equivalent model and the behavior of the battery should be observed. The Dual Polarization Model was chosen as the model. Model parameters were determined according to OCV graphs. Voltage and current values were measured at high current with the Counting Method. These values became the input for the designed Extended Kalman Filter. By using OCV and Coulomb Counting methods together, model-based equations of state are derived. The accuracy of the model used with the designed Extended Kalman Filter was investigated and the correct prediction values were obtained.

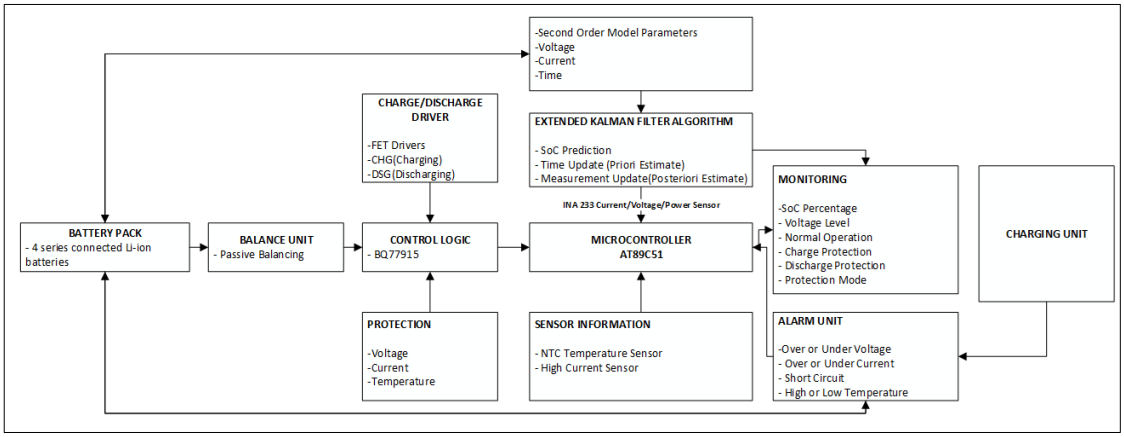

Figure 3.1. General system architecture

3.1. LITHIUM-ION BATTERY PACK

The smallest basic component that constitutes the battery management system is the battery. Generally, a battery can hold a value that corresponds to between 1-6 Volts. A battery pack usually consists of several cells connected in series or parallel. These battery packs can be combined with each other coupled in series or parallel depending on the intended use. Batteries can be classified according to parameters such as high power, high energy, high endurance, longer battery life. In addition to these parameters, the C and E ratios are also important. The C ratio is a measure of the rate at which a battery is discharged relative to its maximum capacity. The 1C rate means that the discharge current given can discharge the entire battery within 1 hour. This means that for a battery with a capacity of 50 Ampere-hours, it will equal a discharge current of 50A. For this battery, the 10C ratio will be 500 Amps and the C/2 ratio will be 25 Amps. The 1E ratio is the discharge power used to discharge the entire battery in 1 hour. State of charge SoC is expressed as a percentage of available battery capacity. In order to understand the characteristics of a one-cell Li-ion battery, its characteristic was extracted in the Cadex C8000 battery tester. Test for one cell coded as LG HG2 is charged with 3A, discharged with 3A. According to the datasheet, the maximum safe operating voltage is 4.25 V, the maximum safe operating charge current is 4A, and the maximum safe discharge current is 10A.

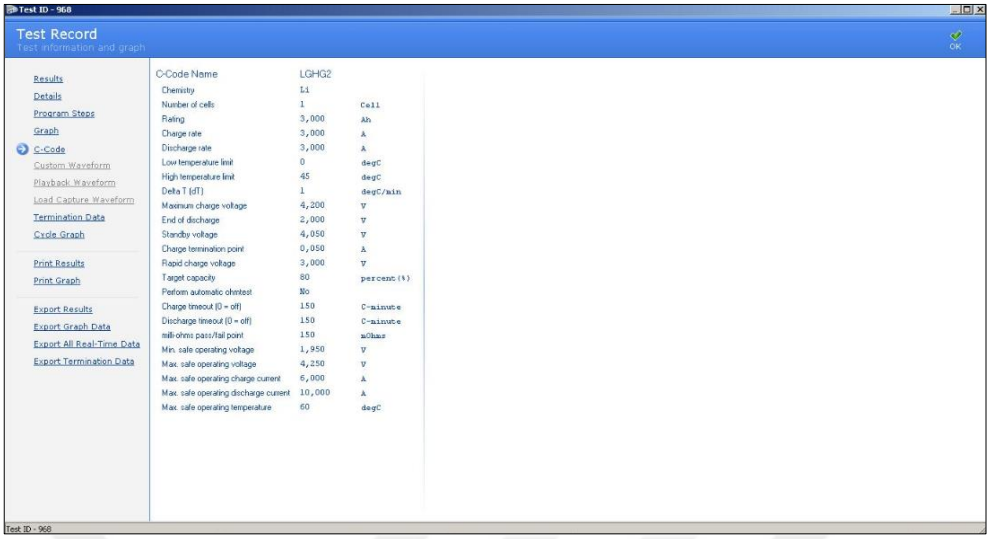

Figure 3.2. C-Code written for Cadex battery device

Figure 3.3 shows the images of testing the batteries connected to the Cadex battery tester.

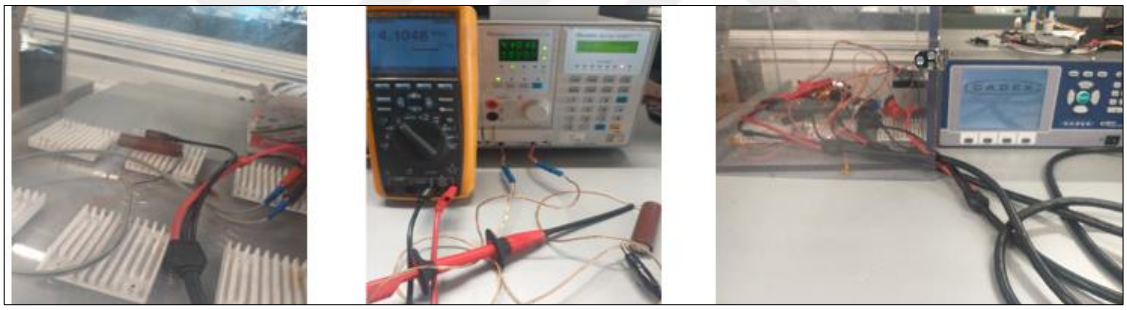

(a) (b) (c)

Figure 3.3 Measurements administered on the Cadex battery tester a) Placing it in the battery cabinet b) Measuring the voltage of the charged battery c) Taking the test

3.2. HARDWARE DESIGN

Proteus program was used for circuit design schematic diagrams. Proteus is a program with which we can draw electronic circuit diagrams and draw printed circuit boards. ISIS is used in electronic circuit design, electronic circuit analysis, printed circuit design, simulation of microprocessor-based projects. ARES provides the opportunity to draw a printed circuit board. In this thesis, Proteus version 8.9 was used. Two separate PCB circuits, Control and Monitoring (Monitor), were created. The reason for this is to prevent undesirable situations such as short circuit that may occur in card printing or material assembly. First of all, the hardware schematics of the circuits were created in Proteus, and then the PCB Layout diagram was drawn. This schematic is taken as a reference for printing PCB boards and correct assembly operations. PCB boards are printed as we call single-sided or single-sided. Single-sided printed circuit boards are preferred in the construction of many electronic projects used in daily life because their production and manufacturing costs are reasonable.

3.2.1. Designing the Battery Management System

The batteBatterygement System design was completed in five steps. These are requirements design, hardware design, algorithm design, software coding, and finally testing and integration phase during which physical tests are performed. In this thesis, a battery management system was designed for a 4 cell Lithium-Ion battery, and a smart cell control was made with the design. The Battery Management System is designed as a data monitoring and protection function. A Microprocessor-based control feature is provided. State of Charge level (SoC) is traceable. State of Charge level can be displayed as a percentage. Battery pack voltage, charge, and discharge status can be monitored. The feature of balancing the cell in package and cellular is provided. A protection function has also been added to protect the battery pack from situations such as overcharging, low voltage, over current, short circuit, open circuit protection, high temperature, etc. Charge or discharge mode, voltage, and, accordingly, SoC value are printed on the LCD screen.

In Figure 3.4, the structure of the Battery Management System Protection Unit, which provides the control and management of the 4-cell Lithium-ion battery during charging and discharging, is given. It is the structure that enables the system to be controlled when the optimum values are exceeded by measuring values such as current, voltage, temperature. ADC0804 component is used for Analog to Digital Converter. This circuit is an IC, that is, an integrated circuit that converts the analog voltage given at the input to a digital output to be equivalent. It provides LCD (Display), State of Charge, charge and discharge status, voltage monitoring feature. Depending on the information it receives from the Battery Management System Protection Unit, the Warning System provides an audible warning to easily control unexpected situations.

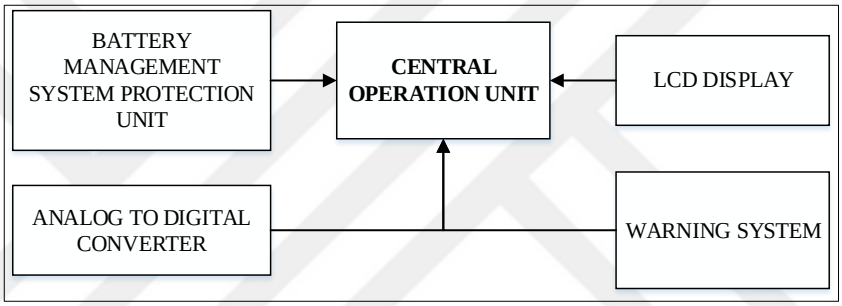

Figure 3.4. Battery management system architecture

The system design is in Figure 3.5 as hardware, charge, discharge, over-temperature charge or discharge with BQ77915 IC, passive cell balancing features are the functional features available in the protection circuit. In terms of software, the information coming from the algorithms protection circuit worked on is converted into digital data with the help of ADC0804, and the messages and operating modes defined by the software loaded on the AT89C51 are printed on the screen.

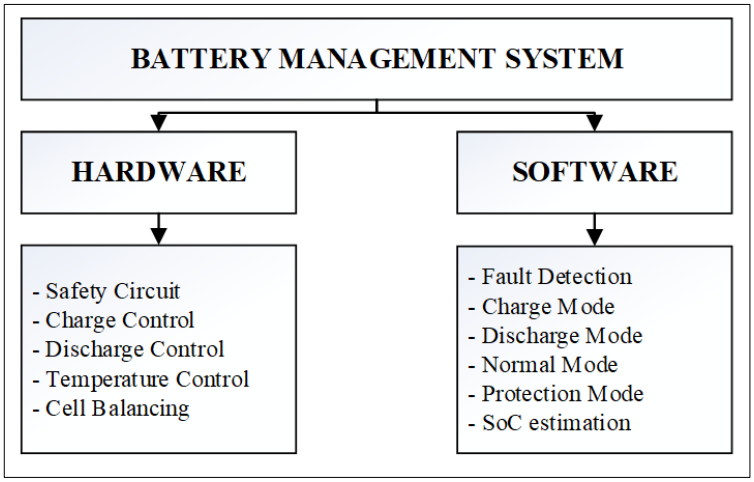

Figure 3.5. Hardware and software features of the battery management system

3.2.2. Control Circuit Design

The main processor of the protection circuit schematic is our IC component BQ77915 of which the manufacturer is Texas Instruments. The reason why the BQ77915 (3-Series to 5-Series Stackable Ultra-Low Power Primary Protector with Autonomous Cell Balancing and Hibernate Mode) device is preferred is that it has many technical and functional features suitable for its intended use. BQ77915 device has an intelligent cell algorithm. It is preferred for Lithium-Ion / Lithium polymer batteries. Protections applied by BQ77915 IC as cell voltage, over-voltage, and under-voltage, over-current charging as current, over current discharge, short circuit discharge, controlling over-temperature or insufficient temperature conditions in charge and discharge as temperature, FET diode protection, battery cell for open wire connection control, Ability to control for 3 or more cells connected in series, overvoltage 3 V to 4.575 V, undervoltage: 1.2 V to 3 V, open-cell and open-wire detection (OW), current protection: overcurrent discharge 1: –10 mV to –85 mV, overcurrent discharge 2: –20 mV to –170 mV, short-circuit discharge: –40 mV to –340 mV, temperature protection: overtemperature charge: 45°C or 50°C, overtemperature discharge: It is between 65°C or 70°C.

It provides battery pack protection via the integrated CHG and DSG NMOS FET drivers, which can be disabled with two control pins in Figure 3.6. CBI pin is “Cell Balancing Input” pin input, CBO “Cell Balancing Output” is cell balancing pin output. It is accomplished by comparing the threshold voltages, evaluating the comparison results, controlling the cell stabilizer FET. SRP and SRN pins are current sensing input pins. Considering these features in Proteus, a 4-cell design scheme was created according to the circuit diagram in the datasheet, as given below. The BQ77915 device is not available in the component insertion section of Proteus, a new circuit element has been created and its library has been added. The temperature control is shown in the schematic with 20k NTC (Negative Temperature Coefficient) using the RTS-PU resistor connected to the VTB and TS pins. Ares, a subprogram of the Proteus program, was used for the layout drawing. With the Ares program, an automatic printed circuit of a diagram drawn in ISIS can be created and allows the circuit to be drawn freely. Figure 3.6 shows the Control Circuit drawn in Proteus.

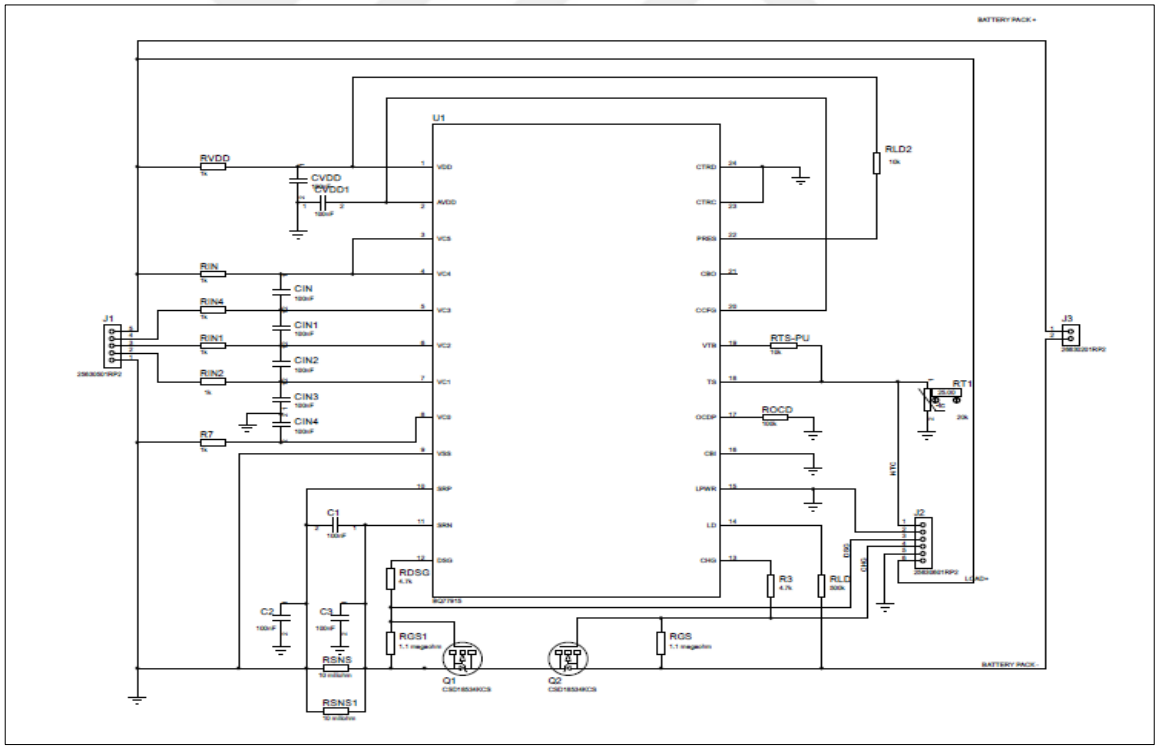

Figure 3.6. Battery management system control circuit diagram

Figure 3.7 Layout drawing of the circuit is made in Ares.

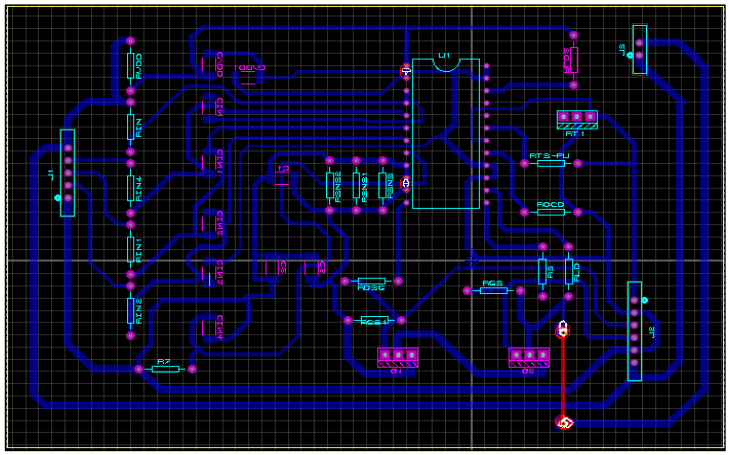

Figure 3.7. Layout drawing

Single-sided PCB image of the drawn board with 3D visualizer shown in Figure 3.8.

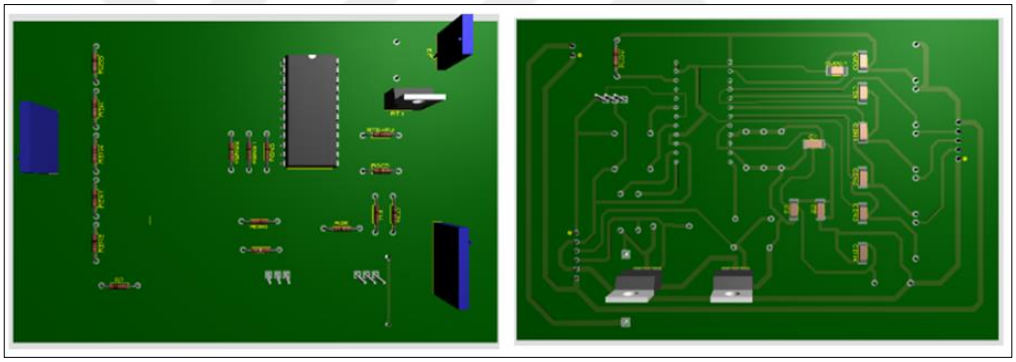

Figure 3.8. 3D Visualizer single-sided PCB ımage

In Figure 3.9, the visuals of the card that this card is arranged on the PCB and can be used in real life are given.

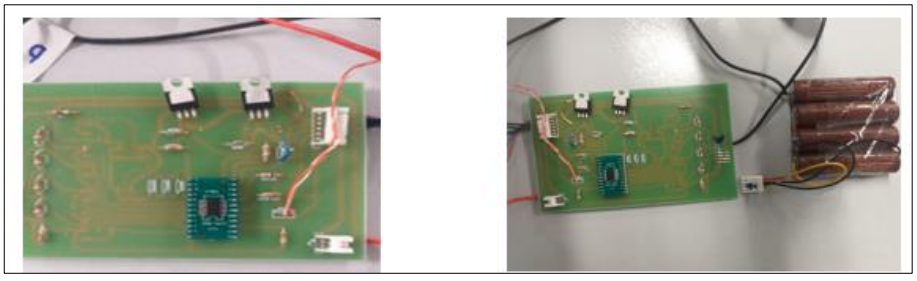

(a) (b)

Figure 3.9. Realized BMS protection board a) Top view b) Installing 4-cell battery in protection circuit

3.2.3. Monitor Circuit Design

The monitor circuit operates many functions to control and print the information from the control circuit, the alarm system with the buzzer, and the State of Charge status. From a design-oriented point of view, the controls are ATMEL AT89C51 8 bit 24 MHz integrated type microcontroller. It is 8 bits and works with a frequency of 24 MHz. 32 of the 40 pins are input and output pins. Analog-to-digital converters are the most commonly used devices for data acquisition. In our Battery Management System design, outputs such as voltage, current, and temperature are obtained. An ADC is used to convert analog signals to digital numbers so that the microcontroller can read and control these values. ADC0804 is an 8-bit converter working with 5V. It can only take one analog signal as input. The digital output can vary between 0-255. The ADC0804 must be interfaced with the AT89C51 and connected to the LCD to measure and display voltage, current, temperature. We aim to measure the voltage supplied at the input of the ADC0804 and show the SoC status of the battery. The information coming from the CHG and DSG inputs from the circuit we designed as the control circuit is given to the AT89C51 with the help of optocouplers. Optocouplers are used to provide isolation between the CHG and DSG inputs and the microcontroller. It acts as input to the ADC0804 pins with the Battery + voltage divider resistors entering the connector. To design the ADC0804 circuit, a 10k resistor and a 150pF capacitor are connected to the CLK R input. The crystal oscillator, together with two 22 pF capacitors, is connected to XTAL1 and XTAL2, which will provide the system clock to the microcontroller. Voltage and SoC value are used ADC0804 to convert analog input to digital format where converted data is shown using AT89C51 and on 16 x 4 LCD. The fuse circuit is made to operate the entire system safely. Serial communication inputs RX (Receiver) and TX (Transmitter) inputs are also shown on the AT89C51. Figure 3.10 shows the Monitor circuit drawn in Proteus.

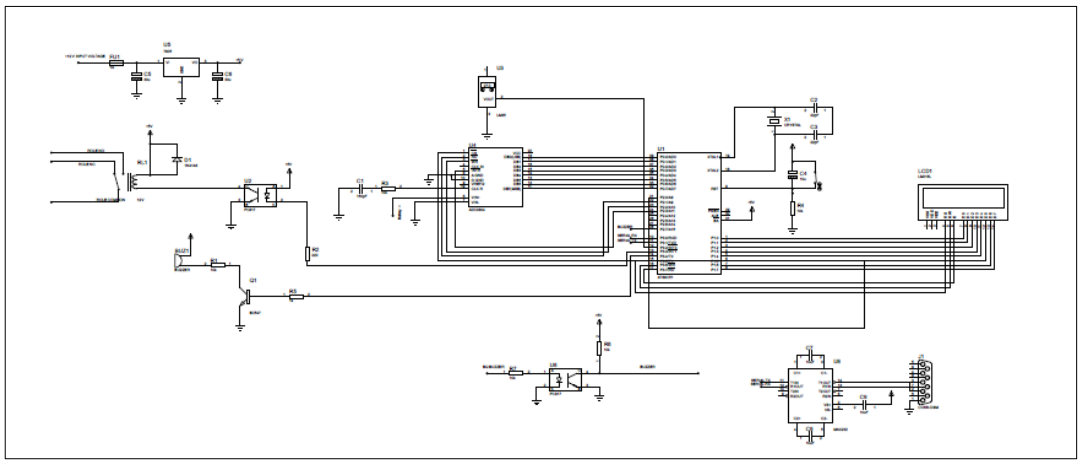

Figure 3.10. Battery management system monitor circuit diagram

Figure 3.11 shows a Layout drawing of the circuit is made in Ares.

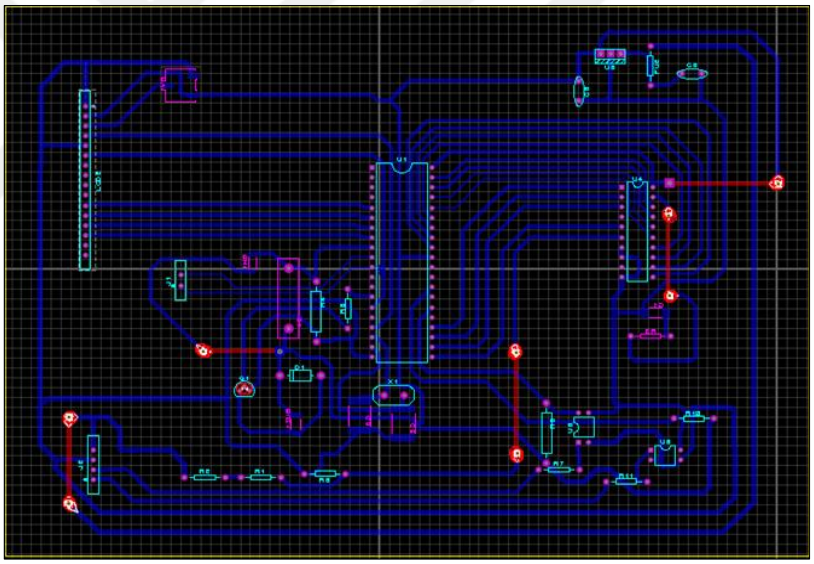

Figure 3.11. PCB layout drawing

In Figure 3.12, a single-sided PCB image of the drawn card is given with a 3D Visualizer

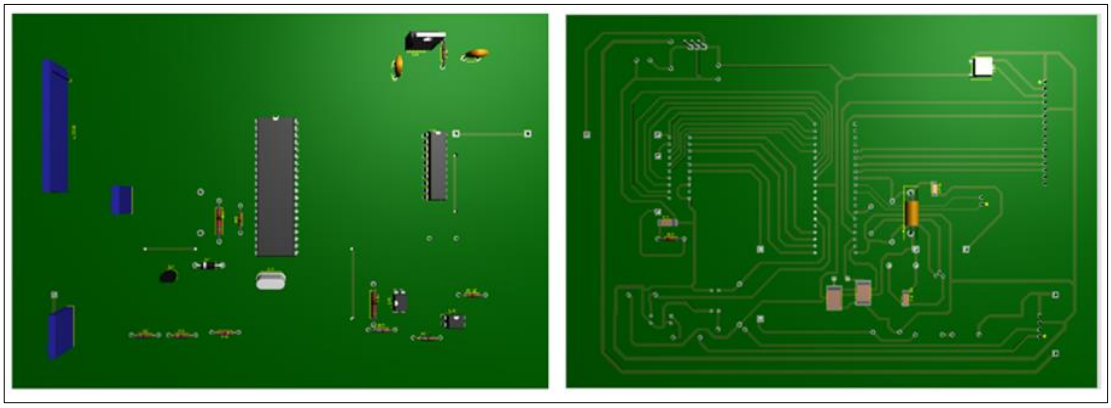

Figure 3.12. 3D Visualizer single-sided PCB ımage

In Figure 3.13, the visuals of the monitor card, which are arranged on the PCB and can be used in real life, are given.

(a) (b)

Figure 3.13. Realized BMS monitor board a) Top view b) Installing a 4-cell battery into the monitor circuit

3.3. SOFTWARE

The microprocessor is the brain of this system. Microprocessors receive digital information through addresses and data and process this information by program instructions stored in a memory unit. It produces a digital output according to the obtained data. Microprocessors are software-controlled circuit elements. As the software of this study is a performance-oriented project, Assembly language was used. Although it reveals the power of our assembly processor well, its footprint is low because it is close to machine language. Written programs run fast. Assembly codes were made in the Keil uVision5 program. The

microprocessor contains a large number of instructions, each action is performed as a result of a command. Assembly language also has an instruction set like other microcontrollers. First of all, a tag is defined in the assembly code, attention is paid to ensure that the defined tag is compatible with the subprogram we will write, each tag name must be different from each other. The "EQU" command is used to define the ports we entered in the AT89C51 and to make a fixed definition without occupying memory, and the "MOV" command is the install command. We use the "CALL" command to call subprograms. We can write the functions we use recursively in a sub-function and call this sub-function in the main program. The RET command is used to exit the subprogram. The unconditional jump instruction is “JMP”, conditional jump instruction is “DJNZ (Decrease, Jump If Not Zero)” “CJNE (Compare, Jump If Not Zero)”, “DPTR” 16-bit register DPH, DPL can also be accessed as 8-bit. “CLR” is used as 0 command and “SET” is used as 1 command. These commands are also the commands that make up our software. In this thesis, the software process has gone from the unit to the whole. Software test and integration plan, battery management system integration, and tests will be started after the tests of the following subsystems are completed as given in Figure 3.14.

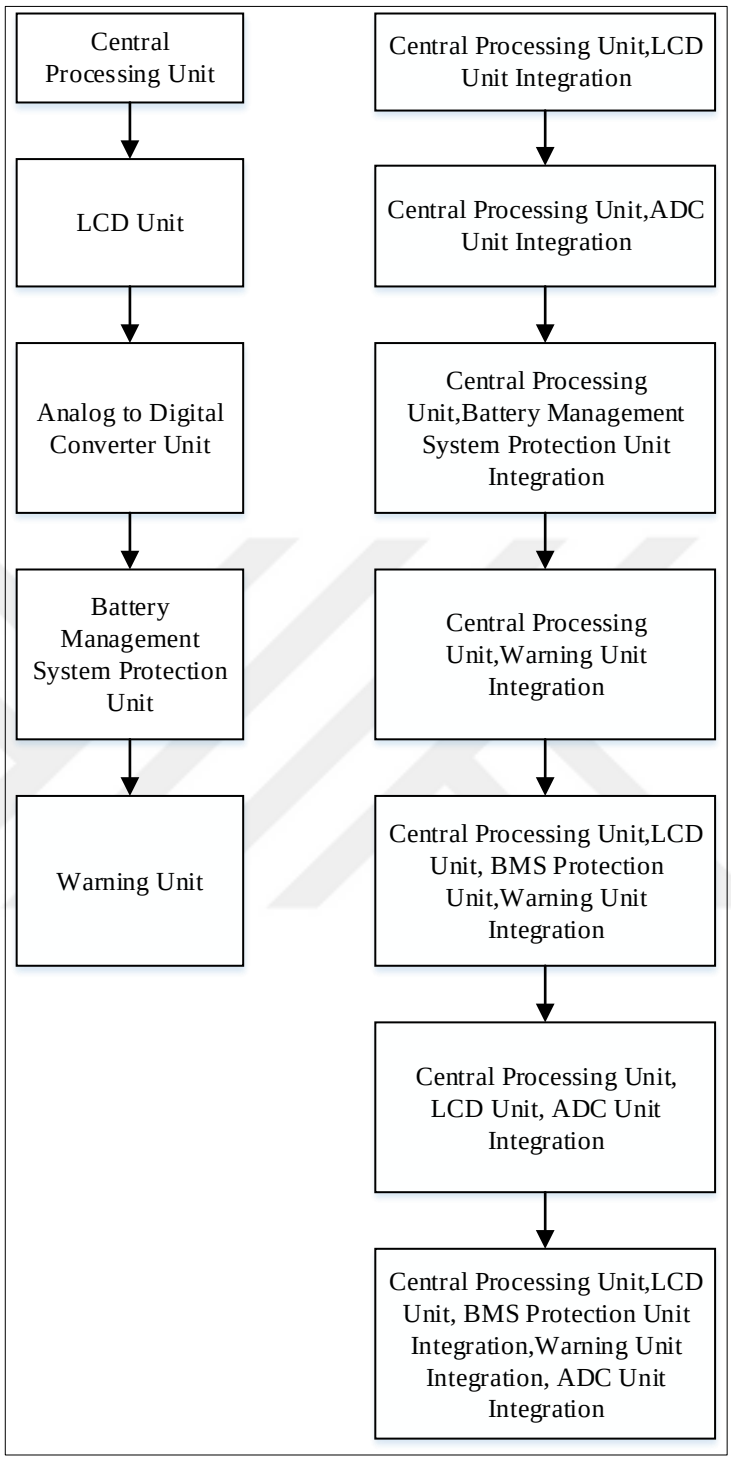

Figure 3.14. Software testing and integration sequence

3.3.1. Analog to Digital Converter (ADC) Software

In this circuit design as given in Figure 3.15, the following circuit is designed to test whether the code written for the analog to digital converter works correctly. There is a potentiometer (POT-HG) to adjust the circuit, this component is connected to the VIN+ input of the ADC. This circuit shows a voltage input ADC. It has two references, the reference and the signal to be measured. The output is an 8-bit digital output that is equal to the input value. The reference voltage is the maximum value that the ADC can convert. With the circuit below, 8-bit ADC values can be converted from 0 volts to reference voltages. This voltage range can be adjusted for 256 different values.

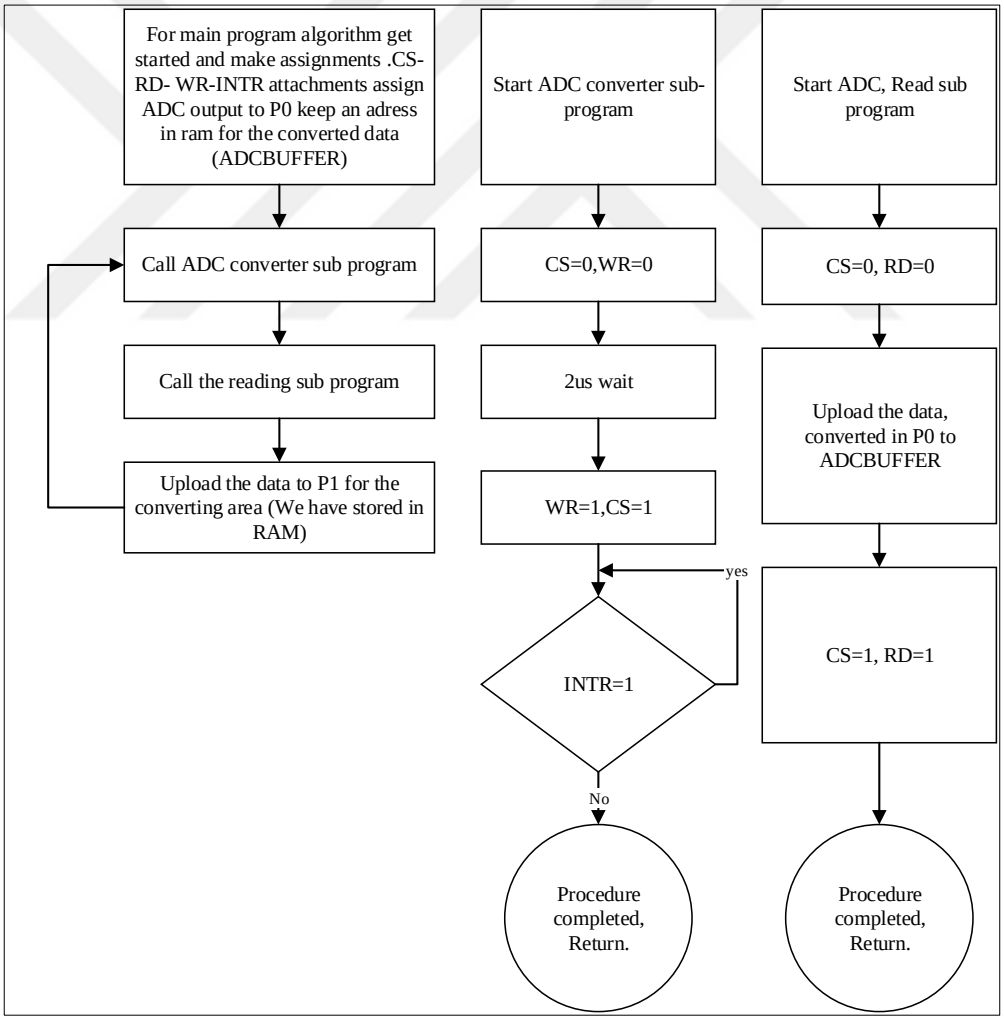

Figure 3.15. Software algorithm made for ADC

3.3.2. Control Circuit Software

The minimum voltage level of the battery pack uses the SRP – SRN resistor voltage to determine if it is in a discharged state with a minimum voltage level lower than VSTATE_D or a charge state greater than VSTATE_C max voltage has occurred. The State comparator uses it to turn on the CHG FET in fault conditions that require the CHG FET to be off, to prevent damage and overheating during discharge. The reverse of this is also true for the DSG FET used during charging, which requires having a DSG FET. The state comparator is used with the CHG and DSG FETs turned on in Normal mode during cell balancing to ensure that the cell balances only while the battery pack is charging. BQ77915 condition comparison conditions are given in Table 3.1.

Table 3.1. BMS state comparison conditions [62]

Mode	**CHG**	**DSG**	**DSG STATE COMP**
Normal Mode, No Cell Balancing	ON	ON	OFF
Normal Mode, Cell Balancing	ON	ON	$V_{STATE\_C\ DETECTION}$
UV, CTRD	ON	OFF	$V_{STATE\_C\ DETECTION}$
OV, UTC, OTC, CTRC	OFF	ON	$V_{STATE\_D\ DETECTION}$
OCD1, OCD2, SCD, OCC, UTD, OTD, OW	OFF	OFF	OFF

[1]

3.3.3. LCD (Liquid Crystal Display) Software and Test

It is very important to monitor the working status of the battery. This monitoring is achieved by displaying the battery status on a small display module. The LCD screen is a commonly used display module for this purpose. The 16x4 module is among the most widely used. The

[1] UV = UnderVoltage, CTRD = DSG Overridecontrol, OV = Overvoltage, UTC=Undertemperature During Charge, OTC = Overtemperature During Charge, CTRC = CHG Signal Override, OCD1 = Overcurrent1 During Discharge, OCD2 = Overcurrent During Discharge ,SCD = Short Circuit Discharge, OCC = Overcurrent During Discharge, UTD = Undertemperature During Discharge , OTD = Overtemperature During Discharge, OW = Open Wire (Cell to PCB disconnection)

LCD allows us to read the voltage of the battery, the SoC value as a percentage, and by reading the input from the screen in which mode it works such as charge, discharge, protection. It can be easily interfaced with an LCD microcontroller. It can be interfaced with a 4 bit or 8 bit LCD microcontroller. In order to activate the LCD, necessary circuit connections have been made in Proteus. VSS is connected to the ground so it is 0V. VDD power supply is +5V. RS means Register Select, RS=0 to select Command Register, RS=1 to select Data Register, R/W means to read and write, R/W=0 to write to the register, R/W=1 to read from is the register pin. In order to write and see a character or number, 8-bit ASCII data is sent to pins between D0 and D7, and control commands are sent to these pins. In our study, these pins were defined first.

3.4. SOFTWARE INTEGRATION INTO BATTERY MANAGEMENT SYSTEM

The software has been integrated into the designed Battery Management System in 3 steps. In the first step, the integration of the Central processing unit, LCD unit, BMS protection unit, and Warning unit is provided. In the second step, the Central Processing Unit, LCD Unit, and ADC unit integration are provided. In the third step, Central Processing Unit, LCD Unit, BMS Protection Unit Integration, Warning Unit Integration, ADC Unit Integration are completed.

3.4.1. Central Processing Unit, LCD Unit, Battery Management System Protection Unit, Warning Unit Integration

The modes transmitted from the inputs in the control circuit to the LCD screen will be combined with the control circuit software and LCD software in the form of messages and will be printed on the screen as given in Figure 3.16.

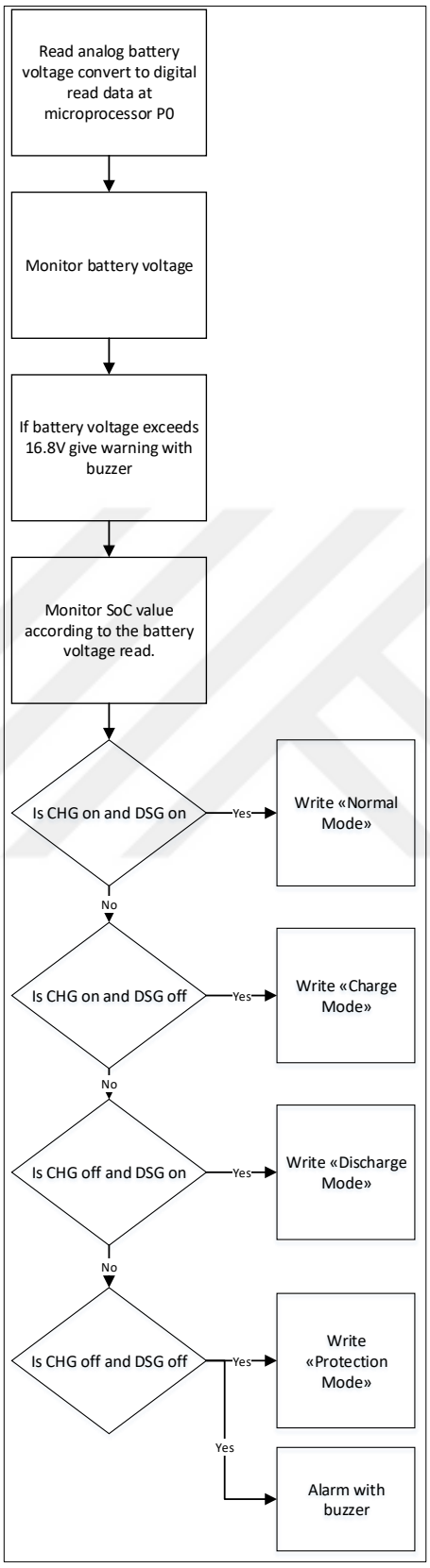

Figure 3.16. Central processing unit, LCD unit, BMS protection unit, warning unit algorithm

3.4.2. Central Processing Unit, LCD Unit, ADC Unit Integration

It simulates the POT-HG battery connected to the ADC VIN+. According to the percentage, we change, the State of Charge status is designed to be visible on the screen.

3.4.3. Central Processing Unit, LCD Unit, Battery Management System (BMS) Protection Unit Integration, Warning Unit Integration, ADC Unit Integration

At this stage, our GUI design for the LCD screen is now finalized. According to the data coming from the control circuit of the battery, the status of the system, how many volts the battery is, and the SoC status respectively is printed on the screen. The point to be considered here is that when the data comes from the CHG and DSG inputs, it does not read any SoC values. While determining the range of SoC values, an estimated and most accurate value table was created for the LG HG2 cell. It is necessary to read 255 values from the ADC converter. The expression 4S is written to express 4 Lithium-Ion Cells. The values we exemplified from the ADC circuit in Table 3.2 were written as binary and the percentage value was calculated.

Table 3.2. Calculation of OCV value and corresponding SoC percent value

OCV	SOC	4S	SAMPLED ADC VALUE	BINARY
4,197	100	16,8	5,01V	#11111111
4,094	90	16,4	4,9V	#11111010
4,021	80	16	4,8V	#11110101
3,908	70	15,6	4,65V	#11101101
3,814	60	15,3	4,55V	#11101000
3,715	50	14,9	4,45V	#11100011
3,643	40	14,6	4,35V	#11011110
3,583	30	14,3	4,25V	#11011001
3,502	20	14	4,2V	#11010110
3,363	10	13,5	4V	#11001100
3,071	0	12,3	3,65V	#10111010

3.5. BATTERY MANAGEMENT SYSTEM AND STATE OF CHARGE

SoC estimation, defined as capacity in lithium-ion batteries, is one of the most important tasks of BMS. It has an important role in controlling the system in charge and discharge situations and evaluating its performance and efficiency. There have been many studies in the literature on SoC estimation. Methods based on artificial intelligence algorithms such as neural networks and fuzzy logic algorithms depend on the accuracy of the learning data. Other methods are calculated by integrating current, known as coulomb counting, and measuring the open-circuit voltage when the circuit is open and not connected to the load. Sensor performance is important in the ampere-hour counting method and an accurate SoC value is required. However, the disadvantage of this method is that it is an open-loop estimation and has a large accumulation of errors [35]. OCV is known to be a good method to accurately predict SoC. In theory, if the OCV values are correctly estimated, the SoC value is also correctly estimated [31]. The accuracy of these methods is linked to the accuracy of the model. The use of model-based methods for SoC estimation is increasing, and understanding the behavior of the battery when tested with an equivalent battery model is of great importance [36]. The linearization parameter in the measurement equation is updated according to the current value of the state variables in the equivalent circuit model, and a standard Extended Kalman filter is used to estimate the SoC according to the linearized value [37].

3.5.1. Battery Modeling

When the literature on modeling the behavior of lithium-ion batteries was reviewed, it was found that different models were created and used. Model types are divided into Electrochemical models, Electrical models, Thermal models, Mechanical/Fatigue models, Interdisciplinary models. It is very important that the designed BMS system is based on a working battery model to calculate battery states and properties efficiently and accurately. Accurate identification of the electrical components of the battery model requires a mathematical second-order the Thevenin model, the ohmic and concentration polarization of the battery can be represented. In fact, a third polarization effect has to be applied, the activation polarization related to chemical reactions on the electrode surface. To implement

this, the second-order ECM Dual Polarization Model shown in Figure 3.17 was used in this thesis [38]. This model describes a voltage source R_{int} internal resistnce (Ω wch defines open circuit voltahe, R_{pa} the activation resistance between the capacitor C_{pa} *(Ω)*, R_{pc} the concentration resistance with the capacitor C_{pc} (Ω), C_{pa} (F), C_{pc}(F), I_{pa} capacitor C_{pa} current (A) I_{pc} capacitor C_{pc} current (A) I_{bat} Battery current (A), U_{OC} Open Circuit Voltage (V), U_{pa} Voltage across the capacitor C_{pa} (V) , U_{pc} Voltage across the capacitor C_{pc},(V), U_{bat} Voltage across the terminals of the battery (V) is used.

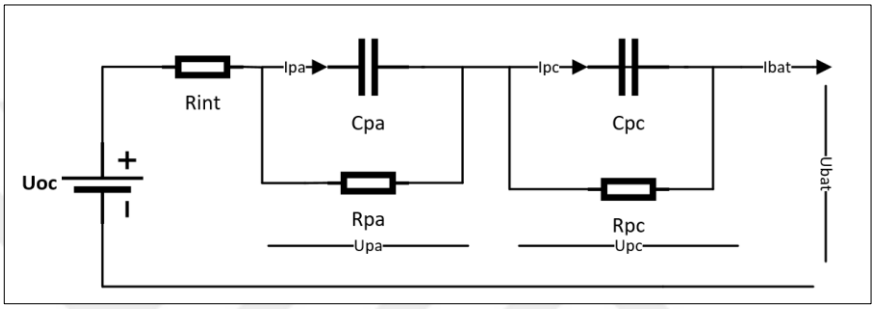

Figure 3.17. Dual polarization model [38]

3.5.2. Measuring Open Circuit Voltage

The correct interpretation of the non-linear relationship between the open-circuit voltage (OCV) and the state of charge (SoC) is required for the SoC estimation of the Li-ion battery. In this thesis, the equivalent circuit Lithium-ion battery charge and discharge voltages and currents of the battery used are combined and the measurement method of the open-circuit voltage is given [39].

3.5.2.1. Identifying the INA238 Sensor

Since each battery system has its own OCV graph, the open-circuit voltage was measured by charge and discharge tests. As shown in Figure 3.18, charge and discharge tests INA238 sensor was used. This sensor works with 2.7V to 5.5V supply but can measure high voltage and current up to 85V. Current is measured by sensing the voltage drop across the shunt resistor at the IN+ and IN- pins. The common-mode voltage range on the input pins is -0.3V to +85V, also suitable for high and low current measurements. This device can also measure the supply voltage via the V_{BUS} pin and the temperature via the temperature sensor integrated into the system. The differential shunt voltage is measured between IN+ and IN- pins. Monitored temperatures can range from -40 ºC to +125 ºC. The INA238 EVM can be

connected to a computer with a USB cable. It provides GUI support to read and write the records of the device, view and save these results. V_{BUS}, V_{SHUNT}, Power, Current, and Temperature data can be recorded and graphic data can be followed instantly.

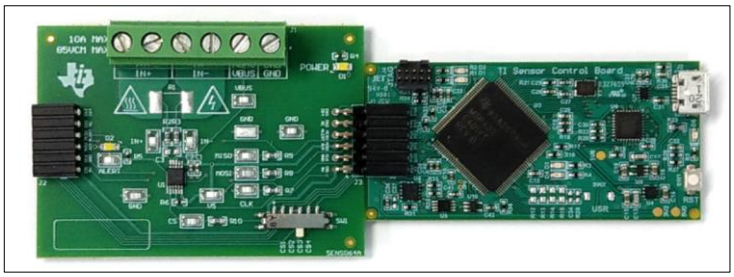

Figure 3.18. EVM (left) connected to SCB controller (right) [41]

3.5.2.2. Connecting the INA238 Sensor to the Battery

It provides accurate monitoring of currents such as the INA238's low offset voltage and low input bias current. To monitor the measured current values with high resolution, the shunt resistor value should be selected so that the sense voltage is within the maximum differential input voltage range specified in the specs. The resistance value selected here is 10mΩ and it is installed on the kit. For other connections on the kit, the +IN input given in Figure 3.19 is connected to the + of the battery, and the -IN input is connected to the load or power supply.

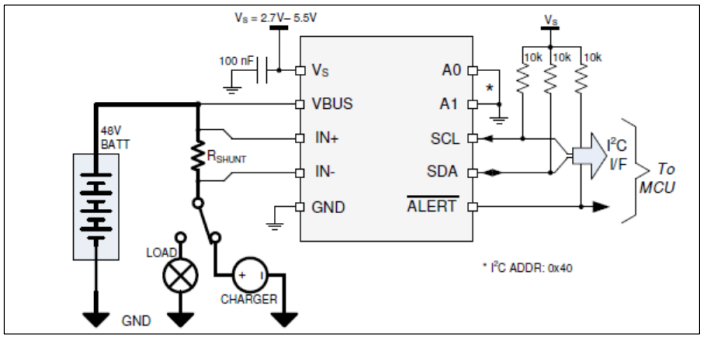

Figure 3.19. INA238 high-side sensing application diagram [40]

The Li-ion BMS circuit shown in Figure 3.20 a is attached to the LG HG2 battery to perform the charge and discharge tests in a controlled manner. To control the opening and closing with a key switched system, a battery connection apparatus is attached. The correct operation of the system with the charged one in Figure 3.20 b was checked with a voltmeter. After the requisite procedures were completed, a battery was inserted into the INA238 kit shown in figure 3.20 c.

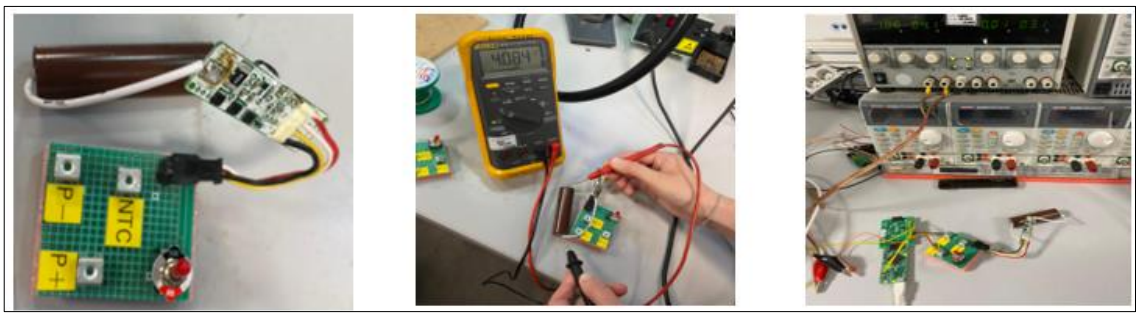

(a) (b) (c)

Figure 3.20. Connecting the battery to the INA238 sensor. (a) Inserting the battery into the battery connector (b) Checking the voltage with the connector (c) Installing the battery in the INA238 EVM kit

3.5.2.3. Connecting the Sensor to the Computer

For the GUI included in the kit to work correctly, the latest version file is installed and run on the computer from the Texas Instruments website. The EVM/SCB Controller Unit is plugged into the computer and the GUI connection is run. After various configuration settings shown in Figure 3.21 are completed, the interface is entered.

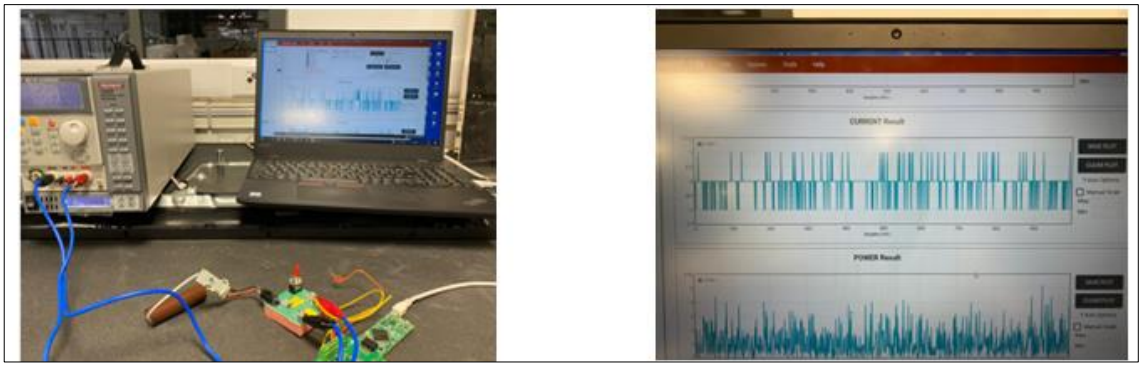

(a) (b)

Figure 3.21. INA238 sensor computer connection (a) Introduction to INA238 EVM result data sheet (b) Current and voltage display

3.5.2.4. Charge and Discharge Test for OCV Measurement with INA238 EVM

The battery was charged before starting the measurement. The measurement settings of the INA238 EVM kit are set to receive data per second as 60000 ms, and the number of samples to be 1000, as indicated in Figure 4.22. Before the battery discharge test, the starting voltage was measured as 4.090 when fully charged, and a discharge test was applied up to 1.5A and

2.347V at constant current. A 1.5A charge test was applied to the battery with 3.125V, and when it reached 4.028V, the charge test was terminated, and charge and discharge graphs were drawn according to the recorded values.

3.5.3. Internal Resistance Calculation

Li-ion batteries have an advantage over other types of batteries with their high energy density and high charge or discharge rate [20]. If we take the battery to charge and discharge tests for a certain period with the changing current in the charging and discharging process, there may be situations that will cause balance problems on the battery. This causes the internal resistance of the battery system to increase and the capacity to decrease on the battery. This situation significantly affects the performance of the BMS system and is one of the important factors that causes the SOH state of the battery, that is, the reduction of its lifespan. If the model works correctly, the SoC prediction is likely to be correct as well [20]. In Table 4.3, as a function of parameters such as current, temperature, and SoC, the measurement of internal resistance is made with different current values and the effect of these values on the internal resistance and the capacity of the battery is studied. It can be determined by estimating V_{OC} by the internal resistance method and calculated from the equation $V_{OC} = V_t + IR.V_{OC}$ is the open-circuit voltage, in other words, the EMF of the battery. V_t is the terminal voltage. *I* is discharge/charge current, *R* is the internal resistance of the battery [42]. During the charging and discharging processes of the battery, the current for the terminal voltage of the battery was measured and recorded in each period. In Equation 3.1, *V* is the voltage on the battery when current is supplied to the load. *I.R* is the voltage equality value transmitted from the device.

$$V = I.R_{eq} + I.R \tag{3.1}$$

3.5.4. Dual Polarization Model Parameter Calculation

The discharges and charge process has been done and this process corresponds to a full charge and discharges cycle. Necessary calculations were made according to the graphs obtained according to the OCV value and the discharge and charge status of the cell. The

R_{int} value was taken as 0.111Ω, corresponding to 10A, from Table 4.3, the internal resistance value measured at different currents. By applying the "the corresponding model-fitting coefficients" method mentioned in [45], the logarithmic Ln value of the voltage values recorded during the discharge process was taken and the regression analysis was performed. According to [46], the initial value of V_{OCV} should be taken.

3.5.5. Extended Kalman Filter and Battery Management System

SoC state estimation is of great importance for the safe operation of lithium-ion batteries and the BMS designed for these batteries. Increasing the accuracy of these prediction results and reducing the algorithm and computational complexity is important for the accuracy of the result. In this thesis, the equivalent circuit model shown in Figure 3.17 is used to simulate the dynamic behavior of the Li-ion battery, where it updates the linearization parameter of the state variables, and then Extended Kalman Filter is used to accurately predict the SoC based on linearization. The studied Extended Kalman Filter for SoC estimation compares the measured cell voltage with the cell model predicted by the battery model. The model also predicts the state of the SoC, which cannot be measured directly. In the second step, it corrects the measurement and model prediction considering their accuracy and a more accurate and corrected prediction value is obtained for the SoC. Figure 3.22 shows the Battery Management System and Extended Kalman Filter relationship.

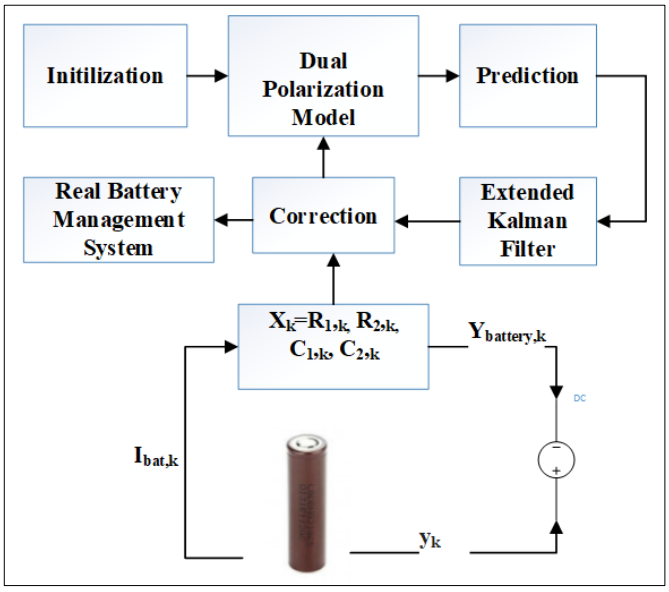

Figure 3.22. Battery management system and Extended Kalman Filter relationship [12]

The Extended Kalman filter is used when trying to predict the state x ∈ R^n of a discrete time-controlled process administered by a linear differential equation. However, the measurement regarding the process or time to be estimated is not linear. We can linearize the estimate close to the current estimate using partial derivatives of the process and measurement functions to calculate estimates against nonlinear measurements similar to the Taylor series [47]. The standard Extended Kalman filter is the estimation method used in linear dynamical systems. However, the system here is nonlinear due to the SoC OCV relationship, so the Extended Kalman filter adapted to the nonlinear system is used for the SoC estimation. Similar to the standard Kalman filter, the Extended Kalman Filter linearizes nonlinear battery systems with the system space model, and then an optimal estimation of the state variables is made using the iterative process of the Extended Kalman filter [51]. Figure 3.23 shows the Extended Kalman Filter Working Flow Chart.

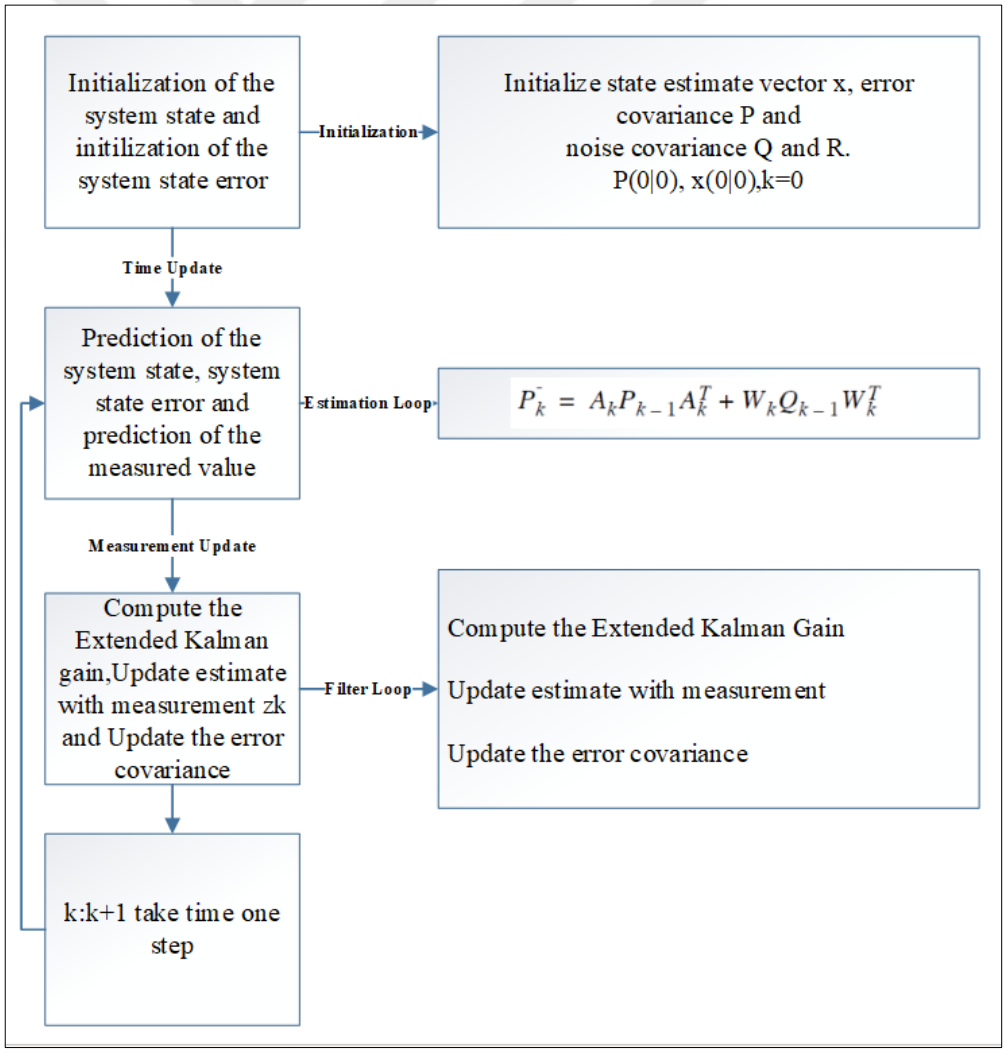

Figure 3.23. Extended Kalman Filter working flow chart

When the current is zero, the OCV (Open circuit voltage) U_{OC} value will be read in the battery. The voltage at the battery terminals is defined as *V*. There is also a nonlinear connection between U_{OC} and SoC. From this relationship, the polynomial functions can be modeled and the coefficients can be found with the curve fitting technique [48]. According to the circuit diagram shown in Figure 3.17, the equations are as follows according to reference [38]:

$$U_{pa} = \frac{-U_{pa}}{R_{pa}.C_{pa}} + \frac{I_L}{C_{pa}} \tag{3.2}$$

$$U_{pc} = \frac{-U_{pc}}{R_{pc}.C_{pc}} + \frac{I_L}{C_{pc}} \tag{3.2}$$

$$U_L = U_{OC} - U_{pa} - U_{pc} - I_L R_0 \tag{3.3}$$

To create a system state space based model, U_{pa} for the voltage drop across the capacitor C_{pa}, U_{pc} and SoC for the voltage drop over the capacitor C_{pc} are considered. The circuit in Figure 3.17 can be modeled with the following equation:

$$U_{bat} = U_{OC} - U_{pa} - U_{pc} - I_{bat}. R_{int} \tag{3.5}$$

If we apply Kirchoff's Law used in reference [48-49] for the battery electrical equivalent model:

$$I = \frac{U_{pa}}{R_{pa}} + C_{pa}\frac{\partial U_{pa}}{\partial t} = \frac{U_{pc}}{R_{pc}} + C_{pc}\frac{\partial U_{pc}}{\partial t} \tag{3.6}$$

$$\dot{U}_{pa}(t) = \frac{U_{pa}(t)}{R_{pa}.C_{pa}} + \frac{I(t)}{C_{pa}} \tag{3.7}$$

$$\dot{U}_{pc}(t) = -\frac{U_{pc}(t)}{R_{pc}.C_{pc}} + \frac{I(t)}{C_{pc}} \quad (3.8)$$

The simplest way to model a battery is to model terminal voltage *V* as the voltage drop of OCV minus internal resistance *R*. When current is drawn, the value read in reference [50] is given in Equation 3.9.

$$V = OCV - I.R \quad (3.9)$$

RMS error is mentioned in [50], and the R value in Equation 3.10 changes according to the state of charge of the battery. Therefore, this change is modeled with a sound. The nominal value of the battery should be calculated and its value will be followed by the Extended Kalman filter. V is the voltage between the terminals and must be measured continuously with a certain error. This model can be improved by adding a constant *C*.

$$V = OCV - I.R + C \quad (3.10)$$

To improve the estimation accuracy, Extended Kalman Filter approach has been tried to be solved. Since SoC and *R* cannot be measured directly, they are chosen as the model for the state space [48]. The state space model $x(k) = [SoC(k)\ R(k),\ U_{pa}(k), U_{pc}(k)]^T$ is defined as follows:

$$\dot{x} = \begin{bmatrix} 0 & 0 & 0 & 0 \\ 0 & 0 & 0 & 0 \\ 0 & 0 & \frac{-1}{R_{pa}.C_{pa}} & 0 \\ 0 & 0 & 0 & \frac{-1}{R_{pc}.C_{pc}} \end{bmatrix} x + \begin{bmatrix} \frac{-1}{Q_{max}} \\ 0 \\ \frac{1}{C_{pa}} \\ \frac{1}{C_{pc}} \end{bmatrix} i + \begin{bmatrix} w_1 \\ w_2 \\ w_3 \\ w_4 \end{bmatrix} \quad (3.11)$$

The Discrete State Space Model is defined as a matrix as follows. ΔT is the sampling frequency [48].

$$x(k+1)=\begin{bmatrix}1 & 0 & 0 & 0\\ 0 & 1 & 0 & 0\\ 0 & 0 & 1-\frac{\Delta T}{R_{pa}.C_{pa}} & 0\\ 0 & 0 & 0 & 1-\frac{\Delta T}{R_{pc}.C_{pc}}\end{bmatrix}x_k+\begin{bmatrix}\frac{-\Delta T}{Q_{max}}\\ 0\\ \frac{\Delta T}{C_{pa}}\\ \frac{\Delta T}{C_{pc}}\end{bmatrix}i+\begin{bmatrix}w_1\\ w_2\\ w_3\\ w_4\end{bmatrix}\Delta T \quad (3.12)$$

Our state space include *x(k)= [SoC(k) R(k),* $U_{pa}(k)$*,*$U_{pc}(k)]^T$

The *R* value changes according to the state of charge of the battery. This change is modeled by sound. The nominal value of the battery should be calculated and followed by the filter. The voltage between the *V* terminals will be measured with a certain error.

State update equations:

$$SOC(k+1)=SOC(k)-I(k)*\frac{\Delta T}{Q_{max}}+w_1 \quad (3.13)$$

$$R(k+1)=R(k)+w_2 \quad (3.14)$$

$$U_{pa}(k+1)=\left(1-\frac{\Delta T}{C_{pa}\cdot R_{pa}}\right)U_{pa}(k)+I(k)\Delta T/C_{pa}+w_3 \quad (3.15)$$

$$U_{pc}(k+1)=\left(1-\frac{\Delta T}{C_{pc}\cdot R_{pc}}\right)U_{pc}(k)+I(k)\Delta T/C_{pc}+w_4 \quad (3.16)$$

Measurement Equation:

$$V(k)=OCV\big(SOC(k)\big)-I(k)*R(k)-U_{pa}-U_{pc}+v \quad (3.17)$$

w_k and v_k in the equation are defined as process and measurement noise, and these independent variables are assumed to have white and normal probability distributions. The state vector is expressed as $x(k)= [SoC(k)\ R(k),\ U_{pa}(k),U_{pc}(k)]^T$. Here, let's assume that the process has a state vector $X \in R_n$, but the process is computed by the nonlinear difference equation $x_k = f(x_k - 1, u_k - 1, w_k - 1)$ with measurement $z \in R_m$, $z_k = h(x_k, v_k)$ The f function relates the state of the k-1 time step which is one step ago to the current time state k. Any driving functions include $u_k - 1$ and zero mean noise w_k as parameters. The nonlinear function h in the measurement equation relates the state x_k to the measurement z_k. x_k and z_k are real state and measurement vectors. In reality it is difficult to know separately the w_k and v_k noise at each time step, the state and measurement vector can be approximately estimated without considering them [47].

$$z(k) = V(k) \tag{3.18}$$

$$h\big(x(k)\big) = OCV\big(SOC(k)\big) - I(k) * R(k) - U_{pa}(k) - U_{pc}(k) \tag{3.19}$$

Since OCV and SoC nonlinear relation, we use Extended Kalman Filter and take the local derivative for the measurement equation.

H is defined in [47] as the Jacobian matrix of partial derivatives of h with respect to x.

$$H\,[i,j] = \frac{\partial h[i]}{\partial x[j]}(\dot{x},0) \tag{3.20}$$

$$H(k) = \frac{\partial h(x(k))}{\partial x}\Big|_{x(k)=x(k+1|k)} = \left[\frac{\partial OCV(SOC(k))}{\partial SOC}\Big|_{SOC(k)=SOC(k+1|k)} \quad -I(k) \quad -1 \quad -1\right] \tag{3.21}$$

Here, $x(k) \in R^{1\times4}$ represents the state variables, and $h(x(k))$ represents the SoC –OCV nonlinear relationship. To find the $H \in R^{1\times4}$ matrix, the experimentally found OCV-SoC graph will be locally derived.

$$SOC(k+1|k) = SOC(k|k) - I(k) * \frac{\Delta T}{Q_{max}} \quad (3.22)$$

$$R(k+1|k) = R(k|k) \quad (3.23)$$

$$U_{pa}(k+1|k) = \left(1 - \frac{\Delta T}{C_{pa} \cdot R_{pa}}\right) U_{pa}(k) + I(k)\Delta T / C_{pa} \quad (3.24)$$

$$U_{pc}(k+1|k) = \left(1 - \frac{\Delta T}{C_{pc} \cdot R_{pc}}\right) U_{pc}(k) + I(k)\Delta T / C_{pc} \quad (3.25)$$

$$F(k) = \begin{bmatrix} 1 & 0 & 0 & 0 \\ 0 & 1 & 0 & 0 \\ 0 & 0 & 1 - \frac{\Delta T}{C_{pa} \cdot R_{pa}} & 0 \\ 0 & 0 & 0 & 1 - \frac{\Delta T}{C_{pc} \cdot R_{pc}} \end{bmatrix} \quad (3.26)$$

If the error covergence $P_k^- = AP_{k-1}A^T + Q$ equation is applied:

$$P(k+1|k) = F(k)P(k|k)F(k)^T + Q(k) \quad (3.27)$$

Compute the Kalman Gain formula is represented as $K_k = P_k^- H^T (HP_k^- H^T + R)^{-1}$

$$K(k+1) = P(k+1|k)H^T(k+1)[H(k+1)P(k+1|k)H^T(k+1) + R(k+1)]^{-1} \quad (3.28)$$

Update estimate with measurement z_k , $\hat{x}_k = \hat{x}_k^-(z_k - H\hat{x}_k^-)$

$$(k+1|k+1) = x(k+1|k) + K(k+1)[z(k+1) - h(x(k+1|k))] \quad (3.29)$$

$$x(k+1|k+1) = x(k+1|k) + K(k+1)[V(k+1) - OCV\big(SOC(k|k)\big) + I(k) * R(k+1|k) + Upa(k+1|k) + Upc(k+1|k)] \quad (3.30)$$

Update the error covariance $P_k = (I - K_k H)P_k^-$

$$P(k+1|k+1) = [I - K(k+1)H(k+1)]P(k+1|k) \quad (3.31)$$

Equation 3.32 shows the process uncertainties. The most appropriate value can be selected by first giving large values to these parameters and then making experiments by reducing them.

$$Q = \begin{bmatrix} \sigma_1^2 & 0 & 0 & 0 \\ 0 & \sigma_2^2 & 0 & 0 \\ 0 & 0 & \sigma_3^2 & 0 \\ 0 & 0 & 0 & \sigma_4^2 \end{bmatrix} \quad (3.32)$$

3.5.6. State of Charge (SoC) Estimation with Extended Kalman Filter

The plotted OCV curve takes the open-circuit voltage estimated by the Extended Kalman filter as input and is used as an output in the function equation that gives the state of charge of the battery according to that voltage value. The Extended Kalman Filter developed for SoC estimation compares the measured cell voltage with the cell voltage value predicted by the cell model specified in Figure 3.16. The Extended Kalman filter provides an adjusted estimate for the SoC, taking into account the measurement and model prediction accuracies. There is no model available that explicitly reflects the real situation [25]. To integrate the model parameters into the Extended Kalman Filter cycle, the battery is charged 4A and discharged with 10A.

3.5.6.1. Procuring Required Data

One of the most used and easy methods to estimate the SoC of a battery is the Coulomb counting method [52]. It is important to measure and integrate the measured current and voltage value. To follow this situation, firstly, the graphics of the pulsed discharge and charging processes were drawn from the Cadex Battery tester. Resting, Charge, Resting, Discharge, Aborted were performed in 5 different orders. It took 20 days, 23 hours, and 23 minutes to conclude the test. The charge rate is 4A, the discharge rate is 10A, Battery Rating (Ah) is 3A. Figures 3.24 and 3.25 show programming details on the Cadex battery tester.

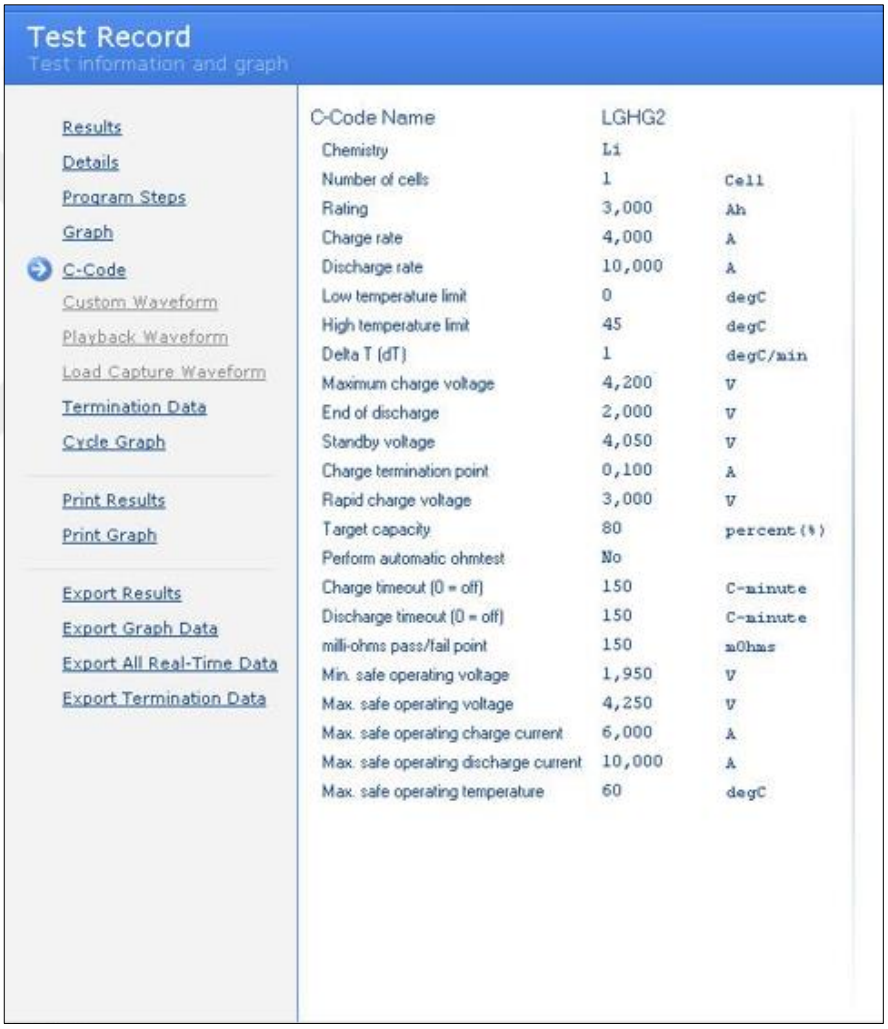

Figure 3.24. C code for pulse charge and discharge test

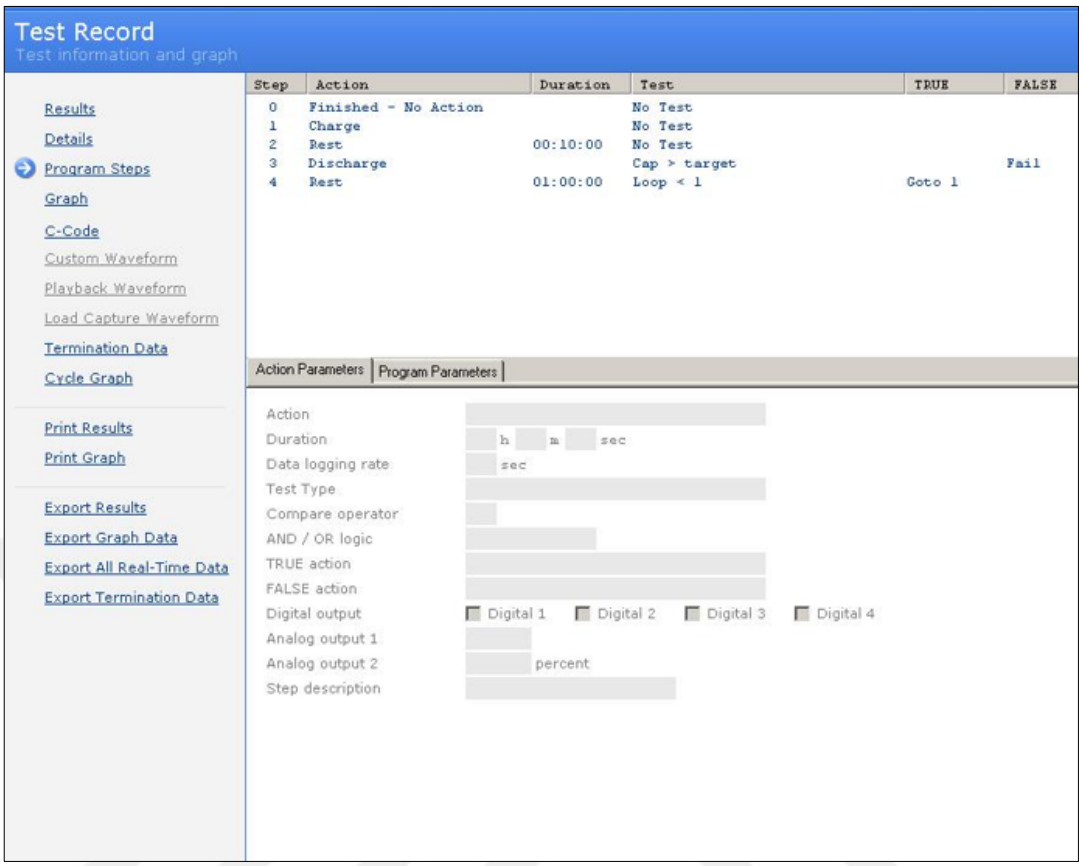

Figure 3.25. Programming steps

3.5.6.2. Subtracting Equations and Following Up with Extended Kalman Filter

Since the R_{int} value, which is found according to the values recorded in milliseconds with the INA238 sensor, varies according to the temperature during this discharge process, it has been calculated experimentally and its changes with R_{int},U_{pa} ve U_{pc} Extended Kalman Filter will be followed up with the Extended Kalman filter. R_{int},R_s,R_p,C_p,C_1,C_2,R_1, R_2 values were calculated according to [46] according to the values obtained as a result of the experiments as shown in Table 4.3. The Rint value found was used as the initial value of the state variable defined for Kalman. The nonlinear correlation between OCV and SoC is experimentally shown in Figures 4.25 and 4.28. This relation is modeled by polynomial fit and the polynomial coefficients are found.

The value read when the current is drawn can be calculated with Equation 3.9. Since an experiment based on Coulomb Counting is performed, the SoC value will decrease from the current-clock capacity depending on the amount of current drawn depending on the current. Since the *R* value will change according to the state of charge of the battery, it is modeled

with a noise. This value will be calculated experimentally and followed by Extended Kalman Filter. The voltage between the terminals will also be measured continuously, including the sensor error. It is assumed that the current value is initially measured without error. An Extended Kalman Filter is defined for this model. *x(k)*$\in R^{4\times1}$ shows the state variables, and *h(x(k))* shows the nonlinear relationship between SoC and OCV. To find the $H \in R^{1\times4}$ matrix, the experimentally found OCV-SoC graph will be locally derived. If the changes are close to each other, the filter will have worked correctly. The covariance matrix progresses over time, and process noise is added accordingly. The filter cycle is defined in Equation 3.22. $K \in R^{4\times1}$ shows the Extended Kalman gain matrix. $R \in R^{1\times1}$ is modeling measurement noise. The values required to run the filter are given.

With the filter cycle, the SoC estimates are updated by advancing the filter over time. In Figure 3.26, we can say that the Extended Kalman Filter algorithm is a closed loop based on the feedback mechanism. In this model, the SoC value can be adjusted dynamically according to the error between the voltage values of the battery model and the estimated voltage values from the battery model. The SoC value and current are fed back from the battery model to be able to read a new predicted battery voltage value.

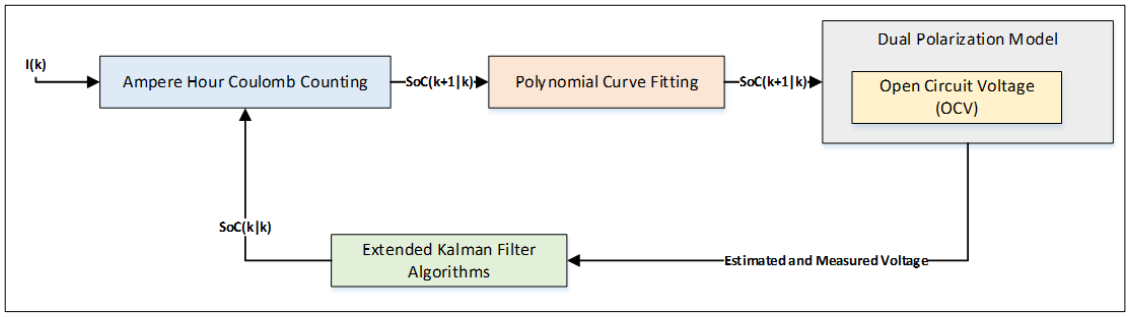

Figure 3.26. Battery model and Extended Kalman Filter flow chart [61]

In Figure 3.27, OCV values were recorded with the INA238 sensor after the charging and discharging processes. Model parameters were calculated according to the OCV graph. Along with the OCV method, 4A charge was discharged with 10A with the Coulomb Counting Method and the voltage values that changed along with the current value were also recorded. These values are input values for the Extended Kalman Filter design. The state vector is defined and error covariance P, noise covariance Q, and R are defined. Parameters have been updated according to equations between Equation 3.2 - 3.32 and Extended Kalman

Filter matrices have been calculated, the flow has been completed with estimation and validation.

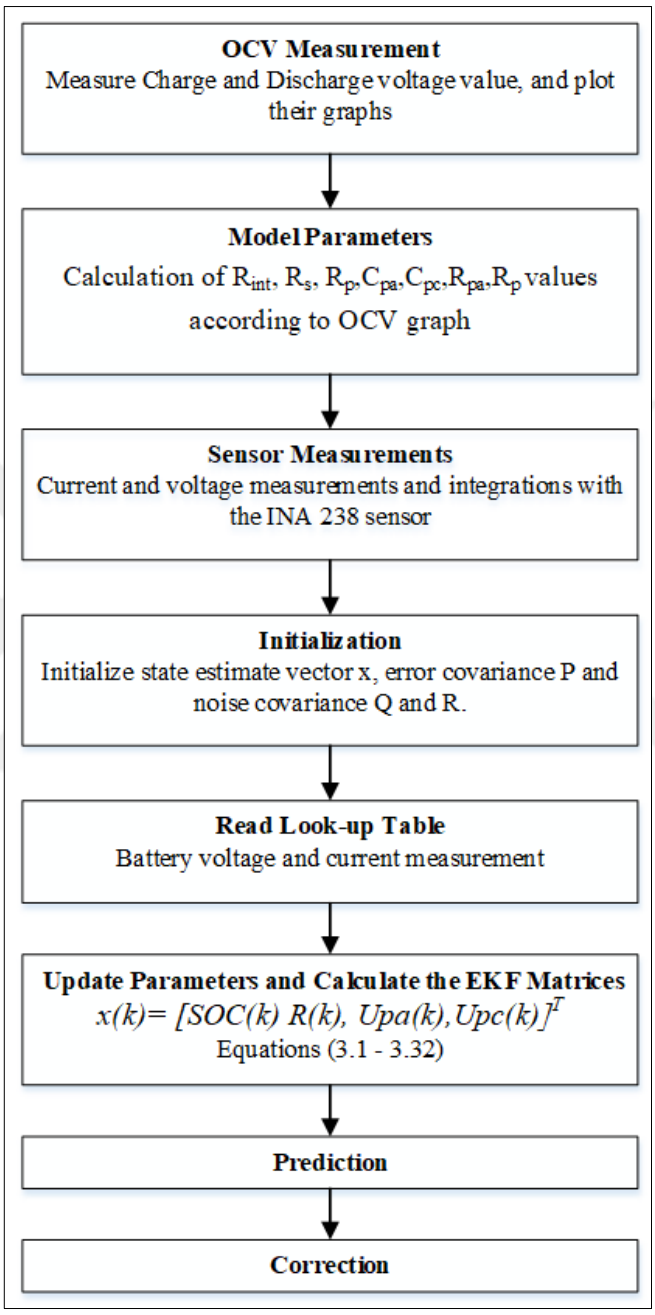

Figure 3.27. SoC estimation of Lithium-ion battery with Extended Kalman Filter

4. EXPERIMENTS AND RESULTS

The charge and discharge graphs of the lithium-ion battery are drawn experimentally. The software and hardware design integration for the BMS card has been tested.

4.1. CHARGE AND DISCHARGE GRAPHS OF LI-ION BATTERY

The battery is charged with 1C. When the battery voltage reaches 4.195 V, the connection is disconnected. The charge curve is shown in Figure 4.1. Over time, the voltage has increased and when it reaches 4.15V, the Cadex battery device disconnects, this voltage will remain stable for a while after reaching 4.194. The maximum current value of 3A, which is kept constant in this average time, starts to decrease after the battery is charged and tends towards zero (0.053A end- 0.050A input to the device). The period when the current is constant and the voltage rises from the minimum value to the maximum value is called constant current charge, when the voltage is constant, it corresponds to 4.194 V, and the period when the current tries to decrease to 0 is called constant voltage charge [47].

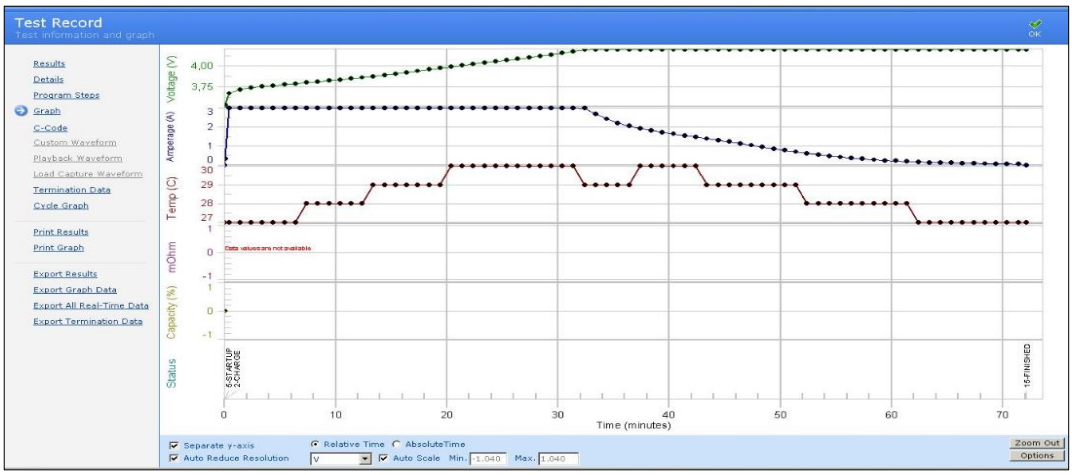

Figure 4.1. Charge graph

The battery was discharged by 1C. The connection is disconnected when the battery voltage reaches 2.108V. The discharge curve is shown in Figure 4.2. Over time the voltage has decreased and when it reaches 2.1 V the Cadex battery device disconnects. It dropped from 4.187V to 2.1V in 60 minutes. The battery is not completely discharged. The end of

discharge written in Cadex is 2V, the end voltage of the discharge is 2.108V. The current constantly draws 3A.

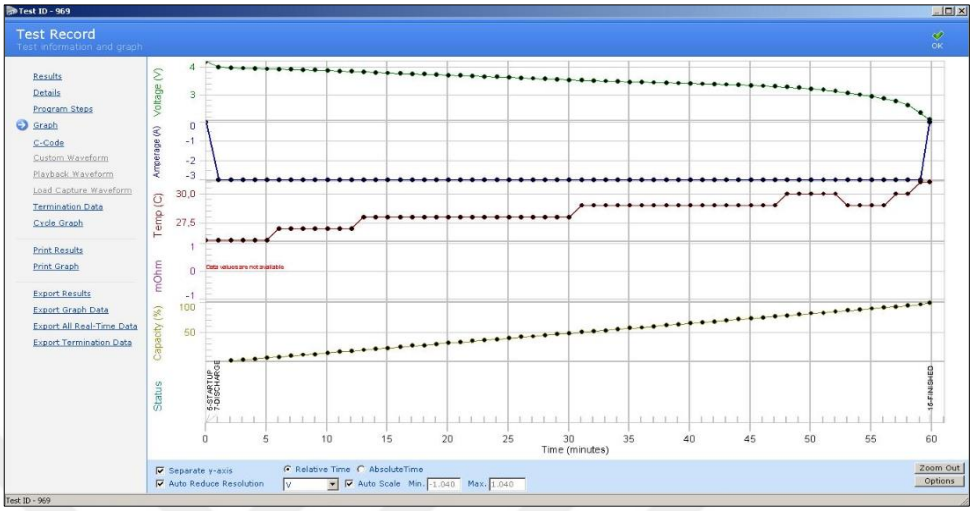

Figure 4.2. Discharge graph

As a result of repeated tests, the battery initially started with 3.53V as seen in Figure 4.2 and was charged up to 4.2V in 1 hour and 12 minutes. The battery was discharged at 3A from 4.19V to 2.1V for 1 hour. Summary values are given in data Table 4.1.

Table 4.1. Charge-discharge summary data table

	Current (A)	***Voltage (V)***	***V_0***	***V_final***	***Duration(ss:dd)***	***T_max***
Charge	3A	4.2V	3.53V	4.2V	01:12	30
Discharge	3A	2V	4.19V	2.1V	01:00	31

4.2. TESTING ANALOG TO DIGITAL CONVERTER (ADC) SOFTWARE

In this thesis, the software has been created so that the ADC can perform its functions, and the software has been integrated into the AT89C51 in the circuit diagram drawn in Proteus and it has been verified that it works. Blue lit LEDs represent "0" status, and unlit LEDs indicate "1" status. Based on the percentage value it receives from the VIN+ input, an 8-bit value is obtained, that is, 0 percent has the value #00000000. If we take another value for example multiplexing; For example, 50 percent is found as #10000000, 35 percent is

#011011001, 70 percent is #10110011. Value reading is performed from bottom to top. In Figure 4.3 and 4.4 given that 0 percent, 50 percent, 35 percent and 70 percent binary values.

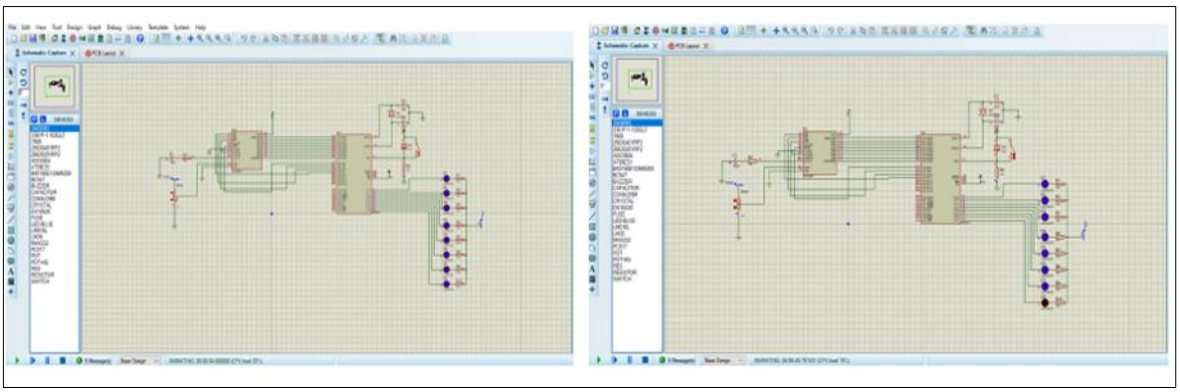

Figure 4.3. Finding 0 percent and 50 percent binary value from Proteus

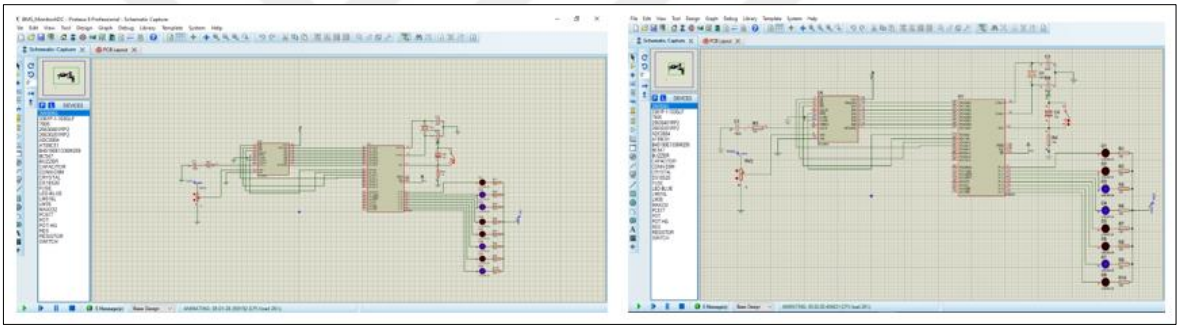

Figure 4.4. Finding 35 percent and 70 percent binary value from Proteus

4.3. TESTING THE CONTROL CIRCUIT SOFTWARE

According to the conditions given in Table 4.2, a circuit consisting of three LED lights was used to check whether the software made in Proteus runs the system correctly. The CHG and DSG inputs are pin inputs to read the inputs from the control circuit, and the buzzer warning system and leads to control the charge and discharge status. Condition checks were made with CHG and DSG commands in the defined main function. “is CHG 1, if 1 goes to X1”, “No, CHG is 0. Is DSG 1? If yes, go to X2”, “CHG=0, DSG=0 status is realized accordingly buzzer ON”, “CHG 0, DSG 1 status is realized”, “So led1 ON”, “If DSG is 1 then go to X3”, “CHG=1 DSG=0 condition is fulfilled. In this case, led2 ON”, “CHG=1 DSG=1 status is realized. Led3 ON” defined software was made.

Table 4.2. Conditions for testing software by state comparison chart

CHG	DSG	LED1	LED2	LED3	BUZZER
OFF	OFF	OFF	OFF	OFF	ON
OFF	ON	ON	OFF	OFF	OFF
ON	OFF	OFF	ON	OFF	OFF
ON	ON	OFF	OFF	ON	OFF

In the Proteus simulation as given Figure 4.5, 15V was given to the CHG input and 15V to the DSG input and it was tested that the buzzer worked according to the situation defined in Table 4.2.

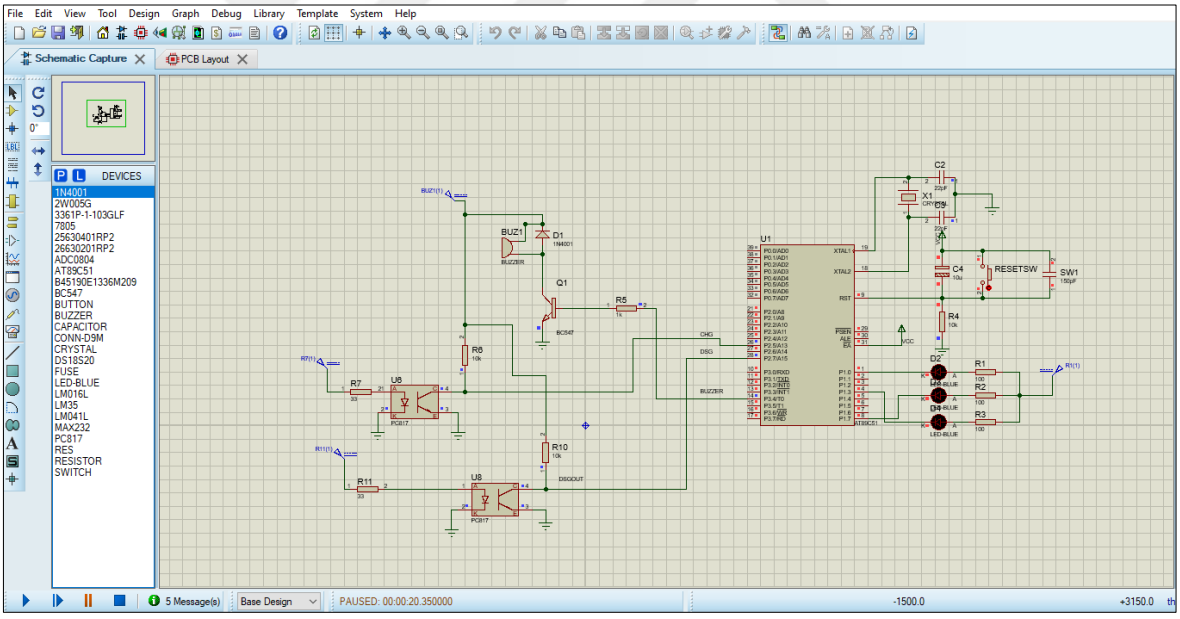

Figure 4.5. CHG = 15 Volt, DSG = 15 Volt (Buzzer)

In the Proteus simulation as given in Figure 4.6, 15V is given to the CHG input and 0V to the DSG input, and it has been tested that Led1 runs according to the situation defined in Table 4.2.

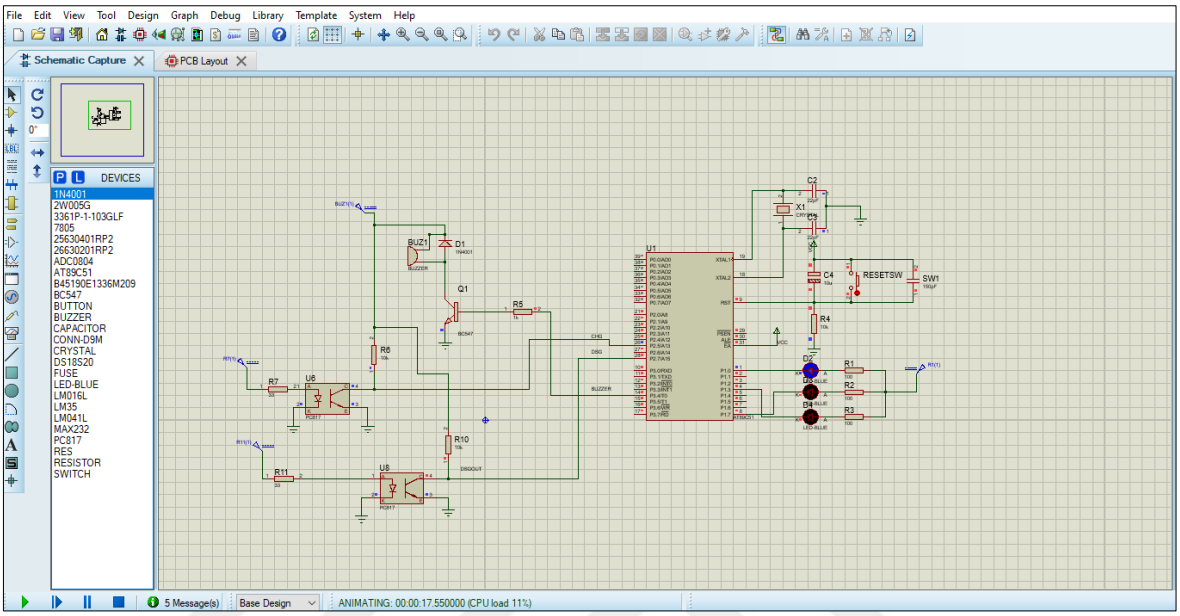

Figure 4.6. CHG = 15 Volts, DSG = 0 Volt (Led1)

In the Proteus simulation as given in Figure 4.7, 0V was given to the CHG input and 15V to the DSG input, and it was tested that Led2 ran according to the situation defined in Table 4.2.

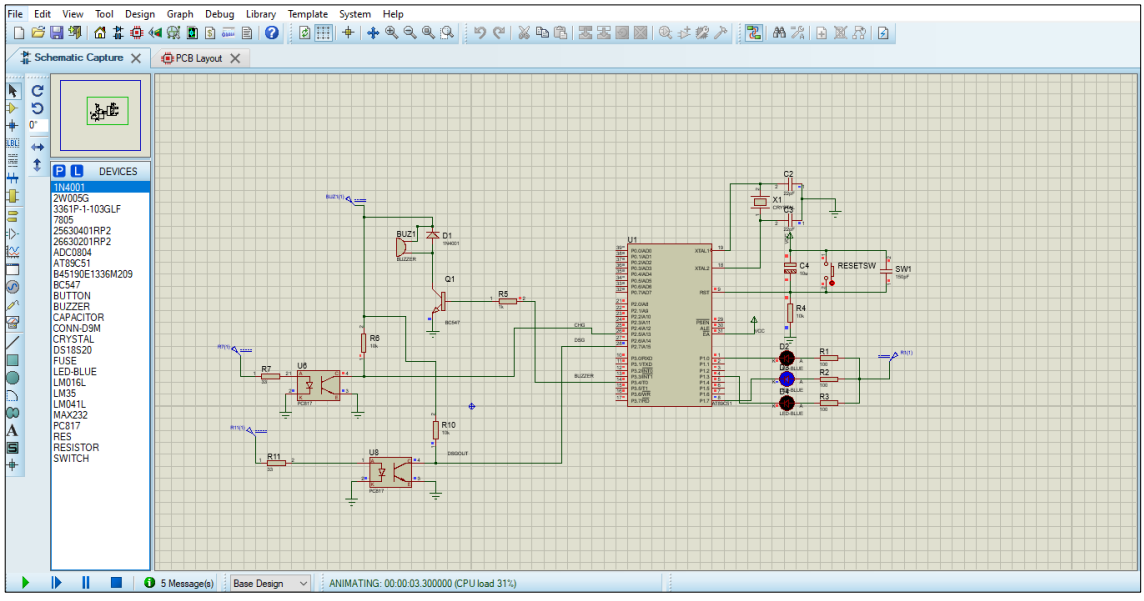

Figure 4.7. CHG = 0 Volt, DSG = 15 Volts (Led2)

In the Proteus simulation as given in Figure 4.8, 0V was given to the CHG input and 0V to the DSG input and it was tested that the Led3 ran according to the situation defined in Table 4.2.

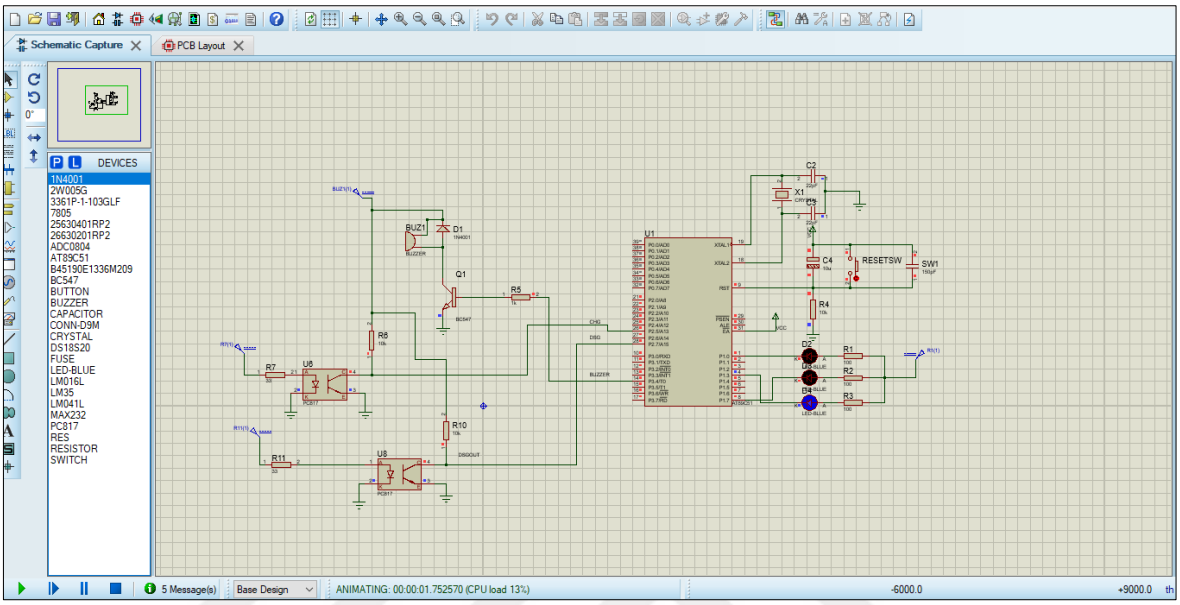

Figure 4.8. CHG = 0 Volt, DSG = 0 Volt (Led3)

4.4. LIQUID CRYSTAL DISPLAY (LCD) SOFTWARE AND TESTING

After the ports are defined, the first line is activated. Four messages are entered, M1, M2, M3, M4. The message M1, M2, M3, M4 has been loaded into the DPTR register and the command to display this message on the LCD has been given. RESETLCD and INITLCD function codes are written. 20h data is sent to LCD for 4 bit mode. 4-bit masking is done. M1 message “BATTERY MANAGEMENT”, M2 message “SYSTEM”, M3 “BALANCE ON”, M4 “PROTECTIONS ON” are messages sent to and read on the LCD. Reading messages on the LCD screen is shown in Figure 4.9.

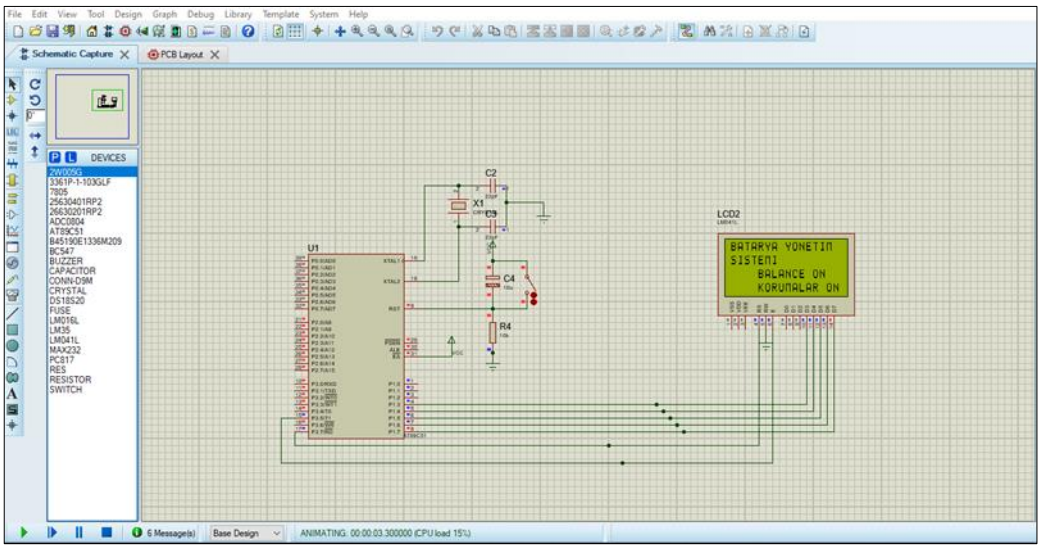

Figure 4.9. Reading messages on the LCD screen

4.5. TESTING THE SOFTWARE INTEGRATION PROCESS TO THE BATTERY MANAGEMENT SYSTEM (BMS)

The software made for BMS was gradually integrated into the system. First, Central Processing Unit, LCD Unit, Battery Management System (BMS) Protection Unit second, Central Processing Unit, LCD Unit, Analog To Digital (ADC) Unit Integration and finally Central Processing Unit, LCD Unit, BMS Protection Unit Integration, Warning Unit Integration, ADC Unit Integration has been completed.

4.5.1. Central Processing Unit, LCD Unit, Battery Management System (BMS) Protection Unit, Warning Unit Integration

The modes coming from the inputs in the control circuit to the LCD screen are combined with the control circuit software and LCD software in the form of messages and printed on the screen. In Figure 4.10 CHG = 15 Volts, DSG = 15 Volts, Normal Mode results are given.

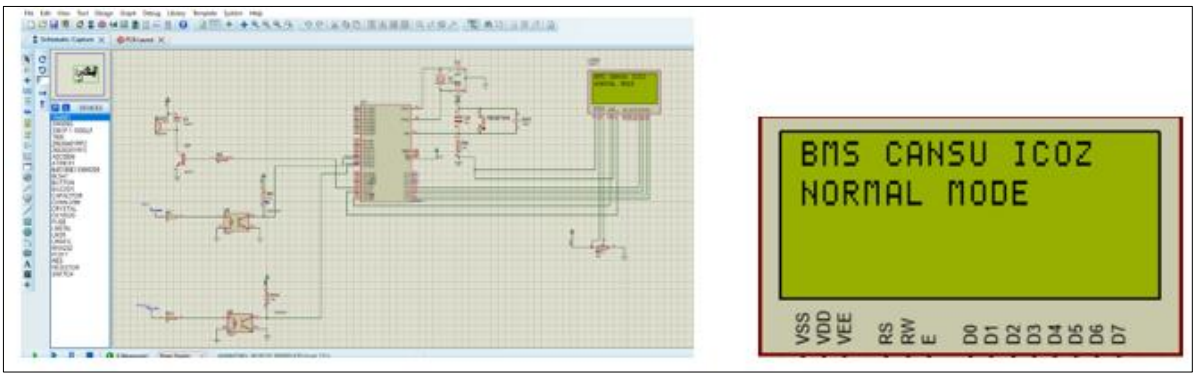

Figure 4.10. CHG = 15 Volts, DSG = 15 Volts, normal mode

Realization of Normal Operating Mode on Board is given in Figure 4.11.

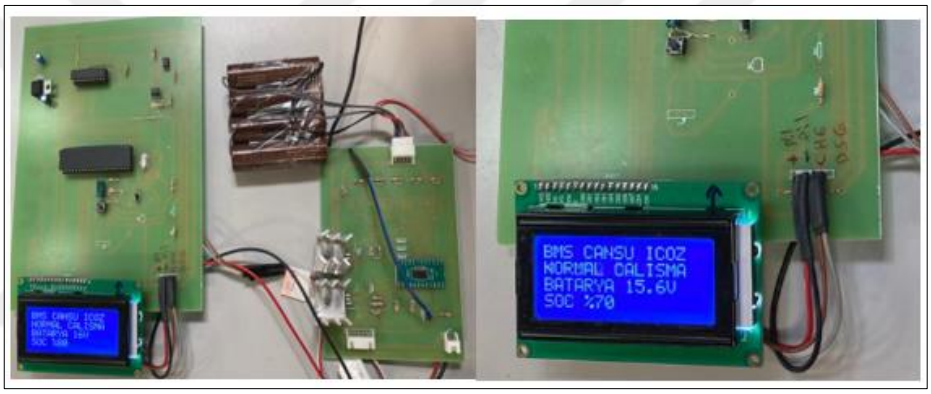

Figure 4.11. Realization of normal operating mode on board

In Figure 4.12 CHG = 15 Volts, DSG = 0 Volts, Discharge Mode results are given.

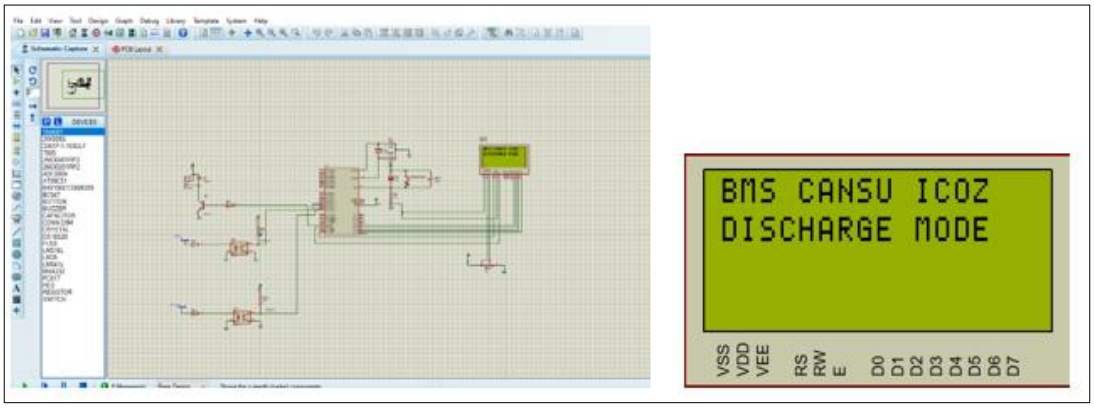

Figure 4.12. CHG = 15 Volts, DSG = 0 Volt, Discharge Mode

Realization of Discharge Mode on Board is given in Figure 4.13.

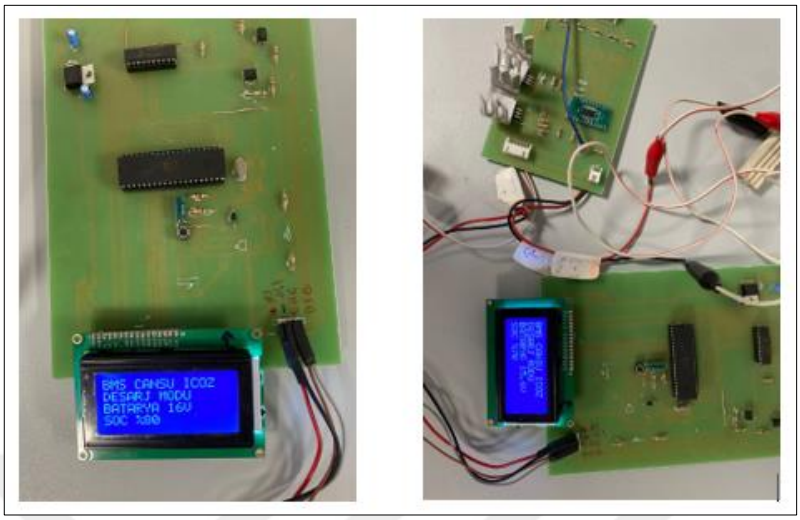

Figure 4.13. Realization of discharge mode on cardboard

In Figure 4.14 CHG = 15 Volts, DSG = 15 Volts, Charge Mode results are given.

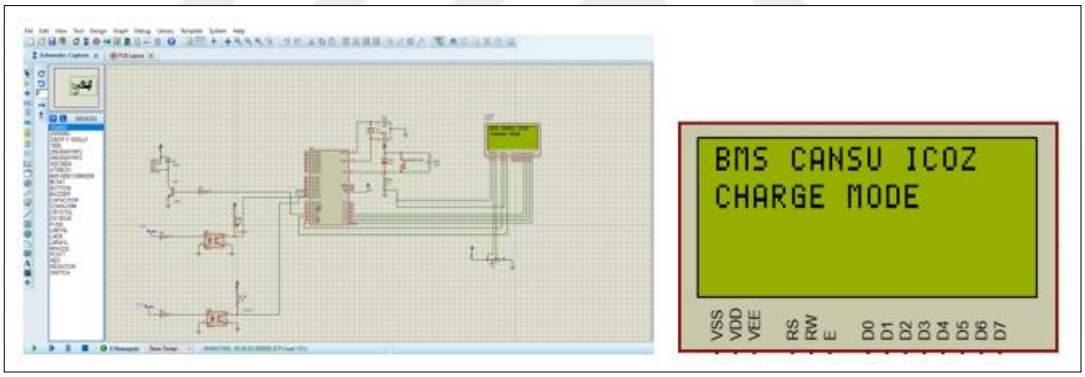

Figure 4.14. CHG = 0 Volt, DSG = 15 Volt, charge mode

Realization of Charge Mode on Board is given in Figure 4.15.

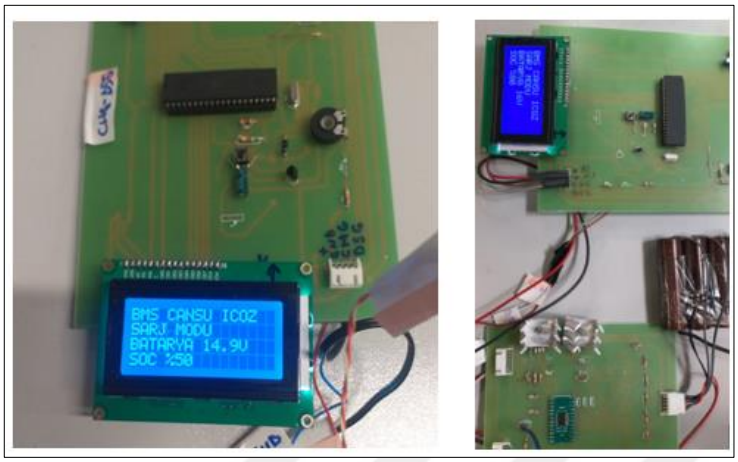

Figure 4.15. Realization of the charge mode on the cardboard

In Figure 4.16 CHG = 0 Volts, DSG = 0 Volts, Protection Mode results are given.

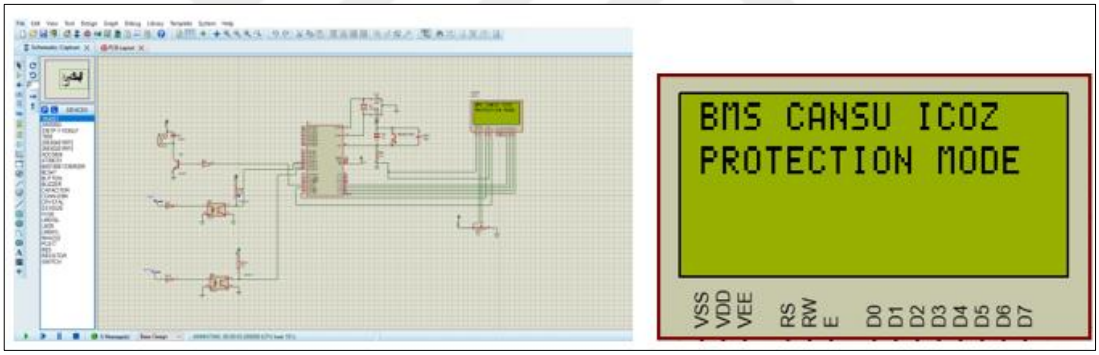

Figure 4.16. CHG = 0 Volt, DSG = 0 Volt, protection mode

Realization of Charge Mode on Board is given in Figure 4.17.

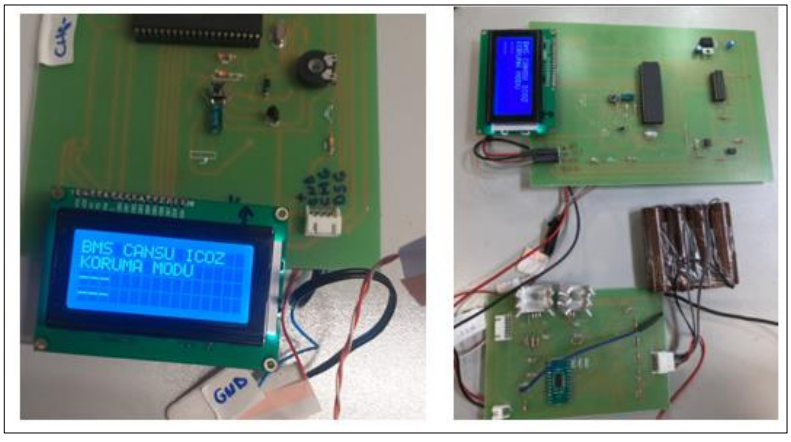

Figure 4.17. Realization of protection mode on the cardboard

4.5.2. Central Processing Unit, LCD Unit, Analog To Digital (ADC) Unit Integration

In Figure 4.18 shown that POT-HG values may vary. For example, when POT-HG is 14 percent, the following value is read.

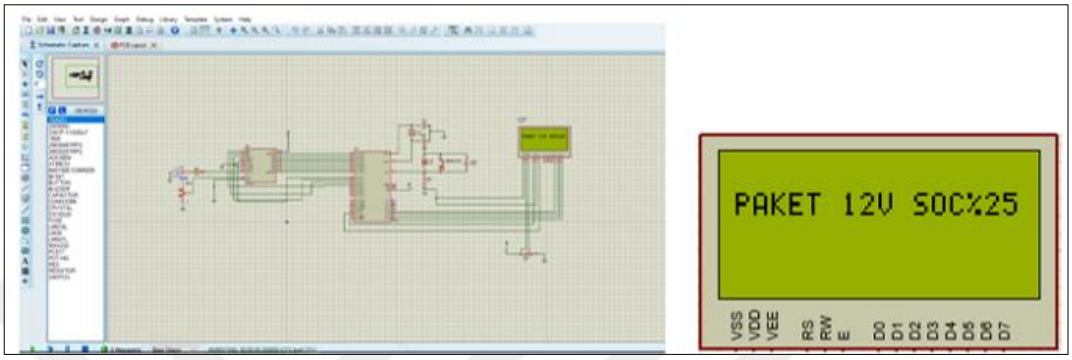

Figure 4.18. Display of central processing unit, LCD Unit, ADC unit ıntegration on the screen

4.5.3. Central Processing Unit, LCD Unit, BMS Protection Unit Integration, Warning Unit Integration, ADC Unit Integration

Once the software is referred and glanced upon, the beginning is taken as 100 percent starting from the value of 255 up to the value of 231, the value of 230 is taken as the beginning of 90 percent and the value of 213 is taken as the beginning of 80 percent. In summary, SoC value at 12.3 Volts is 0 percent, SoC value at 13.5 Volts is 10 percent, SoC value at 14 Volts is 20 percent, SoC value at 14.3 Volts is 30 percent, SoC value at 14.6 Volts is 40 percent, SoC value at 14.9 Volts is 50 percent, SoC value at 15.3 Volts is 60 percent, SoC value at 15.6 Volts is 70 percent, SoC value is 80 percent at 16 Volt, SoC value is 90 percent at 16.4 Volt, SoC value is 100 percent at 16.8 Volt. In the GUI design, the input sentence is 'CANSU ICOZ', and according to the information transmitted from the inputs, 'NORMAL OPERATION', ' DISCHARGE MODE', 'CHARGE MODE', 'PROTECTION MODE' and '--- ' to not read the SoC value in protection mode while the BMS design is working. It has been validated in the simulation environment and on cardboards.

In Figure 4.19 shown that Reading Mode and SoC on LCD Screen.

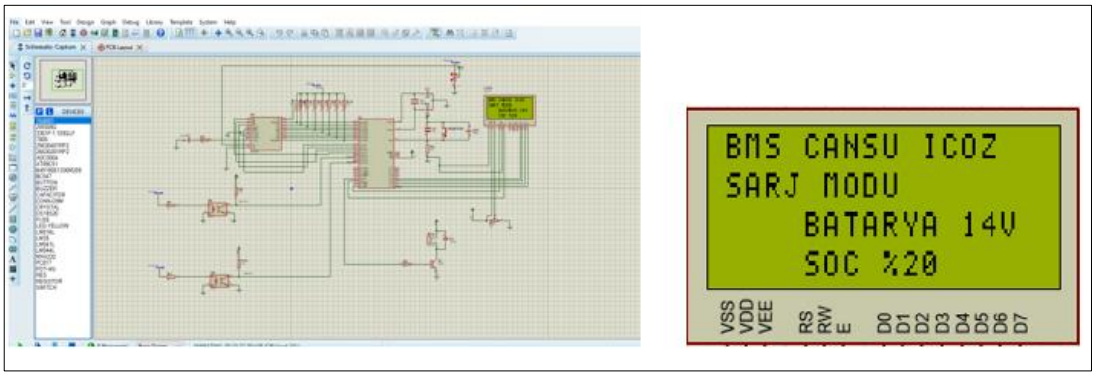

Figure 4.19. Reading mode and SoC on LCD screen

In Figure 4.20 shown that Verification of Values on BMS Card by Measurement.

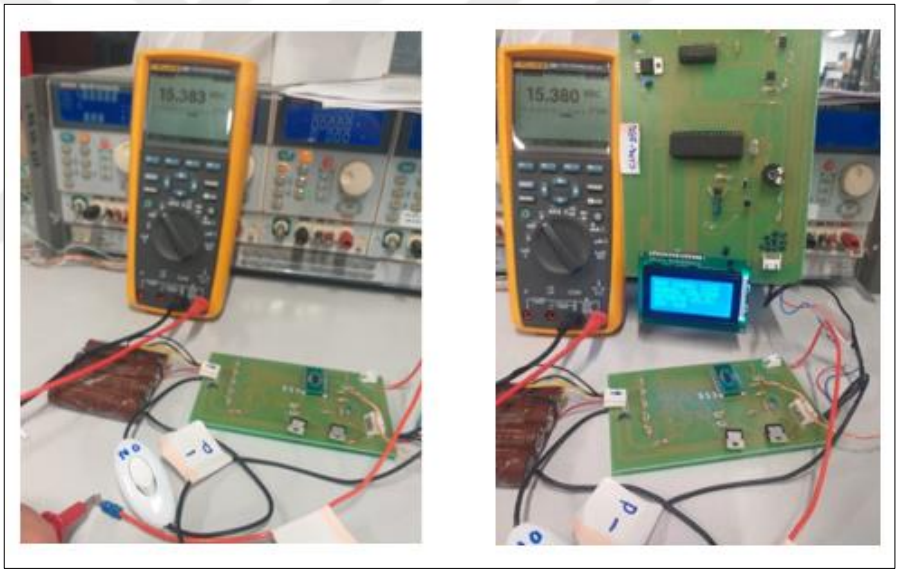

Figure 4.20. Verification of values on BMS card by measurement

Figure 4.21 shows verifying that the SoC Value is Not Read on the LCD Display in Protection Mode.

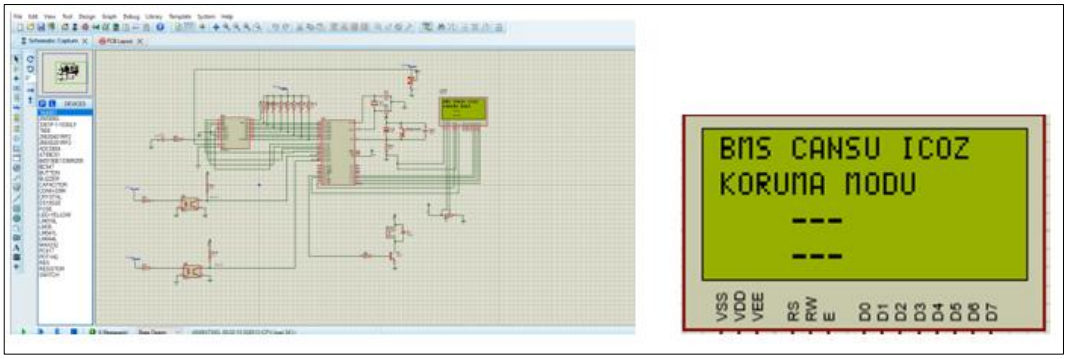

Figure 4.21. Verifying that the SoC value is not read on the LCD display in protection mode

4.5.4. Measurement Results of Internal Resistance

The aging of the battery causes a loss of battery capacity and an increase in internal resistance. Reduction of battery capacity occurs due to repeated charging and discharging processes. The capacity estimation of a battery can be calculated by various methods and can give near-accurate results. Although the methods studied give accurate results, it increases the computational complexity and the error rate in the operations performed, and it is not frequently used in online estimation methods. Various applications have been made aiming to estimate the capacity of a battery effectively. According to different opinions, these methods are divided into four categories: Direct measurement, Book-keeping estimation, Adaptive Systems, and Hybrid methods. [43,44]. The internal resistance values measured at different currents are given in Table 4.3.

Table 4.3. Table of internal values measured at different currents

Steps	V no-load gauge	V no-load Electronic Load	Electronic Load Load Re-sistance	V load Electronic Load	V Load Gauge	I Electronic Load	Internal Re-sistance (Ω)
0.1A	4.16V	4.15V	40R	4.12V	4.15V	0.102A	0,392
0.2A	4.15V	4.15V	20R	4.1V	4.15V	0.204A	0,098
0.5A	4.15V	4.15V	8R	4.03V	4.14V	0.503A	0,012
1A	4.15V	4.15V	3.9R	3.91V	4.13V	1.002A	0,002
1.5A	4.15V	4.15V	2.5R	3.72V	4.11V	1.48A	0,277
1.7A	4.14V	4.14V	2.1R	3.63V	4.09V	1.72A	0,278
2A	4.13V	4.13V	1.8R	3.62V	4.08V	2.002A	0,238
2.5A	4.11V	4.11V	1.4R	3.49V	4.05V	2.497A	0,222
5A	4.11V	4.11V	0.65R	3.22V	3.99V	5.03A	0,143
10A	4.1V	4.1V	0.275R	2.72V	3.85V	9.98A	0,111

4.6. CHARGE AND DISCHARGE TESTS WITH INA238

In the graph given in Figure 4.22, the battery is charged up to 4.1V and the Li-ion battery is discharged in constant current mode. For the battery to be discharged safely, it has been tested with the battery's own BMS circuit and since the cut-off voltage is 2V, it has not fallen below this voltage as shown in Figure 4.23.

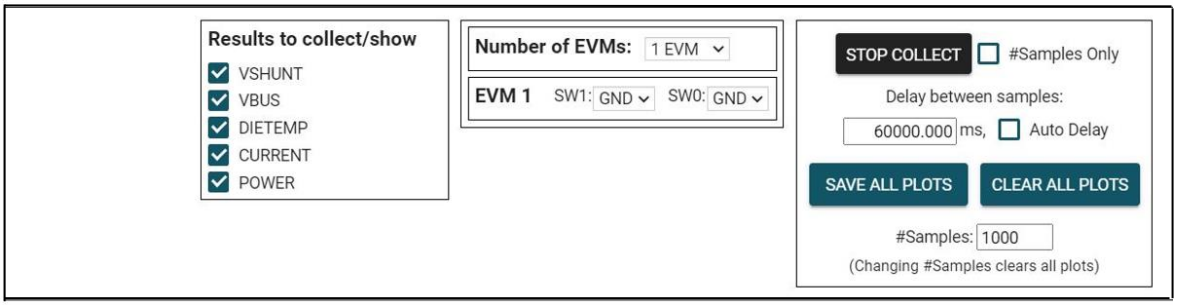

Figure 4.22. Adjusting the INA238 EVM sampling interval and sampling number setting

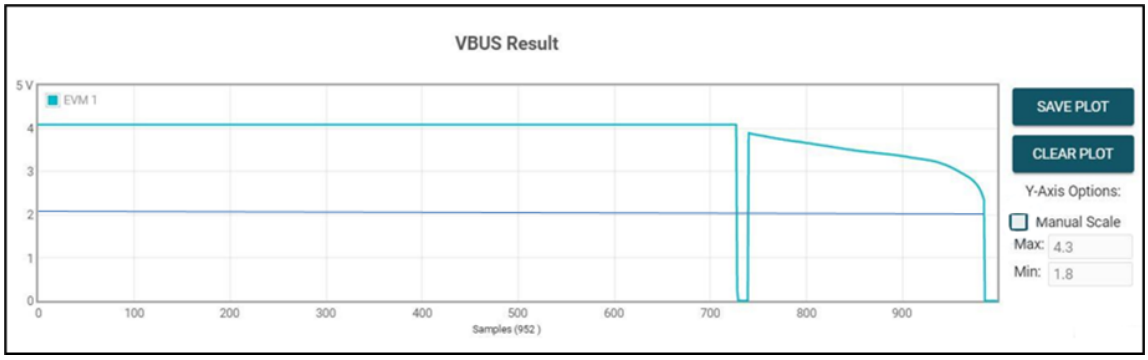

Figure 4.23. VBUS voltage graphic

The discharge current is 1.5A. When the Li-ion battery is discharged, the initial discharge current should not be too large. As the graph in Figure 4.24, excessive current causes internal heating that can cause permanent damage [39].

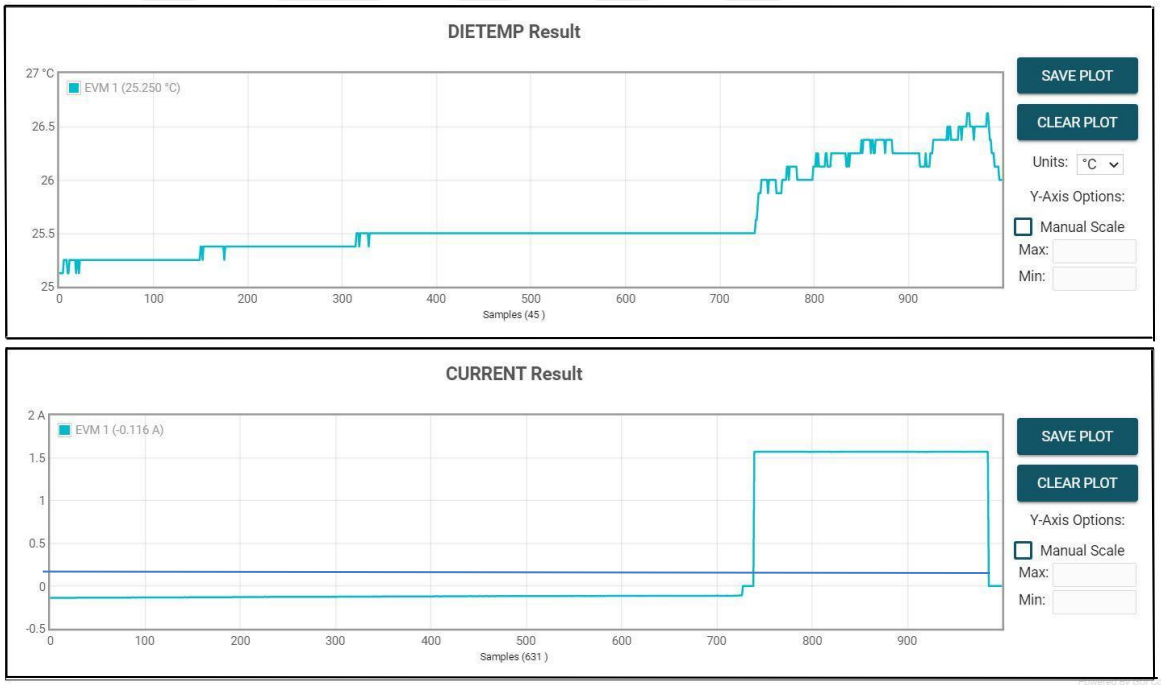

Figure 4.24. Temperature and current graphics

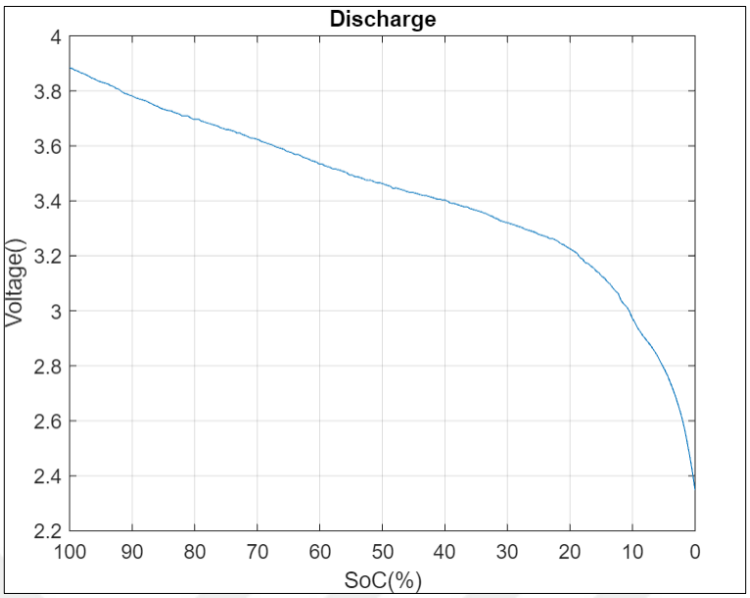

Figure 4.25. Discharge graphic

The lithium-ion battery uses constant current at constant voltage when in charging mode. Here, charging with 1.5A is applied. The battery voltage is gradually increased to 4.028V as shown in Figure 4.26. The change in charge voltage is recorded instantly with the INA 228 sensor.

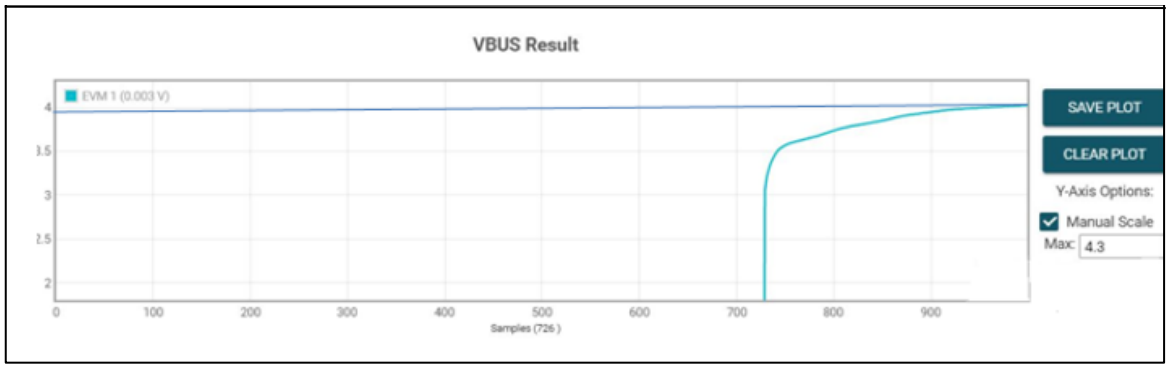

Figure 4.26. VBUS graphic

In Figure 4.27 shows that when the current reaches a certain range, it enters the slow charging phase, continues to charge at a constant rate, and ultimately the battery is fully charged.

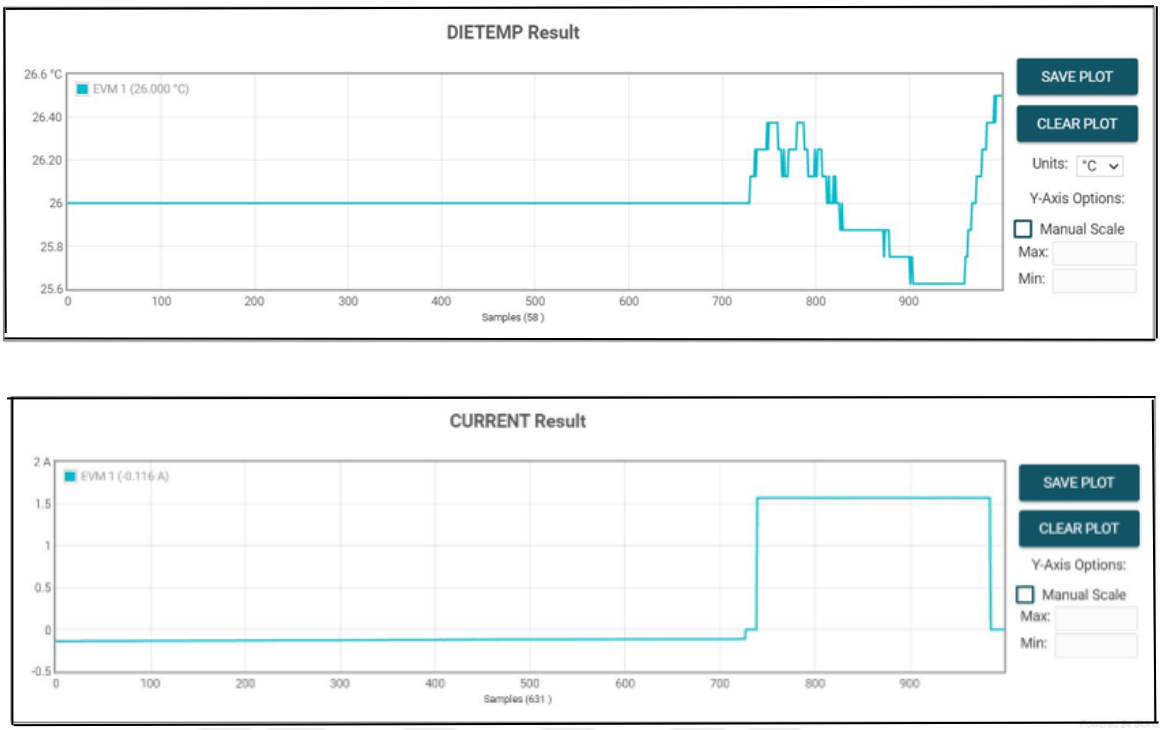

Figure 4.27. VBUS temperature and current graphic

With the data collected from the sensor, a constant current charging graph was obtained in MATLAB, from 0 percent to 100 percent in the charging state as shown in 4.28.

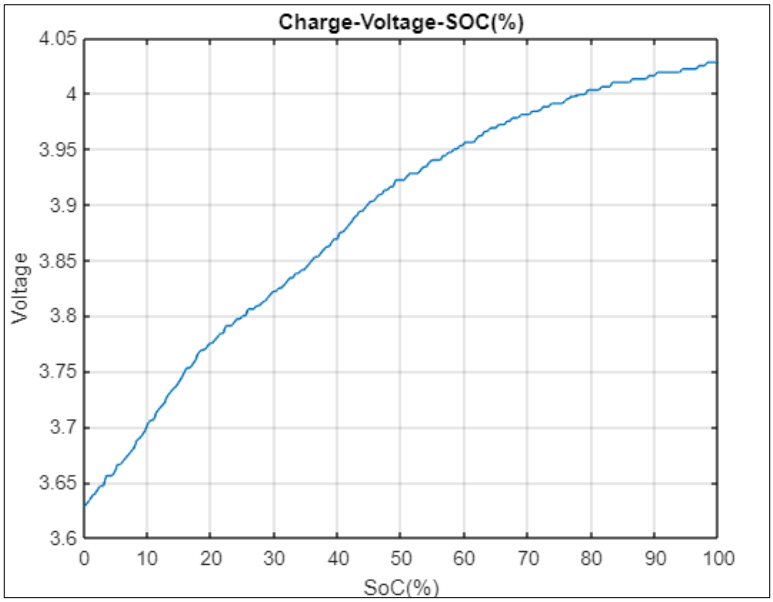

Figure 4.28. Charge graphic

4.7. EXTENDED KALMAN FILTER-BASED STATE OF CHARGE ESTIMATION

In the study carried out with C code in Cadex Battery device, charge with 4A and discharge with 10A were performed as shown in Figure 4.29. To prevent the battery from over-discharging, the voltage at which the discharge will end is 2V and the voltage at which it will be charged is 4.2V. To obtain OCV data during discharge, the charged battery is charged, the charged battery rests for 10 minutes [54]. It rests for 1 hour after discharge. The test implementation was continued until the capacity of the battery reached the levels of 84 percent, 84 percent, 84 percent and 33 percent.

Figure 4.29. Summary data of pulse charge and discharge process

While the lithium-ion battery is being discharged, the discharge current should not be too large. Excessive current here can cause permanent damage. If the discharge termination voltage value is not lower than 2V, it may cause over-discharge voltage and permanently damage the battery [39]. Current and voltage waveforms during charging and discharging are shown in Figure 4.30.

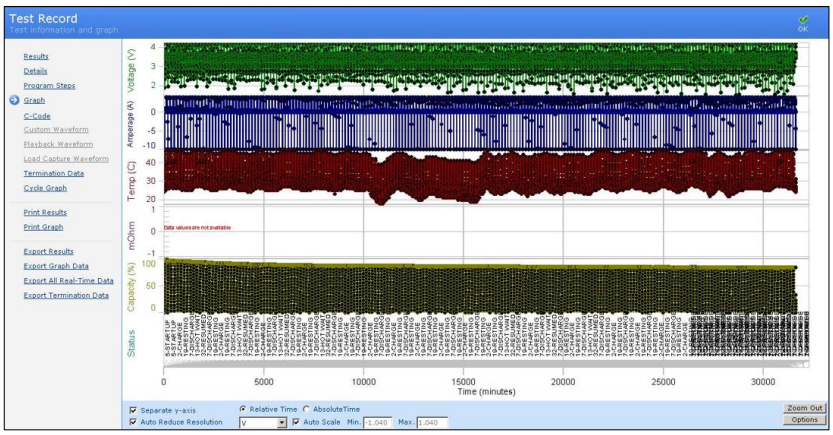

(a)

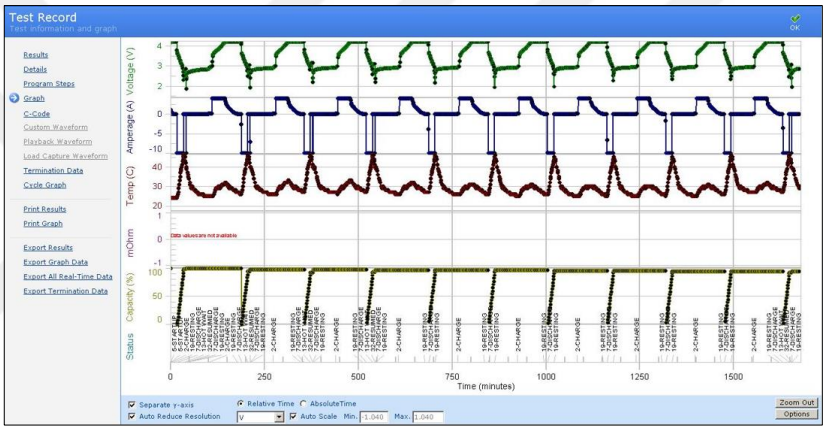

(b)

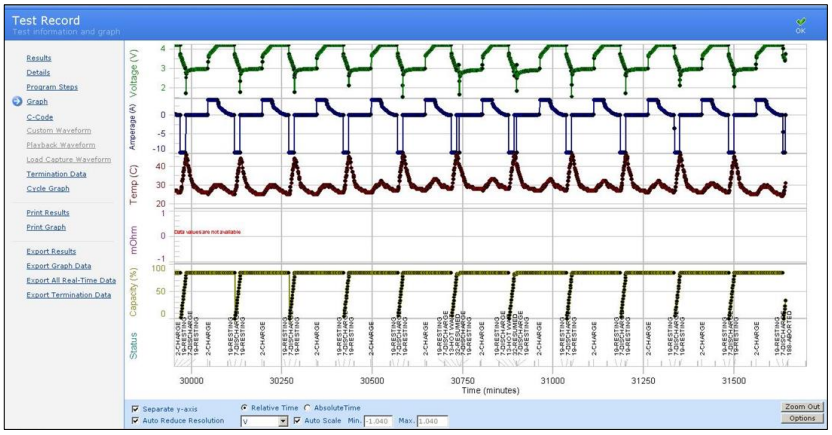

(c)

Figure 4.30. (a) Charging with 4A and discharging with 10A (b) Graph of the first 10 data (c) Graph of the last 10 data

According to the data received with the INA238 Sensor, current and voltage graphs are also drawn. In this experiment to obtain the relationship between the OCV and the state of charge of the battery, the applied test procedure consists of 10A current pulses to discharge the battery, that is, to reduce the SoC value from 100 percent to 0 percent. The open circuit voltage of the battery is the gradual rise of the battery to a constant voltage value after a discharge pulse and removing the load [46]. The extracted pulse discharge voltage value is shown in Figure 4.31.

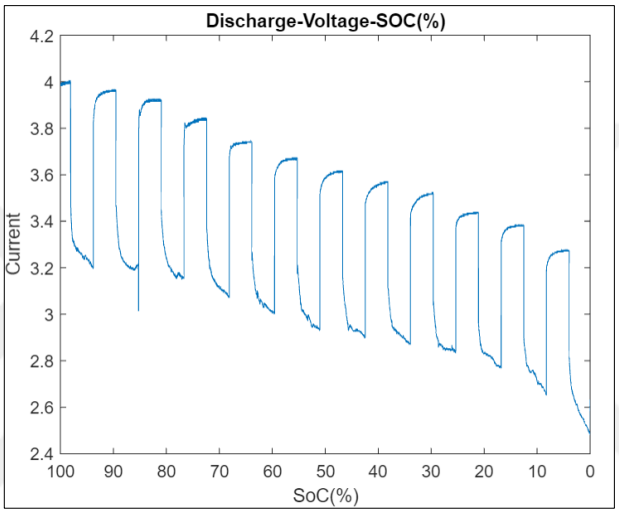

Figure 4.31. Discharge voltage pulses

In Figure 4.32 shows that the current value initiated with 10A has decreased to approximately 6A.

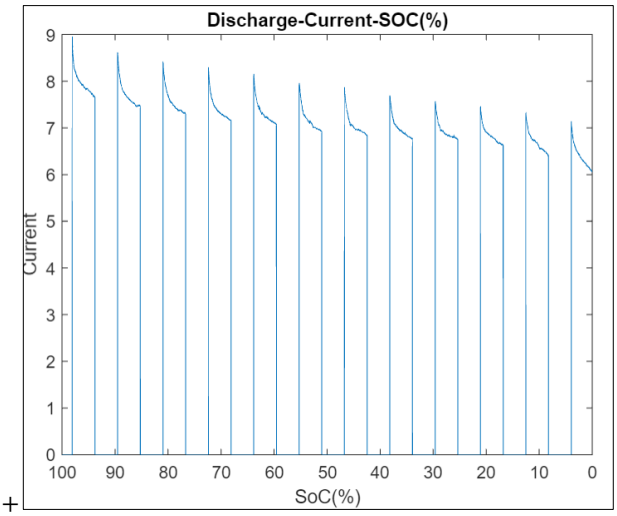

Figure 4.32. Discharge current pulses

4.7.1. Dual Polarization Model Parameter Calculation

According to the measured data, V_{OCV} = 4.0906 was specified. The value of R_s is the voltage that first drops from the initial value after a certain period of time when it starts to draw current with the OCV voltage, the first voltage it drops after V_{OCV} is 3.8843V and is divided by the constant discharge current I_{bat} [46].

$$R_s = \frac{3.996-3.309}{10} = 0.0687\ \Omega \tag{4.1}$$

The R_p voltage is the second voltage at which it drops a certain amount after the first drop voltage. The second drop is the voltage value it shows. The parameters of the Dual Polarization Model were calculated according to reference [46].

$$R_p = \frac{3.309-3.207}{10} = 0.0102\ \Omega \tag{4.2}$$

The value of R_1 is found by dividing the coefficient K_1 by the constant discharge current I_{bat}.

$$R_1 = \frac{0.006}{10} = 0.0006\ \Omega \tag{4.3}$$

The R_2 value is found by dividing the K_2 coefficient by the constant discharge current I_{bat}.

$$R_2 = \frac{0.1212}{10} = 0.01212\Omega \tag{4.4}$$

a coefficient value is taken as 0.482847564 and b coefficient value is taken as 0.009706373429.

$$C_1 = \frac{1}{0.4828475648 \times 0.0006} = 3451.745004 \text{ F} \quad (4.5)$$

$$C_2 = \frac{1}{0.009706373429 \times 0.01212} = 8500.42 \text{ F} \quad (4.6)$$

Model parameter values are given in Table 4.4.

Table 4.4. Dual polarization model parameters

Parameter	Value	Unit
R_{int}	0.111	Ω
R_s	0.0687	Ω
R_p	0.0102	Ω
C_1	3451.745004	F
C_2	8500.42	F
R_1	0.0006	Ω
R_2	0.01212	Ω

4.7.2. SoC Value Graph Results with Extended Kalman Filter

Based on the linearization, the designed Extended Kalman Filter described with equations in Section 3.5.5 is used to estimate the SoC. The result of the Coulomb Counting method is in Figure 4.31 and Figure 4.32, the charge and discharge current, voltage data recorded with the INA238 sensor are graphically shown and these values are chosen as a reference to increase the accuracy of the SoC estimation. The sensor data is 14000 in total, that is, 14000 data has been obtained. The terminal voltage of the battery and OCV estimation are shown in Figure 4.33.

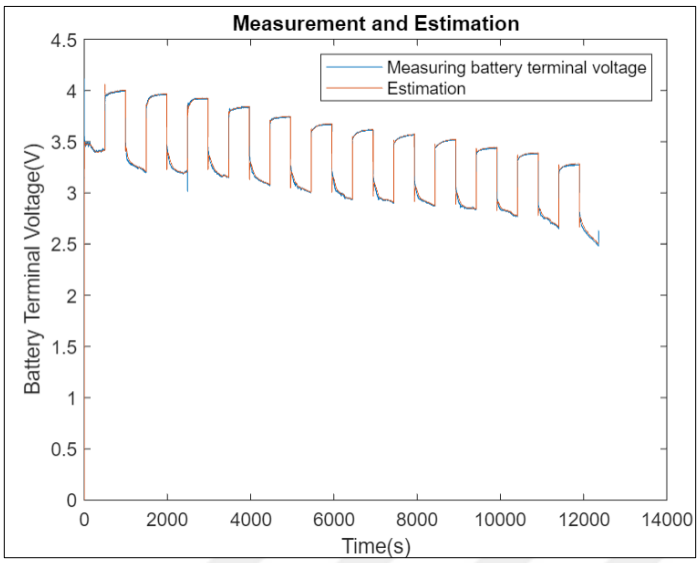

Figure 4.33. Measuring battery terminal voltage and estimation

There is a measurement error of 0.3 V in the sampling with a sampling frequency of $0{,}2*10^4$ sec. The designed Extended Kalman Filter is used to simulate real field conditions where the SoC at the start of use is unknown and to test its self-healing ability. The blue line shows the measured terminal voltage, and the red line shows the predicted value. We can see from Figures 4.33 and 4.34 that the SoC values converge to a certain value with the Extended Kalman Filter estimations. The SoC converged at the same level, regardless of its initial value, close to its true value. Sudden dips and spikes in the measurement are not observed in the estimation.

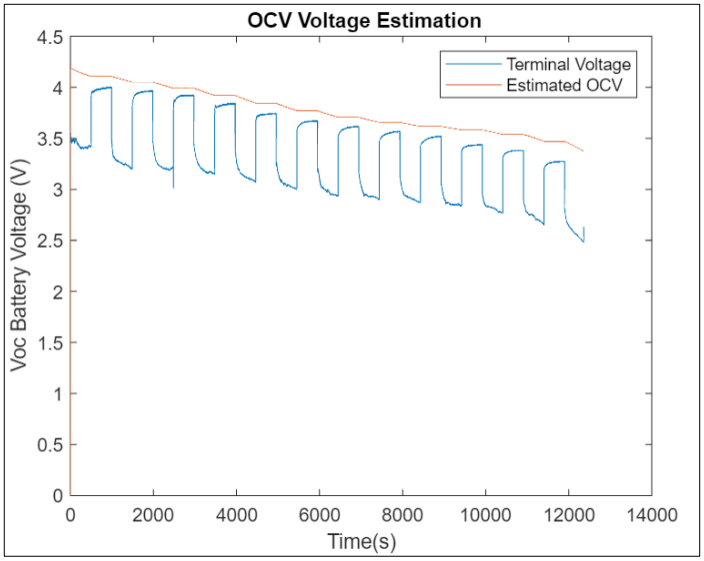

Figure 4.34. Figure battery terminal voltage and OCV results

The values measured during the charging and discharging process of the battery are the online identification data of the equivalent circuit parameters and have been the input for the designed Extended Kalman Filter. The defined parameters are used to update the filter system parameters. In theory, OCV values are expected to change continuously and smoothly as SoC changes, and the estimation results are shown in Figure 4.33 shows this change.

We can see that the SoC can adjust itself to the actual value even when the current is zero [61]. The reason for this is that the battery voltage does not remain constant but changes as a result of dynamic effects even when the current defined as the variable is zero. The model and the Extended Kalman Filter algorithm will adjust the SoC to follow the actual terminal voltage. Although the estimate deviates from the true SoC due to the initial erroneous estimate, it converges to the true SoC value as more measurements are made as shown in Figure 35.

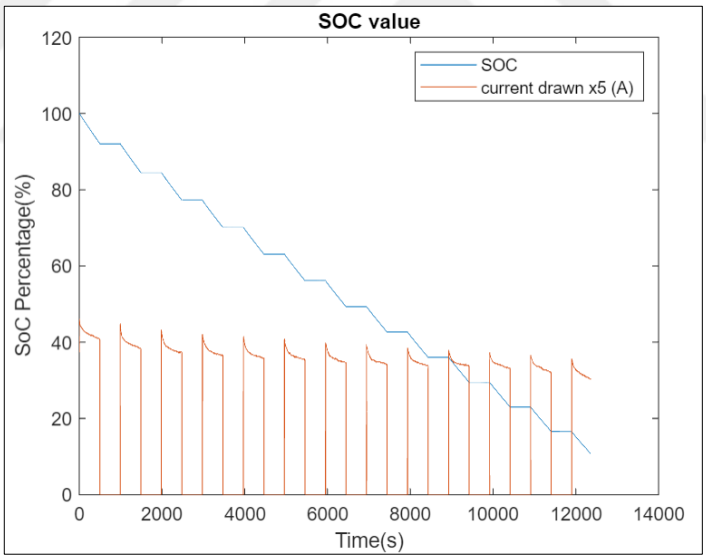

Figure 4.35. SoC value and current drawn

Figure 4.36 shows that considering the change of R_{int} value according to the drawn current, it can be said that it does not change much and is indeed consistent.

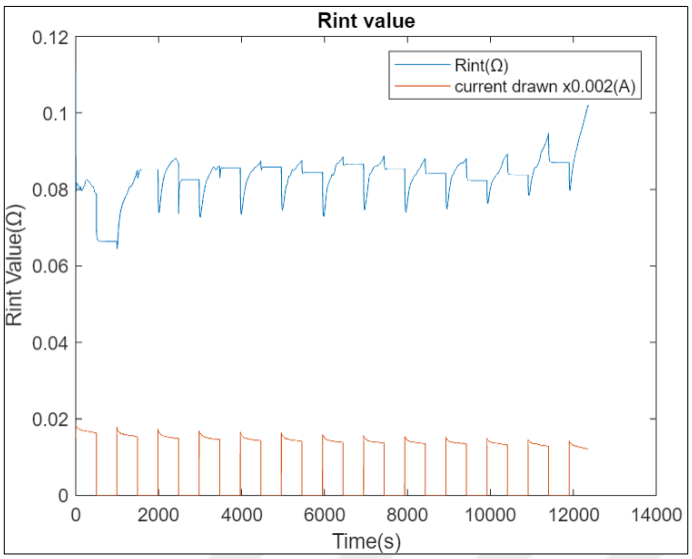

Figure 4.36. R_{int} value and current drawn (x 0,002)

While the current value is zero as shown in Figures 4.37 and 4.38, the covariance value of SoC and R-value does not change. U_{pa} and U_{pc} values, on the other hand, change because the current is discharged in themselves. SoC and R covariance values will change when the current is in the negative or positive direction. In the ideal case, it is assumed that a constant current is drawn, but as the current draws, there are voltage drop effects and the current does not remain constant.

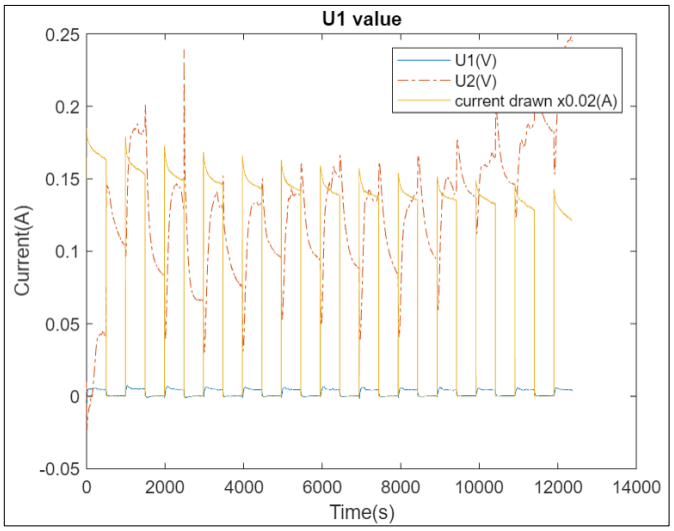

Figure 4.37. U_1, U_2 and current drawn (x 0.02)

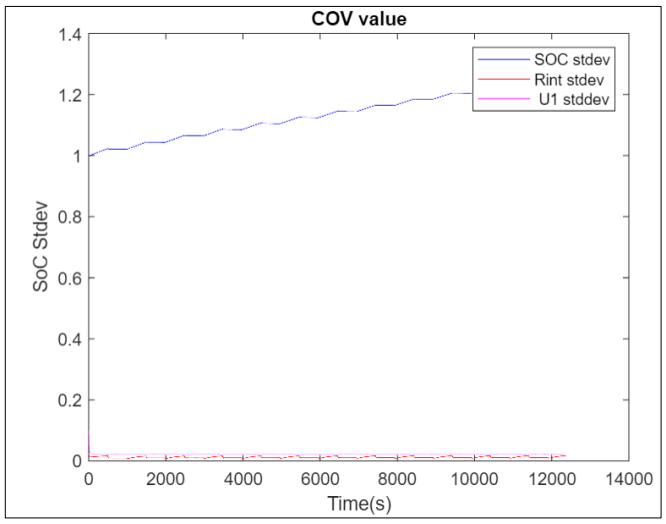

Figure 4.38. SoC, R_{int} and U_1 values

According to the graph in Figure 4.39, the reason for this increasing of SoC covariance is that the uncertainty of the SoC increases as the battery is used. The battery fullness will continue to increase until it reaches 0 percent from 100 percent, it does not increase infinity. The highest uncertainty is seen at 0 percent battery charge rate.

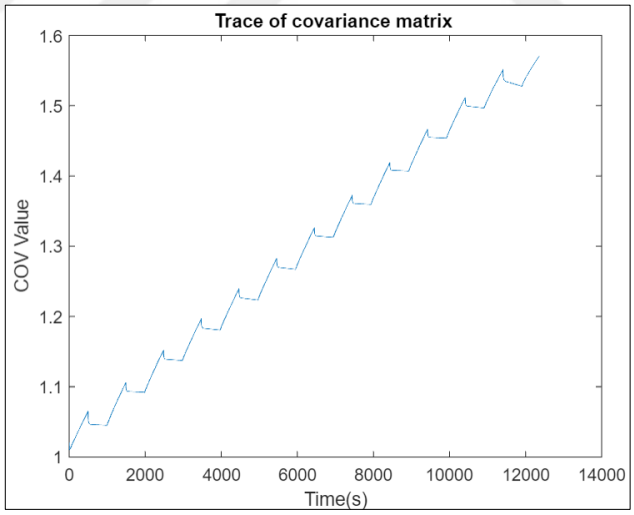

Figure 4.39. Trace of covariance matrix

5. CONCLUSION

One of the most important components of the Li-ion battery is the BMS (Battery Management System). A BMS collects and monitors information about the battery's voltage, current, and temperature operating conditions. A BMS consists of multiple series or parallel connected battery cells for high voltage and current applications. Consisting of more than one cell, it must be connected in series or parallel. The BMS allows the battery to continue to operate safely by controlling the operating voltage, current, and temperature. This thesis proposes a BMS circuit design for a battery system consisting of four series-connected cells. The system is designed to provide two basic features of BMS, namely monitoring and protection. Functional features of BMS such as battery status estimation, temperature control, cell balancing, charge, and discharge control are observed with Texas Instruments device BQ77915 sensors and controlled and analyzed with the help of a microprocessor. The BQ77915 IC has made the design more efficient with its many functional features. A circuit topology has been developed to monitor battery performance, program and improve algorithms. By transferring other peripherals to the BMS circuit with the help of Mosfets, the user allowed to monitor the charge, discharge, protection, and standard operating conditions on the LCD. The design was made both in the simulation phase, and the usability of the cards as a protection circuit in real life was tested. The designed BMS can provide protection up to 16.8V. By ensuring that the system it is used in works in an optimized way, it prevents overcharge and discharge and ensures that the battery capacity is at the highest level, ensuring that the voltage values of each cell are balanced. In case of overvoltage or low voltage in the battery pack and deterioration of voltage values, when optimal values such as high temperature, low temperature, leakage current are exceeded, the circuit is protected. This situation can be reported to the user with a buzzer. Monitoring instant data provides controls such as voltage status, charge status, and current status.

One of the important parameters required to ensure safe charging and discharging is the SoC. Actual-time SoC estimation helps battery management determine the battery system's stability. Inaccurate estimation of the SoC value can cause overcharge or over-discharge, resulting in permanent damage to the battery. The techniques used for estimating the SoC of a battery can be classified as direct computation methods or intelligent computation methods. Direct calculation methods can measure the SoC of the battery using the Coulomb Counting

Method, Open Circuit Voltage, or internal impedance and directly calculate it based on its relationship to the battery parameters. These methods are widely used because they are easy to implement. In this thesis, the Coulomb Counting Method was used. The method used for SoC estimation is Coulomb Counting, OCV and model-based method. Coulomb Counting has been sampled with an accurate SoC value and high current to avoid cumulative errors. Open circuit voltage revealed the nonlinear relationship between OCV-SoC. Sampling was done with an accurate SoC value and high current to prevent cumulative errors. It was concluded that the values did not give a direct and net result in the sampling made with low current.

The model-based method is used as the state equation of the battery system. This method requires high accuracy measurement and estimation, so the model-based method is combined with an algorithm. Extended Kalman Filter is one of the most widely used algorithms in SoC estimation. This thesis proposes an accurate and comprehensive battery charge state estimation method using Extended Kalman Filter. The Extended Kalman Filter was designed in Matlab to accurately predict the battery SoC using the battery model and estimated Open Circuit Voltages (OCV). Values recorded with the INA238 sensor, with a sampling frequency of 5 and a number of Extended Kalman filters of 4, were used in the order of time, voltage, and current. For k=1, an estimation loop and filter are applied.$SOC(k+1|k)$ is a priori estimation and the measurement at step *k* is used. z_{k+1} is the measurement we made at the instant *k+1*. When we estimate using the measurement in step *k+1*, it is the estimate we make using the most recent measurement. Since we have taken a new measurement, namely data, the uncertainty decreases, and it has been observed that the posterior covariance is lower than the a priori covariance. *H* is the Extended Kalman Filter measurement matrix, which determines the relationship between the defined state and the measurement we made. *K* was used as the gain factor that minimizes the posterior error covariance. It is defined as *x(k)= [SoC(k) R(k),* U_{pa}*(k),*U_{pc}*(k)]*^{T} state vector. *z(k)* is defined as our actual state vector, and *V(k)* as our measurement. *Q* is defined as the process noise covariance, which means how much it can change over time. Since it is a variance calculation, it is squared, and its standard deviation is calculated as 0.01. It has been calculated experimentally, as we do not expect much change in the values from one second to one second in cases where the aging of the batteries changes over time, such as the characteristics of the battery. The initial uncertainty in SoC $p_{11}^2 = 1^2$, the uncertainty of the

Rint resistance $p_{22}^2 = 0.001, p_{33}$, the uncertainty of the U_{pa} voltage $p_{33}^2 = 0.1^2$, the uncertainty of the p_{44} U_{pc} voltage $p_{44}^2 = 0.1^2$ are taken into consideration. When we compare it with the filter values, it has been observed that there is not a notable difference between the measured values and the predicted values for the internal resistance, U_{pc}, U_{pa}, SoC-OCV relationship, during the time we run the filter, since it is set to the correct values experimentally. In case the Q value is too high, it means that it changes too much from time to time, and the difference between the measurement and prediction results will increase, it directly reflects the result from the measurement, and the result is undue and countless noise. If we insert too many low values, it means that they do not change during the process, it is obtained that the values do not change. *R* is the measurement covariance, the voltmeter error performance is checked, and the error is selected as 0.3V. An uncertainty of 1 percent is given for the initial covariance matrix of the filter. For R_{int}, U_{pc},U_{pa}, values are given as 0.001, 0.01, 0.01. The initial vector is defined for the 4 state variables that we want to predict. The values converting from SoC to OCV and from OCV to SoC are fit with a 6th degree polynomial according to the graph given in Figure 4.25, according to the OCV-SoC graph, and inverted. These coefficients were also taken in the Extended Kalman Filter. In the graphs obtained, it is seen that the values obtained as a result of the measurement are close to the estimated values.

The proposed model demonstrates that the system predicts SoC more accurately than commonly used methods, which can help to improve battery performance and lifespan. Evaluation of the adaptability of the battery model used to calculate the SoC value and the robustness of the SoC estimation algorithm was also verified. The results indicated that the estimation method using the Extended Kalman Filter based on the Dual Polarization model performed well by harmonizing the Coulomb Counting and OCV methods.

With the designed BMS and the Extended Kalman Filter used, SoC estimation can be widely used in electric vehicles, mobile phones, computers, renewable energy systems, telecommunications, energy storage units. It is of utmost importance for the protection of high-capacity, high-cost battery systems.

6. FUTURE WORK

In the future, the Extended Kalman Filter can be integrated into the cards designed in this thesis. The designed Extended Kalman Filter is left in the simulation phase. If the system is to be used in advanced battery technologies, since the designed BMS will have more battery cells, these cards can be used more than once for each battery pack. The motherboard is defined as the master can receive current, voltage, and temperature data from the cards defined as the slave. The communication of this designed system with each other can be provided by standard or specially designed RS232, RS485, Controller area network (CAN) communications. In addition to displaying the SoC battery charge rate, the State of Health (SoH) value can also provide the user with information that how much of the battery's lifetime is consumed and how long it takes to be replaced. Direct measurement, Book-keeping estimation, Adaptive Systems, and Hybrid methods can be used for Li-ion battery and their accuracy can be investigated for SoC. With the Extended Kalman Filter method, charge and discharge tests of Pb-acid, Ni-MH, Li-Polymer batteries can be applied, and the estimation accuracy can be compared with the Li-ion battery. The voltage and current values obtained by modeling the battery model in Simulink can be plotted from the experimentally measured data. OCV and SoC values can compare**.** Computational intelligence algorithms, such as the artificial neural networks (ANNs),fuzzy-logic, and support vector machines (SVMs) methods can be applied to all battery types, and excellent prediction performance can be explored if the training data is sufficient to cover all loading conditions.

7. REFERENCES

1. Yao LW, Aziz JA, Kong PY, Idris NRN. Modeling of lithium-ion battery using MATLAB/simulink. In: *IECON Proceedings (Industrial Electronics Conference).* 2013. p. 1729–34.

2. Mousavi G. SM, Nikdel M. Various battery models for various simulation studies and applications. Vol. 32, *Renewable and Sustainable Energy Reviews*. 2014. p. 477–85.

3. Xu J, Li S, Mi C, Chen Z, Cao B. SOC based battery cell balancing with a novel topology and reduced component count. *Energies*. 2013;6(6):2726–40.

4. Koseoglou M, Tsioumas E, Jabbour N, Mademlis C. Highly Effective Cell Equalization in a Lithium-Ion Battery Management System. *IEEE Transactions on Power Electronics*. 2020 Feb 1;35(2):2088–99.

5. Saxena S, Raman SR, Saritha B, John V. A novel approach for electrical circuit modeling of Li-ion battery for predicting the steady-state and dynamic I–V characteristics. *Sadhana - Academy Proceedings in Engineering Sciences.* 2016 May 1;41(5):479–87.

6. Lotfi N, Fajri P, Novosad S, Savage J, Landers RG, Ferdowsi M. Development of an experimental testbed for research in lithium-ion battery management systems. *Energies.* 2013;6(10):5231–58.

7. Asghar F, Talha M, Kim SH, Ra IH. Battery State of Charge Estimation using Kalman Filter.

8. Castano-Solis S, Serrano-Jimenez D, Gauchia L, Sanz J. The influence of BMSs on the characterization and modeling of series and parallel Li-ion packs. *Energies*. 2017;10(3).

9. Waag W, Fleischer C, Sauer DU. Critical review of the methods for monitoring of lithium-ion batteries in electric and hybrid vehicles. Vol. 258, *Journal of Power Sources*. 2014. p. 321–39.

10. Maitreya S, Jain H, Paliwal P. Scalable and De-centralized Battery Management System for Parallel Operation of Multiple Battery Packs. In: *2021 Innovations in Energy Management and Renewable Resources, IEMRE 2021*. *Institute of Electrical and Electronics Engineers* Inc.; 2021.

11. Steinhorst S, Lukasiewycz M, Narayanaswamy S, Kauer M, Chakraborty S. Smart cells for embedded battery management. In: *Proceedings - 2nd IEEE International Conference on Cyber-Physical Systems, Networks, and Applications, CPSNA 2014*. *Institute of Electrical and Electronics Engineers* Inc.; *2014*. p. 59–64.

12. Loniza E, Situmorang JA, Kusuma DDA, Cahyadi AI, Wahyunggoro O. Passive balancing of battery lithium polymer using shunt resistor circuit method. In: *AIP Conference Proceedings. American Institute of Physics* Inc.; 2016.

13. Wu H. Hardware-in-loop verification of battery management system. In*: 2011 4th International Conference on Power Electronics Systems and Applications, PESA 2011*. 2011.

14. Baboselac I, Hederić Ž, Benšić T. MatLab simulation model for dynamic mode of the Lithium-Ion batteries to power the EV. *Tehnički glasnik*. 2017 Jul 1;11(1-2):7-13.

15. Wey CL, Jui PC. A unitized charging and discharging smart battery management system. In *2013 International Conference on Connected Vehicles and Expo (ICCVE)* 2013 Dec 2 (pp. 903-909). IEEE.

16. Liu Y, Gene Liao Y, Lai MC. Lithium-ion polymer battery for 12-voltage applications: Experiment, modelling, and validation. *Energies*. 2020;13(3).

17. Zhang C, Jiang J, Zhang W, Sharkh SM. Estimation of state of charge of lithium-ion batteries used in HEV using robust extended Kalman filtering. *Energies*. 2012;5(4):1098–115.

18. Jiani D, Youyi W, Changyun W. Li-ion battery SOC estimation using particle filter based on an equivalent circuit model. In: *IEEE International Conference on Control and Automation, ICCA*. 2013. p. 580–5.

19. Pei L, Zhu C, Wang T, Lu R, Chan CC. Online peak power prediction based on a parameter and state estimator for lithium-ion batteries in electric vehicles. *Energy*. 2014 Mar 1;66:766–78.

20. Li X, Li N, Chen L, Shen Y, Wang Z, Zhu Z. An improved LEACH for clustering protocols in wireless sensor networks. In *2010 International Conference on Measuring Technology and Mechatronics Automation* 2010 Mar 13 (Vol. 1, pp. 496-499). IEEE.

21. Chen N. Design of Intelligent Battery Management System. *In Scitepress*; 2017. p. 346–50.

22. Gismero A, Schaltz E, Stroe DI. Recursive state of charge and state of health estimation method for lithium-ion batteries based on coulomb counting and open circuit voltage. *Energies*. 2020 Apr 1;13(7).

23. Zhang S, Sun H, Lyu C. A method of SOC estimation for power Li-ion batteries based on equivalent circuit model and extended Kalman filter. In*: Proceedings of the 13th IEEE Conference on Industrial Electronics and Applications, ICIEA 2018. Institute of Electrical and Electronics Engineers* Inc.; 2018. p. 2683–7.

24. Cheng KWE, Divakar BP, Wu H, Ding K, Ho HF. Battery-management system (BMS) and SOC development for electrical vehicles. *IEEE Transactions on Vehicular Technology*. 2011 Jan;60(1):76–88.

25. Rzepka B, Bischof S, Blank T. Implementing an extended Kalman filter for SoC estimation of a Li-ion battery with hysteresis: A step-by-step guide. *Energies.* 2021 Jul 1;14(13).

26. Li Z, Zhang P, Wang Z, Song Q, Rong Y. State of Charge Estimation for Li-ion Battery Based on Extended Kalman Filter. In: *Energy Procedia. Elsevier* Ltd; 2017. p. 3515–20.

27. Ren H, Zhao Y, Chen S, Wang T. Design and implementation of a battery management system with active charge balance based on the SOC and SOH online estimation. *Energy*. 2019 Jan 1;166:908–17.

28. Tian Y, Xia B, Sun W, Xu Z, Zheng W. A modified model based state of charge estimation of power lithium-ion batteries using unscented Kalman filter. *Journal of Power Sources*. 2014 Dec 15;270:619–26.

29. Wang A, Jin X, Li Y, Li N. LiFePO4 battery modeling and SOC estimation algorithm. In: *Proceedings of the 29th Chinese Control and Decision Conference, CCDC 2017. Institute of Electrical and Electronics Engineers* Inc.; 2017. p. 7574–8.

30. Chung DW, Yang SH. SOC estimation of lithium-ion battery based on kalman filter algorithm for energy storage system in microgrids. In: *E3S Web of Conferences. EDP Sciences*; 2018.

31. da Costa SCL, Araujo AS, Carvalho ADS. Battery State of Charge estimation using Extended Kalman Filter. In: *2016 International Symposium on Power Electronics, Electrical Drives, Automation and Motion, SPEEDAM 2016. Institute of Electrical and Electronics Engineers* Inc.; 2016. p. 1085–92.

32. Fathoni G, Widayat SA, Topan PA, Jalil A, Cahyadi AI, Wahyunggoro O. Comparison of State-of-Charge (SOC) estimation performance based on three popular methods: Coulomb counting, open circuit voltage, and Kalman filter. In *2017 2nd International Conference on Automation, Cognitive Science, Optics, Micro Electro-Mechanical System, and Information Technology (ICACOMIT)* 2017 Oct 23 (pp. 70-74). IEEE.

33. Li T, Martínez López L, Li Y, Institute of Electrical and Electronics Engineers. *Proceedings of the 2017 12th International Conference on Intelligent Systems and Knowledge Engineering (ISKE)* : IEEE ISKE 2017 : November 24-26, 2017, NanJing, JiangSu, China.

34. Meena N, Baharwani V, Sharma D, Sharma A, Choudhary B, Parmar P, et al. Charging and discharging characteristics of Lead acid and Li-ion batteries. In*: 2014 Power and Energy Systems Conference: Towards Sustainable Energy, PESTSE 2014*. IEEE Computer Society; 2014.

35. Khalil IU, Ahsan M, Ullah I, Adnan A, Khan N, Nawaz S. SOC prediction of lithium-ion battery using extended Kalman filter. *In2018 International Symposium on Recent Advances in Electrical Engineering (RAEE)* 2018 Oct 17 (pp. 1-5). IEEE.

36. Baccouche I, Jemmali S, Manai B, Omar N, Essoukri Ben Amara N. Improved OCV model of a Li-ion NMC battery for online SOC estimation using the extended Kalman filter. *Energies.* 2017 Jun 1;10(6).

37. Yu Z, Huai R, Xiao L. State-of-charge estimation for lithium-ion batteries using a Kalman filter based on local linearization. *Energies*. 2015 Aug 1;8(8):7854–73.

38. Nikolian A, De Hoog J, Fleurbay K, Timmermans JM, Van De Bossche P, Van Mierlo J. Classification of Electric modelling and Characterization methods of Lithium-ion Batteries for Vehicle Applications. In *Proceedings of the European Electric Vehicle Congress, Brussels, Belgium* 2014 Dec 4 (pp. 2-5).

39. Lei H, Han YY. The measurement and analysis for Open Circuit Voltage of Lithium-ion Battery. In: *Journal of Physics: Conference Series. Institute of Physics Publishing*; 2019.

40. INA228-Q1 AEC-Q100, 85-V, 20-Bit, Ultra-Precise Power/Energy/Charge Monitor With I2C Interface (Rev. A): Texas Instruments: [cited 2021, June]. Available from: https://www.ti.com/document-viewer/INA228-Q1/datasheet

41. INA228, INA229, INA237, INA238, and INA239 EVM User's Guide.Texas Instruments: https://www.ti.com/tool/INA228_237_238EVM

42. Prasad S VK, Divakar BP. Real Time Estimation of SoC and SoH of Batteries. Vol. 8. 2018.

43. Xavier LS, Amorim WCS, Cupertino AF, Mendes VF, do Boaventura WC, Pereira HA. Power converters for battery energy storage systems connected to medium voltage systems: a comprehensive review. *BMC Energy.* 2019 Dec;1(1).

44. Lei G, Luo X, Cai L, Gao L, Dai N, Xu Q, et al. Research on smart EFK algorithm for electric vehicle battery packs management system. *Journal of Intelligent and Fuzzy Systems*. 2020;38(1):257–62.

45. Pang H, Zhang F. Experimental Data-Driven Parameter Identification and State of Charge Estimation for a Li-Ion Battery Equivalent Circuit Model. Available from: www.mdpi.com/journal/energies

46. NEMES RO, CIORNEI SM, Mircea RU, MARTIS C. Parameters identification using experimental measurements for equivalent circuit Lithium-Ion cell models. In *2019 11th International Symposium on Advanced Topics in Electrical Engineering (ATEE)* 2019 Mar 28 (pp. 1-6). IEEE.

47. Welch G, Bishop G. An Introduction to the Kalman Filter [Internet]. Available from: http://www.cs.unc.edu/~gb

48. Jokić I, Zečević Ž, Krstajić B. State-of-charge estimation of lithium-ion batteries using extended Kalman filter and unscented Kalman filter. In: *2018 23rd International Scientific-Professional Conference on Information Technology, IT 2018. Institute of Electrical and Electronics Engineers* Inc.; 2018. p. 1–4.

49. Pulavarthi C, Kalpana R, Parthiban P. State of Charge estimation in Lithium-Ion Battery using model based method in conjunction with Extended and Unscented Kalman Filter. In: *2020 IEEE International Conference on Power Electronics and Renewable Energy Applications, PEREA 2020*. Institute of Electrical and Electronics Engineers Inc.; 2020.

50. He W, Williard N, Chen C, Pecht M. State of charge estimation for electric vehicle batteries using unscented kalman filtering. *Microelectronics Reliability*. 2013;53(6):840–7.

51. Li B, Bei S. Estimation algorithm research for lithium battery SOC in electric vehicles based on adaptive unscented Kalman filter. *Neural Computing and Applications*. 2019 Dec 1;31(12):8171–83.

52. Chen C, Xiong R, Yang R, Shen W, Sun F. State-of-charge estimation of lithium-ion battery using an improved neural network model and extended Kalman filter. *Journal of Cleaner Production*. 2019 Oct 10;234:1153–64.

53. ZHANG L, WANG S-L, CHEN L, WANG Y, SU J. Study on the Charging and Discharging Characteristics of the Lithium-ion Battery Pack. *DEStech Transactions on Computer Science and Engineering*. 2018 Sep 13;(cmsms).

54. Shen JC. Time efficient state-of-charge estimation using open circuit voltage and the logarithmic modelling for battery management system (Doctoral dissertation, University of British Columbia).

55. Lin L, Fukui M. An OCV estimation algorithm for lithium-ion battery using kalman filter. In: *IEEE Region 10 Annual International Conference, Proceedings/TENCON. Institute of Electrical and Electronics Engineers* Inc.; 2020. p. 1086–9.

56. Kim J, Seo GS, Chun C, Cho BH, Lee S. OCV hysteresis effect-based SOC estimation in extended Kalman filter algorithm for a LiFePO 4/C cell. In: *2012 IEEE International Electric Vehicle Conference, IEVC* 2012. 2012.

57. Ilies AI, Chindris G, Pitica D. A Comparison between State of Charge Estimation Methods: Extended Kalman Filter and Unscented Kalman Filter. In: *2020 IEEE 26th International Symposium for Design and Technology in Electronic Packaging, SIITME 2020 - Conference Proceedings. Institute of Electrical and Electronics Engineers* Inc.; 2020. p. 376–81.

58. Dao VQ, Dinh MC, Kim CS, Park M, Doh CH, Bae JH, et al. Design of an effective state of charge estimation method for a lithium-ion battery pack using extended kalman filter and artificial neural network. *Energies*. 2021 May 1;14(9).

59. Rahmoun A, Biechl H, Rosin A. SOC estimation for Li-Ion batteries based on equivalent circuit diagrams and the application of a Kalman filter. In: *PQ 2012: 8th International Conference - 2012 Electric Power Quality and Supply Reliability, Conference Proceedings*. 2012. p. 273–6.

60. Fridholm B, Wik T, Nilsson M. Robust recursive impedance estimation for automotive lithium-ion batteries. *Journal of Power Sources*. 2016 Feb 1;304:33–41.

61. Yuan S, Wu H, Yin C. State of charge estimation using the extended Kalman filter for battery management systems based on the ARX battery model. *Energies*. 2013;6(1):444–70.

62. BQ77915 3-Series to 5-Series Stackable Ultra-Low Power Primary Protector with Autonomous Cell Balancing and HIBERNATE Mode. Texas Instruments [cited 2020, September] Available from: https://www.ti.com/lit/ds/symlink/bq77915.pdf

63. Kharisma MD, Ridwan M, Ilmiawan AF, Nurman FA, Rizal S. Modeling and Simulation of Lithium-Ion Battery Pack Using Modified Battery Cell Model. In *2019 6th International Conference on Electric Vehicular Technology (ICEVT)* 2019 Nov 18 (pp. 25-30). IEEE.